DYNAMICS AND CONTROL OF VIBRATING WEBS IN A ROLL-TO-ROLL SYSTEM

BY

SAJID ALI

A Dissertation Presented to the

DEANSHIP OF GRADUATE STUDIES

KING FAHD UNIVERSITY OF PETROLEUM & MINERALS

DHAHRAN, SAUDI ARABIA

In Partial Fulfillment of the
Requirements for the Degree of

DOCTOR OF PHILOSOPHY

In

MECHANICAL ENGINEERING

DECEMBER 2017

In the name of Allah, the Most Gracious and the Most Merciful

KING FAHD UNIVERSITY OF PETROLEUM & MINERALS

DHAHRAN- 31261, SAUDI ARABIA

DEANSHIP OF GRADUATE STUDIES

This thesis, written by **SAJID ALI** under the direction of his thesis advisor and approved by his thesis committee, has been presented and accepted by the Dean of Graduate Studies, in partial fulfillment of the requirements for the degree of **DOCTOR OF PHILOSOPHY IN MECHANICAL ENGINEERING.**

Dr. Muhammad Hawwa
(Advisor)

Dr. Zuhair Mattoug Gasem
Department Chairman

Dr. Yehia A. Khulief
(Member)

Dr. Salam A. Zummo
Dean of Graduate Studies

Dr. David E. Hardt
(Member)

3/4/18
Date

Dr. Hussain M. Al-Qahtani
(Member)

Dr. Sami El-Ferik
(Member)

©SAJID ALI

2017

Dedicated

to

My Beloved Parents, Brothers, Sisters,

My wife, Son and Daughter

ACKNOWLEDGMENT

I pay my sincere acknowledgment to ALLAH ALMIGHTY with his help it would not be possible for me to complete this research work well on time. May peace be upon the prophet Muhammad (PBUH), on his family, and companions.

I want to acknowledge Department of Mechanical Engineering and King Fahd University of Petroleum and Minerals (KFUPM) to give me an opportunity to pursue my PhD degree. I am thankful to Deanship of Research at King Fahd University of Petroleum and Minerals for funding this work through Project No. MIT13101/02.

I am highly thankful to my thesis advisor Dr. Muhammad Hawwa professor department of Mechanical Engineering King Fahd University of Petroleum and Minerals (KFUPM) who always helped me and guide me throughout my thesis and provided me a valuable opportunity to conduct my experimental work at Massachusetts Institute of Technology (USA). I am highly thankful to Professor. David Hardt for his intense help and guidance in performing my experiments at MIT. I am highly grateful to the committee members, Dr. Sami, Dr. Khulief, and Dr. Husain for giving me their precious time and valuable comments.

I am thankful to my Parents, brothers, sisters, and my wife for their support in every aspect of my life. I am thankful to my colleagues at the university specially Sikandar Khan, Khwaja Muhammad and Usama Siddique for their help, prayers and providing me a good company during my study at KFUPM.

TABLE OF CONTENTS

ACKNOWLEDGMENT ..... **v**

TABLE OF CONTENTS ..... **vi**

LIST OF TABLES ..... **ix**

LIST OF FIGURES ..... **x**

LIST OF ABBREVIATIONS ..... **xiii**

ABSTRACT ..... **xviii**

ملخص الرسالة ..... **xx**

CHAPTER 1 INTRODUCTION **22**

1.1 Introduction **22**

1.1.1 Roll-to-Roll Manufacturing Systems **23**

1.1.2 Axially Moving Webs **31**

1.2 Research Objectives **34**

1.3 Dissertation Organization **35**

CHAPTER 2 LITERATURE REVIEW **39**

2.1 Literature Review **39**

2.1.1 Vibration of Axially Moving Webs **40**

2.1.2 Vibration Control of Axially Moving Webs **47**

CHAPTER 3 WEB VIBRATION IN A SINGLE-SPAN ROLL-TO-ROLL SYTEM **51**

3.1 Roll-to-Roll Dynamics **51**

3.1.1 Web Tension Velocity Relationship **52**

3.1.2 Equation of Motion of the Roll **54**

3.1.3 Roll Radius and Moment of Inertia 56

3.1.4 Numerical Solution of Roll-to-Roll Dynamics 59

3.2 Web Vibration Model 64

3.2.1 Model Validation 72

3.2.2 Effect of Axial Speed on Web Vibration Response 74

3.2.3 Effect of Roll-Borne Disturbances on Web Vibration Response 79

3.2.3.1 Parametric Analysis 80

3.3 The Coupled Web Vibration 86

CHAPTER 4 WEB VIBRATION IN A TWO-SPAN ROLL-TO-ROLL SYTEM 92

4.1 Roll-to-Roll Dynamics 92

4.1.1 Web Tension Velocity Relationship 93

4.1.2 Equation of Motion of the Roll 93

4.1.3 Numerical Solution of Two-Span Roll-to-Roll System 94

4.1.4 Roll-to-Roll System Parameters 98

4.2 The Coupled Web Vibration 105

CHAPTER 5 MULTI-SPAN ROLL-TO-ROLL PRINTING SYSTEM 111

5.1 Roll-to-Roll Dynamic 111

5.2 Validation of Web Dynamic Model 117

5.2.1 Tension Measurement/Control System 119

5.2.2 Fiber Optic Micro Displacement Measurement Systems (μDMS) 122

5.2.2.1 Operation of Fiber Optic Micro Displacement Measurement Systems (μDMS) 124

5.3 Results & Discussion 125

5.3.1 Frequency Comparison at Different Web Speeds 126

5.3.2 Transverse Displacement Comparison at Variable Web Speed 129

CHAPTER 6 WEB VIBRATION SUPPRESSION 134

6.1 Mathematical Model 134

6.1.1 Problem Formulation 134

6.1.2 Finite Difference Model 139

6.1.3 Numerical Solution and Discussion 141

6.2 Experimental Setup & Results 148

6.2.1 Results 150

CHAPTER 7 CONCLUSIONS AND RECOMMENDATIONS 153

REFERENCES 157

APPENDIX 167

VITAE 178

LIST OF TABLES

Table 3.1 Parameters of the roll-to-roll R2R System 60
Table 4.1 Parameters of Two-Span R2R configuration..... 95
Table 5.1 Parameters of Four-Span R2R configuration..... 113

LIST OF FIGURES

Figure 1.1 Schematic of a Roll-to-Roll process [1] 24
Figure 1.2 Active dancer system in a Roll-to-Roll process [3] 24
Figure 1.3 (a) The proposed six-roll configuration (b) the final six-roll design comprising two idler rolls for web guidance [4] 25
Figure 1.4 Stress-strain curve of PET 26
Figure 1.5 (a) Dished Roll (b) Wrinkling in the web (c) Telescoping [6] 28
Figure 1.6 Schematic of an R2R process and its possible applications [7] 31
Figure 1.7 Example of large-area high-throughput roll-to-roll patterning systems [8] 32
Figure 1.8 Schematic of process integration (CVD & μCP) [9] 32
Figure 3.1 One Span R2R System 51
Figure 3.2 Free Body Diagram of the Roll (Torques acting on a roll) 55
Figure 3.3 Geometry of unwinding and rewinding rolls 57
Figure 3.4 Angular speed variation of rolls 61
Figure 3.5 Angular displacement variation of rolls 61
Figure 3.6 Radii variation of rolls with time 62
Figure 3.7 Axial web velocity variation with time 63
Figure 3.8 Web-transmitted tension variation with time 64
Figure 3.9 Deformation / Velocity diagram 65
Figure 3.10 Transverse Response Comparison at $v* = 0.1$ & $x* = 0.5$ 74
Figure 3.11 Transverse displacement at $x* = 0.25$ for webs having different speeds 75
Figure 3.12 Transverse displacement at $x* = 0.5$ for webs having different speeds 75
Figure 3.13 Transverse displacement at $x* = 0.75$ for webs having different speeds 76
Figure 3.14 Frequency of response at $x* = 0.5$ for webs having different speeds 77
Figure 3.15 Frequency vs axial speed 77
Figure 3.16 Comparison of first three mode shapes at different velocities 78
Figure 3.17 Transverse displacement at $x* = 0.5$ & Ω = 0.6 for webs having different speeds 80
Figure 3.18 Transverse displacement at $x* = 0.5$ & Ω = 1.2 for webs having different speeds 81
Figure 3.19 Transverse displacement at $x* = 0.5$ & Ω = 1.4 for webs having different speeds 81
Figure 3.20 Transverse displacement at $x* = 0.5$ & Ω = 1.7 for webs having different speeds 82
Figure 3.21 Transverse displacement at $x* = 0.5$ & Ω = 3.4 for webs having different speeds 82
Figure 3.22 Frequency-domain response of displacement at $x* = 0.5$ & Ω = 0.6 for webs having different speeds 83

Figure 3.23 Frequency-domain response of displacement at $x* = 0.5$ & Ω = 1.2 for webs having different speeds 84
Figure 3.24 Frequency-domain response of displacement at $x* = 0.5$ & Ω = 1.4 for webs having different speeds 84
Figure 3.25 Frequency-domain response of displacement at $x* = 0.5$ & Ω = 1.6 for webs having different speeds 85
Figure 3.26 Frequency-domain response of displacement at $x* = 0.5$ & Ω = 3.4 for webs having different speeds 85
Figure 3.27 Web-transmitted tension variation with time 87
Figure 3.28 Transverse displacement at $x* = 0.25$ for the axially moving web 88
Figure 3.29 Transverse displacement at $x* = 0.50$ for the axially moving web 88
Figure 3.30 Transverse displacement at $x* = 0.75$ for the axially moving web 89
Figure 3.31 Transverse displacement (at $x* = 0.5$) and web speed (dimensionless) 89
Figure 3.32 Frequency-domain response of displacement at different points on the web 90
Figure 4.1 Dual Span R2R System 92
Figure 4.2 Angular velocity variation of rolls 96
Figure 4.3 Web-transmitted tension (T_2) variation with time 97
Figure 4.4 Web-transmitted tension (T_3) variation with time 97
Figure 4.5 Angular velocity variation of rolls, (a) J_b = 0.0001, (b) J_b = 0.001 & (c) J_b = 0.01 99
Figure 4.6 Comparing the web-transmitted tension (T_2) at different idler roll inertia ... 100
Figure 4.7 Comparing the web-transmitted tension (T_3) at different idler roll inertia ... 101
Figure 4.8 Web transmitted tension, T_2 102
Figure 4.9 Web transmitted tension, T_3 102
Figure 4.10 Time history of angular speed (Rur = 0.04 m & Rrr = 0.02 m) 103
Figure 4.11 (a) Web transmitted tension, T_2 (Rrr = 0.02 m & 0.04 m) 104
Figure 4.12 Web transmitted tension, T_3 (Rrr = 0.02 m & 0.04 m) 104
Figure 4.13 Transverse displacement at $x* = 0.25$ (Unwinding Span) 107
Figure 4.14 Transverse displacement at $x* = 0.50$ (Unwinding Span) 107
Figure 4.15 Transverse displacement at $x* = 0.75$ (Unwinding Span) 108
Figure 4.16 Transverse displacement at $x* = 0.25$ (Rewinding Span) 109
Figure 4.17 Transverse displacement at $x* = 0.50$ (Rewinding Span) 109
Figure 4.18 Transverse displacement at $x* = 0.75$ (Rewinding Span) 110
Figure 5.1 Four Span Roll-to-Roll System 111
Figure 5.2 Angular velocity variation of (a) Unwinding & Rewinding rolls, and (b) Idler & Impression rolls 114
Figure 5.3 (a) Angular displacement variation and (a) Radii variation of Unwinding & Rewinding rolls 115
Figure 5.4 Web transmitted-tension variation with time (a) T_2, (b) T_3, (c) T_4 and (d) T_5 116

Figure 5.5 Experimental setup 117
Figure 5.6 System's critical component layout [2] 118
Figure 5.7 FMS web tension measurement 120
Figure 5.8 Tension control process 121
Figure 5.9 Fiber optics probes (D-Model) 122
Figure 5.10 Fiber optics probes (RC-Model) 123
Figure 5.11 D-Model (reflectance dependent) 123
Figure 5.12 RC-Model (reflectance compensated) 124
Figure 5.13 Measured transverse displacement 125
Figure 5.14 Frequency of transverse displacement 126
Figure 5.15 Frequency variation against speed & tension (Experimental) 127
Figure 5.16 Frequency variation against speed & tension (String) 128
Figure 5.17 Frequency variation against speed & tension (Membrane) 129
Figure 5.18 Axial web speed 130
Figure 5.19 Simulated & experimental transverse response comparison at $x* = 0.50$. 131
Figure 5.20 Simulated & experimental transverse response comparison at $x* = 0.75$. 131
Figure 5.21 Simulated & experimental transverse response comparison with at $x* = 0.50$ 132
Figure 5.22 Simulated & experimental transverse response comparison with at $x* = 0.75$ 133
Figure 6.1 With & without control transverse displacement at $x* = 0.25$ & $v* = 0.5$.. 141
Figure 6.2 With & without control transverse displacement at $x* = 0.50$ & $v* = 0.5$.. 142
Figure 6.3 With & without control transverse displacement at $x* = 0.75$ & $v* = 0.5$.. 142
Figure 6.4 Transverse displacement at $x* = 0.25$ for webs having different speeds 144
Figure 6.5 Transverse displacement at $x* = 0.50$ for webs having different speeds 144
Figure 6.6 Transverse displacement at $x* = 0.75$ for webs having different speeds 145
Figure 6.7 Axial speed comparison 146
Figure 6.8 Transverse displacement at $x* = 0.25$ for webs having variable speed 147
Figure 6.9 Transverse displacement at $x* = 0.50$ for webs having variable speed 147
Figure 6.10 Transverse displacement at $x* = 0.75$ for webs having variable speed 148
Figure 6.11 Modification 149
Figure 6.12 Modified Experimental Setup 149
Figure 6.13 Transverse Response Comparison at $x* = 0.25$ 150
Figure 6.14 Transverse Response Comparison at $x* = 0.50$ 151
Figure 6.15 Transverse Response Comparison at $x* = 0.75$ 151

LIST OF ABBREVIATIONS

$\boldsymbol{\tau}$	:	Kinetic energy
$\boldsymbol{U}$	:	Potential energy
$\boldsymbol{W^{NC}}$	:	Work done by non-conservative forces
$\boldsymbol{\rho}$	:	Density of the web
A	:	Area of web
$\boldsymbol{t}$	:	Time (Sec)
$\boldsymbol{t_*}$	:	Time (Dimensionless)
$\boldsymbol{v}$	:	Axial speed of the web
$\boldsymbol{v_y}$	:	Transverse component of the web axial speed
$\boldsymbol{v_x}$	:	Longitudinal component of the web axial speed
$\boldsymbol{w(x,t)}$	:	Transverse displacement (Dimensional)
$\boldsymbol{w_*(x_*,t_*)}$	:	Transverse displacement (Dimensionless)
T	:	Axial tension (N)
$\boldsymbol{v_*}$	:	Axial speed of the string (Dimensionless)
$\boldsymbol{a(x_*)}$	:	Initial displacement

$\boldsymbol{b(x_*)}$	:	Initial velocity
$\boldsymbol{g_n^R(t_*)}$	:	Real component of the generalized coordinate
$\boldsymbol{g_n^I(t_*)}$	:	Imaginary component of the generalized coordinate
$\boldsymbol{g_n^R(0)}$	:	Initial value of real component of the generalized coordinate
$\boldsymbol{g_n^I(0)}$	:	Initial value of imaginary component generalized coordinate
$\boldsymbol{E}$	:	Modulus of elasticity
I	:	Moment of inertia
$\boldsymbol{\alpha}$	:	Dimensionless flexural rigidity
$\boldsymbol{dx}$	:	Step size
$\boldsymbol{dx_*}$	:	Step size (Dimensionless)
FR	:	Flexure rigidity
$\boldsymbol{R_1(t)}$	:	Radius of unwind roll
$\boldsymbol{R_2(t)}$	:	Radius of rewind roll
$\boldsymbol{R_r}$	:	Radius of roll
L	:	Length of the web
$\mathbf{L_0}$	:	Initial length of the web
$\boldsymbol{\varepsilon}$	:	Elastic strain

$\boldsymbol{\sigma}$	:	Stress
$\mathbf{a}$	:	Length of sliding zone
$\boldsymbol{\mu}$	:	Coefficient of friction
$\Omega_{\boldsymbol{k}}$	:	Angular speed of roll
$\boldsymbol{B_k}$	:	Motor constant
$\boldsymbol{J_k}$	:	Polar moment of inertia of roll
$\boldsymbol{C_k}$	:	Frictional torque
$\boldsymbol{R_{01}}$	:	Initial radius of unwinding roll
$\boldsymbol{R_{02}}$	:	Initial radius of rewinding roll
$\boldsymbol{\theta_1}$	:	Angular displacement of unwinding roll
$\boldsymbol{\theta_2}$	:	Angular displacement of rewinding roll
$\boldsymbol{h}$	:	Web thickness
$\boldsymbol{J_r}$	:	Polar moment of inertia of the roll material
$\boldsymbol{J_{W1}(t)}$	:	Polar moment of inertia of web material on unwinding roll
$\boldsymbol{J_{W2}(t)}$	:	Polar moment of inertia of web material on rewinding roll
$\boldsymbol{m_r}$	:	Mass of the roll (Without web)
$\boldsymbol{\rho_r}$	:	Density of the roll (Without web)

$\boldsymbol{m_{w1}}$	:	Mass of the web material on unwinding roll
$\boldsymbol{m_{w2}}$	:	Mass of the web material on rewinding roll
W	:	Width of the roll
$\boldsymbol{R_{id}}$	:	Radius of the idler roll
$\Omega_{\boldsymbol{id}}$	:	Angular speed of the idler roll
Ω	:	External disturbance frequency
GITT	:	Generalized integral transform technique
$\boldsymbol{R_{ur}}$	:	Radius of the unwinder roll
$\boldsymbol{R_{rr}}$	:	Radius of the rewinder roll
$\boldsymbol{R_b}$	:	Radius of the idler roll
$\boldsymbol{J_b}$	:	Polar moment of inertia of the idler roll
$\Omega_{\boldsymbol{rr}}$	:	Angular speed of the rewinder roll
$\Omega_{\boldsymbol{ur}}$	:	Angular speed of the unwinder roll
$\Omega_{\boldsymbol{b}}$	:	Angular speed of the idler roll
$\boldsymbol{L}$	:	Web span length
$\boldsymbol{J_{ur}(t)}$	:	Polar moment of inertia of the unwinder roll
$\boldsymbol{J_{rr}(t)}$	:	Polar moment of inertia of the rewinder roll

$\boldsymbol{C}$	:	Coupled
$\boldsymbol{NC}$	:	Uncoupled

ABSTRACT

Full Name : Sajid Ali

Dissertation Title : Dynamics and control of vibrating webs in a roll-to-system

Major Field : Mechanical Engineering

Date : December, 2017

Vibration is a limiting factor of printing small features on a web within R2R systems, since it diversely affects the quality of the printed features. This dissertation focuses on understanding the transverse web vibrations coupled with R2R system's dynamics; it also provides a unique method for controlling web vibration by combining torque regulation and energy dissipation at the rewinding roll. The dynamics of three roll-to-roll systems, including two rolls-one web span, three rolls-two web spans, and five rolls-four web spans, was analyzed to realize the axial speed-tension relationships. Rigorous analytical treatment is provided to examine the coupling between the roll-to-roll dynamics and the transverse vibration of the aforementioned axially moving webs between the rolls. Mathematical models of coupled differential equations are solved by utilizing a finite difference scheme / state space technique which helped in transforming hyperbolic partial differential equation into first-order ordinary differential equations. It was shown that the web axial speed and web-transmitted tension are not constants over time, while certain amount of web material is transferred from the unwinding roll to the winding roll; they vary nonlinearly after a short transient period. Based on the R2R system's dynamics, the transverse vibration of the axially moving web between rolls was found to be non-periodic,

with a higher frequency response corresponding to rapid changes in the web axial speed and a lower frequency response corresponding to slow changes in the web axial speed. In order to control the web transverse vibration of the axially moving web, the torques applied at the rewinding / unwinding rolls were regulated to make the web axial speed close to constant over the time of material transfer. This is combined with changing the rewinding roll radius to allow for an optimal web slope to minimize the vibration amplitude. Experiments conducted showed that the numerical results obtained for the control approach generated reasonable results.

ملخص الرسالة

الاسم : ساجد علي

عنوان الاطروحة العلمية: ديناميكية والسيطرة على اهتزازات الأشرطة المتحركة بين البكرات

التخصص: الهندسة الميكانيكية

التاريخ : ديسمبر 2017

الاهتزاز عامل يحد من إمكانية طباعة المميزات الصغيرة على الأشرطة المتحركة بين البكرات. تركز هذه الأطروحة على فهم الاهتزازات المتعامدة على الشريط المتحرك والمقرونة مع الأنظمة الديناميكية للبكرات، أيضاً توفر الأطروحة كذلك طريقة فريدة للتحكم باهتزازات الشريط وذلك بدمج العزم المنظم مع طاقة مبددة عند البكرة الأخيرة. الديناميكا لأنظمة مكونة من بكرتين وشريط واحد، ثلاث بكرات وشريطين، وخمس بكرات وأربعة أشرطة تم تحليلها باعتبار علاقات سرعة الشريط ومقدار شده. تحليل شامل ودقيق تم تقديمه لاختبار الاقتران بين ديناميكا البكرات والاهتزاز العرضي للأشرطة المتحركة السابقة ذكرها بين تلك البكرات. بناءً على أدلة من التجارب، جميع الأشرطة تم نمذجتها كخيوط. نماذج رياضية مكونة من معادلات تفاضلية مقترنة تم حلها باستخدام طريقة الفرق المحدود، والتي ساعدت بتحويل المعادلات التفاضلية الجزئية لمعادلات تفاضلية عادية من الدرجة الأولى. أيضاً تم اظهار بأن سرعة الأشرطة وشدها لقيم متغيرة مع الزمن، في حين أن كمية معينة من الشريط تم نقلها من البكرة الأولى إلى البكرة الأخيرة؛ كلاهما يتغير بشكل لا خطي، الاهتزاز العرضي للأشرطة المتحركة طولياً بين البكرات تميز بأنه غير دوري، مع تردد يتغير مع التغيرات في سرعة الشريط الطولية. من أجل التحكم في الاهتزازات المعامدة للشريط المتحرك طولياً، العزم المبذول عند البكرة الأولى تم تنظيمه لجعل سرعة الشبكة الطولية قريبة شبه ثابتة مع الزمن.

بالإضافة لجعل نصف قطر البكرة الأخيرة مؤدياً للميل المثالي لتقليل مقدار الاهتزاز. التجارب التي تم عملها أظهرت بأن النتائج التحليلية والرقمية المستقاة من النماذج للنمذجة الميكانيكية ونماذج التحكم أدت إلى نتائج معقولة.

CHAPTER 1

INTRODUCTION

1.1 Introduction

Roll-to-roll (R2R) web processing is traditionally the preferred method for the high rate automated production of papers, textiles, sheet metals, thin polymers, and laminated composites. R2R production has the added benefit of guaranteeing rapid fabrication along with a standardized level of quality. At high transport velocities and levels of fluctuation in transport speed, problems with a loss of stability may be encountered. In these mechanical systems vibrations of the axially moving materials undermine their efficiency.

Generally, vibration is an unwanted phenomenon but due to the high web speeds it is inevitable. In a band saw application transverse vibration can result in undesirable cutting forces, as well as poor cutting quality. In a printing press, printing quality cannot be achieved in the presence of vibrations. This is especially true in the chemical vapor deposition (CVD) process used for the synthesis of a carbon nanotube (CNT) forest where the accuracy of the product strongly depends on the movement of the web. Very small fluctuations in the web can severely affect the mechanical properties of the produced CNT forest. Therefore, an understanding of dynamic analysis is vital for vibration control of the webs between rolls to attain the desired level of performance metrics and the efficiency.

In an axially moving web, disturbance in the speed of the web can result from various sources such as, non-circularity of the roller or imperfect bearings, web sliding, air entrainment and windage effects, in addition to thermal or magnetic effects. In a roll-to-roll system, the quality, as well as the productivity of the process, strongly depends on the web tension and vibration.

1.1.1 Roll-to-Roll Manufacturing Systems

One has to consider R2R systems with their system dynamics model as encompassing all of a system's components; namely, the axially moving web(s), the rotating rolls, and other accessories such as dancers and brakes. (i) A web is a continuous flexible material in strip form which is very long in comparison to its width and very wide compared to its thickness. Examples of webs include all forms of paper, fabric, plastic wrap, adhesive tape, photographic film, and strip metals [1]. (ii) Every web-handling machine starts with an unwind reel, which is a specialized roll meant to carry a large roll of raw web material. (iii) Most web-handling machines end in a rewinding process, with a rewind reel. (iv) Both the unwind and rewind reels are driven by servomotors. (v) Idler rolls are used in addition to the winding and rewinding rolls for removing the effects of time-varying variables from the system [2]. (vi) Sometimes an additional roll (dancer) is used in the system to overcome the tension fluctuations, shown in Fig. 1.2. A dancer mechanism is used as a feedback element in the tension control of the system [3].

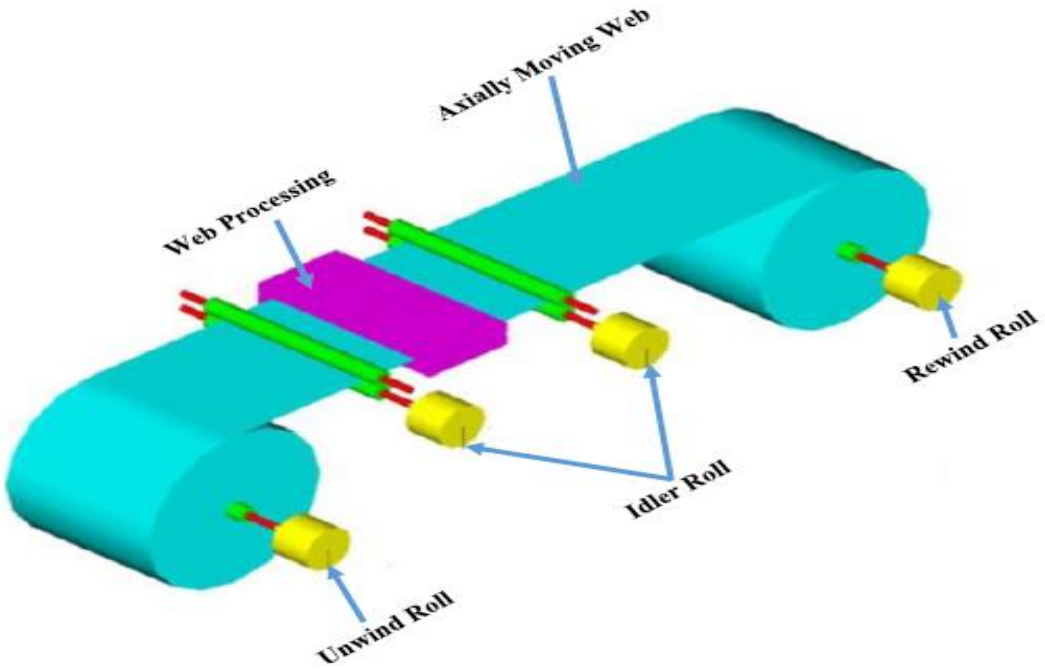

Figure 1.1 Schematic of a Roll-to-Roll process [1]

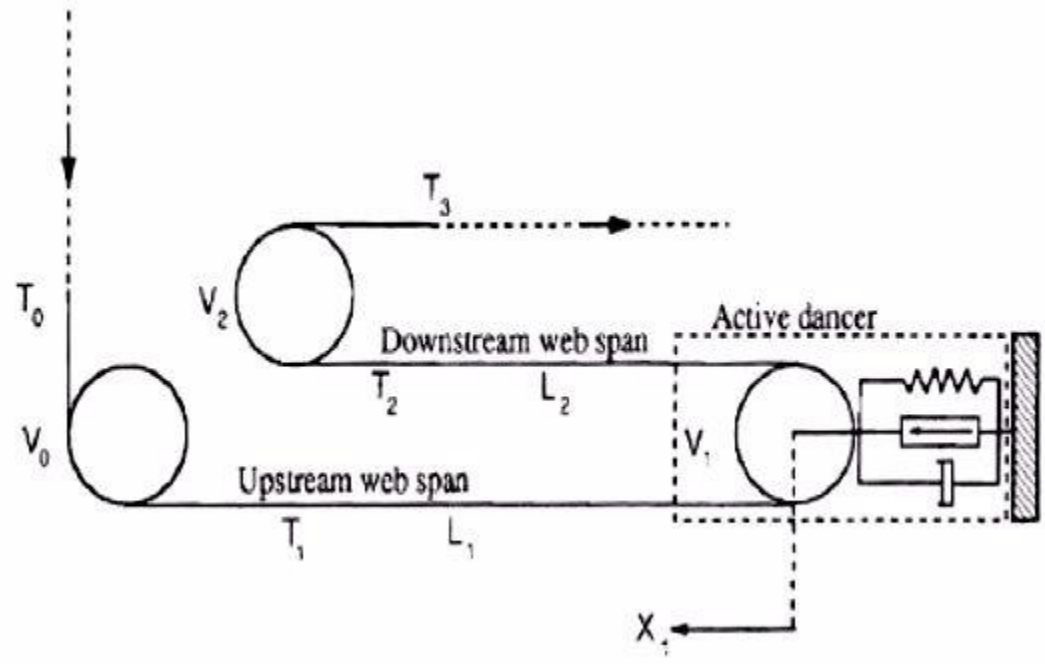

Figure 1.2 Active dancer system in a Roll-to-Roll process [3]

A μFLEX machine, designed and developed with the objective to implement the best practices regarding roll-to-roll microcontact printing [4]. Starting with an eight-roll

configuration, a three and four-roll configuration are considered, then finally a six-roll configuration is selected for the implementation, shown in Fig. 1.3.

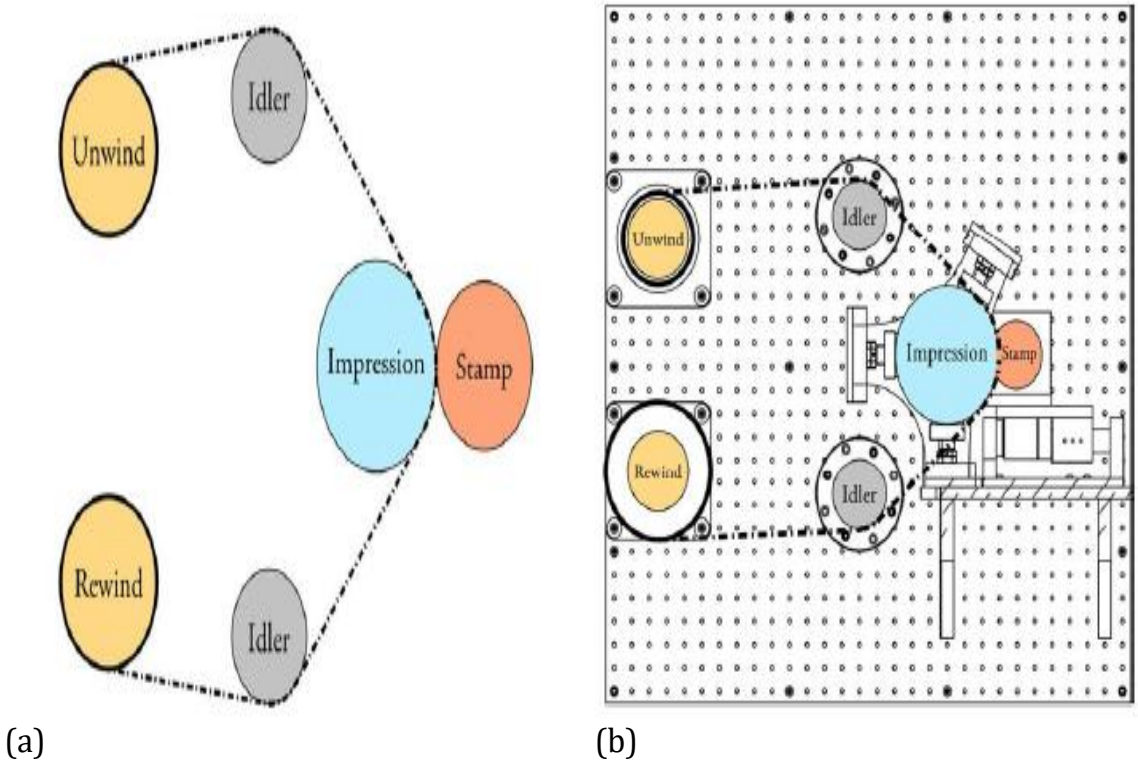

Figure 1.3 (a) The proposed six-roll configuration (b) the final six-roll design comprising two idler rolls for web guidance [4]

The μFLEX machine consists of the winding roll, unwinding roll, printing roll, impression roll and two idler rollers. The sizes of the winding and unwinding roll vary constantly during the process. To compensate for this, idler rolls are installed to ensure a constant wrap angle around the impression roll.

A typical stress-strain curve of poly ethylene terephthalate (PET) is shown in Fig. 1.4, [7]. The linear elastic region for PET is around 160 MPa.

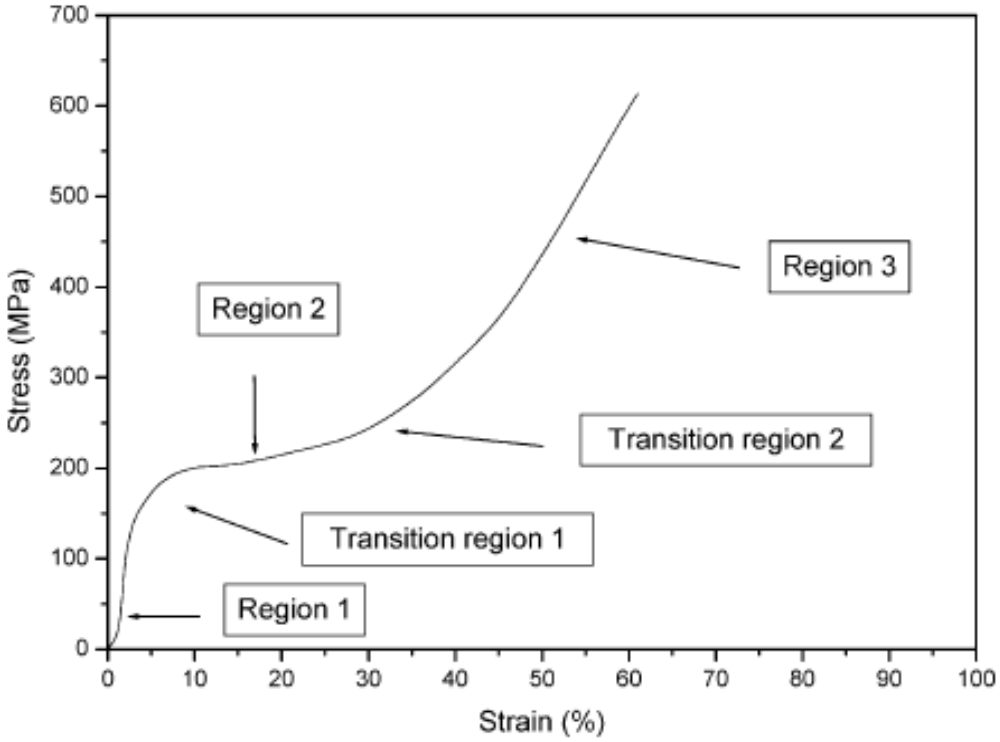

Figure 1.4 Stress-strain curve of PET

Tension in the web is defined as applied force in the direction of the machine. Normally, tension is measured in Pounds per Linear Inch (PLI). Multiplying the total width with the PLI gives the amount of tension in the web. In simple words, tension in the web can be considered as the weight hanging off the edge. Throughout the process, the web must be "in traction" with the driven rolls as well as with the idler rolls. According to the web handling principle, an axially moving web will always try to seek to align itself perpendicular to both the driven and the idler rolls. In situations, such as when webs have no traction with either the driven or idler rolls, the web handling principle is not applicable [5]. This means that, in the case where the web slips off the rolls, it will only ramble from side to side and will not follow the desired path. When web tension is high, stretching of the web in the direction of the machine and compression of the web in a cross-machine

direction will occur. Because of this stretching and compression, the web width will narrow and will cause wrinkles in the web. In case of low web tension, the shrinking of the web width in the direction of the machine and widening in the cross-machine direction will occur. This shrinking and widening in the width will produce wrinkles in the web [6] as shown in Fig. 1.5. Limiting factors in R2R manufacturing include excessive web stretching and web wrinkling, which are normally avoided by using tension control schemes.

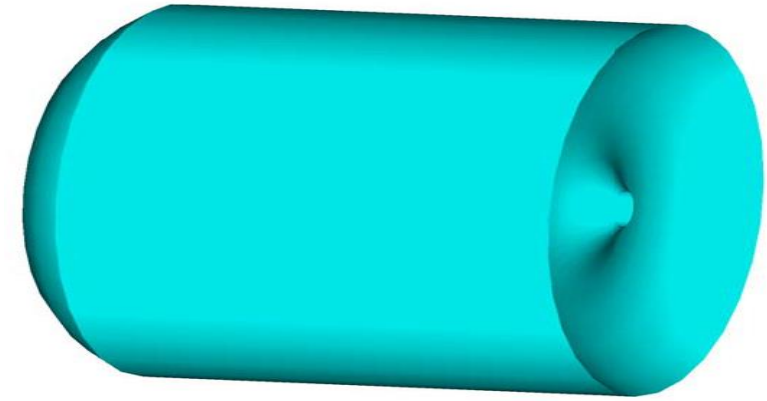

(a)

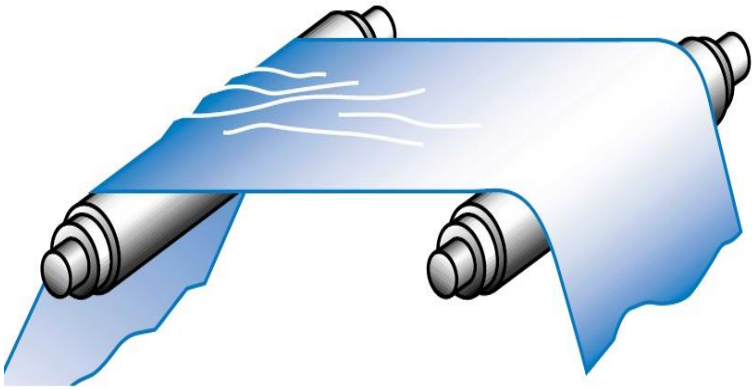

(b)

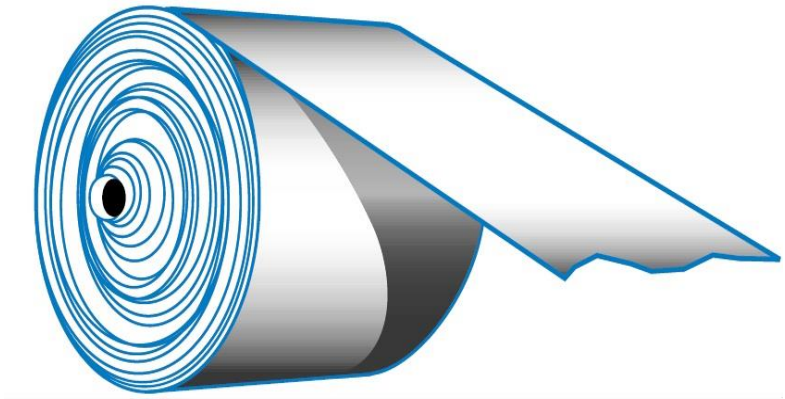

(c)

Figure 1.5 (a) Dished Roll (b) Wrinkling in the web (c) Telescoping [6]

Generally, in roll to roll web systems tension zones are classified as, unwinding, internal and rewinding zones as shown in Fig. 1.1. It is important to independently control each zone because each zone is unique. In addition, it is possible to have multiple zones of each type. Because of independent control of the tension, tension in each zone may differ from each other. The amount of torque required to produce the desired level of web tension is equal to the measured tension in the web times the radius of the roll. As the diameter of the unwinding section decreases linearly, the driving torque of the unwinding shaft must also decrease linearly throughout the process to provide constant tension to web. In contrast, the diameter of the rewinding roll increases linearly throughout the process, therefore the driving torque in the rewinding shaft must increase linearly to provide constant web tension. The web tension in these two zones (rewinding & unwinding) behaves dynamically. Both in the rewinding and unwinding zones, the diameter of the roll changes constantly. Therefore, to achieve constant web tension, the driving torque and speed must be adjusted to counter the diameter change. In internal zones, both speed and web tension remain stable as the diameter of the roll remains constant throughout the machine run. However, some kind of control is also required in the internal zones to sustain the desired level of web tension. Tension in the internal zones can be affected by problems like splices, defects in the web, reference machine speed and defects in the machine.

The simplest way to control the web tension is manually. Manual control can be applied in all of the tension zones. As there is no feedback response involved the manual control method is the least reliable. The diameter control method is also used for controlling the web tension. This method is very useful in the unwinding tension zone, as well as in the rewinding zone. As the basic principle involved in this method is to generate a driving

torque in response to the increasing and decreasing diameter in the rewinding and unwinding zone respectively, it cannot be used for the internal zone.

There are also tension control techniques which are based on the tension measurement. The load cell and the dancer roll are two types of this control technique. Both types are closed loop control methods. The basic control principle involved in these methods is to generate a control signal in response to the measured tension in the web. In dancer roll and load cell methods, compensation for changes in the tension because of the diameter change are made. Also, web tension changes due to the mechanical losses, bearing imperfection and other forces on the machine are also compensated for in this technique. As the tension measurement control techniques are closed loop and the drive signals are generated in response to the actual web tension, this control technique can be applied to all three web tension zones.

Process performance relies heavily on vibration control. Vibration can be controlled by either active vibration control methods or passive vibration control methods. In passive vibration control method, the focus is to introduce modifications into the original design of the system to optimize damping and stiffness in order to minimize the fluctuations in the system. In active vibration control strategy, the system parameters are measured through external sensors and the driving forces required to counter the vibration are generated through actuators.

Numerous control strategies have been developed such as, active and passive vibration control. Based on the theories and concepts involved in these methods several active and passive vibration control techniques have been developed over the years for axially moving materials.

1.1.2 Axially Moving Webs

An important factor that influences the quality of the web processing is mechanical vibration that can naturally arise as an unavoidable phenomenon in the system's dynamics. Mechanical vibrations in R2R systems can originate at the rolls if their round shape is distorted, or they are out of balance, misaligned, or if they accelerate, decelerate or stop. Web vibrations can also be caused by an intermittent processing style that typically characterizes material deposition, ink printing, and physical and chemical curing. The present work is motivated by the dynamic and vibration control problem in R2R systems such as, (i) Plasma coating and Nano-Imprinting, shown in Fig. 1.6, (ii) R2R Pattering, shown in Fig. 1.7, and (iii) Integrated Chemical Vapor Deposition (CVD) and Microcontact Printing, shown in Fig. 1.8.

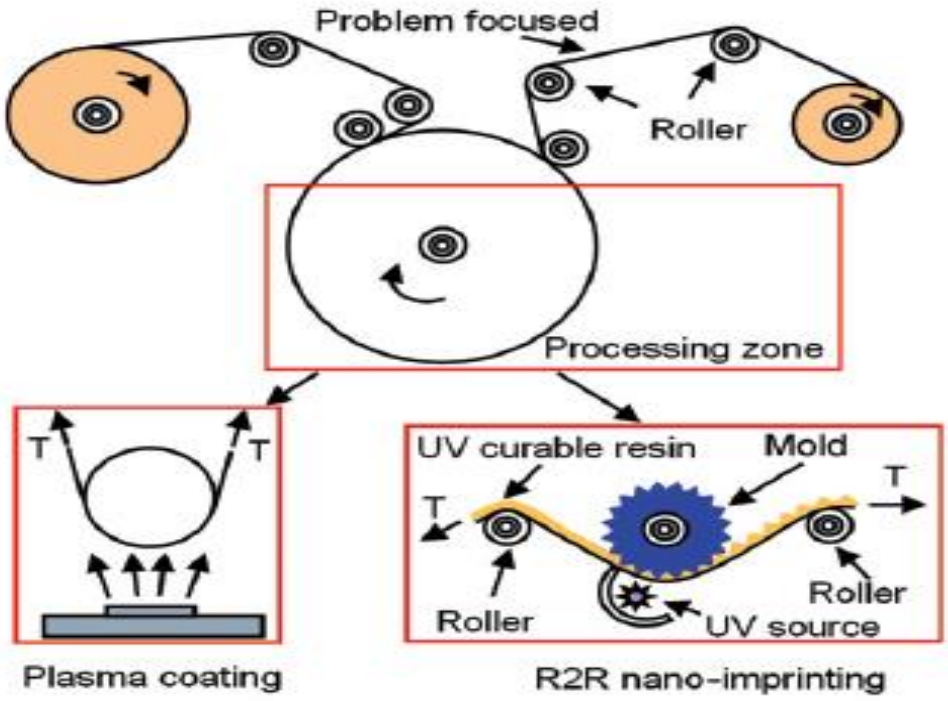

Figure 1.6 Schematic of an R2R process and its possible applications [7]

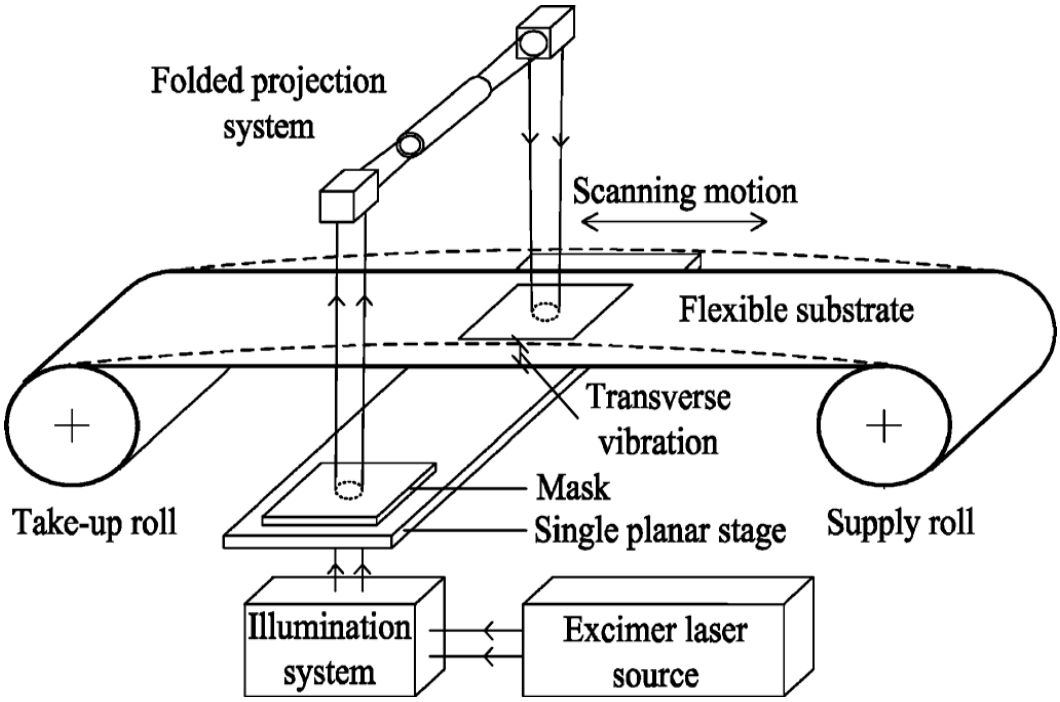

Figure 1.7 Example of large-area high-throughput roll-to-roll patterning systems [8]

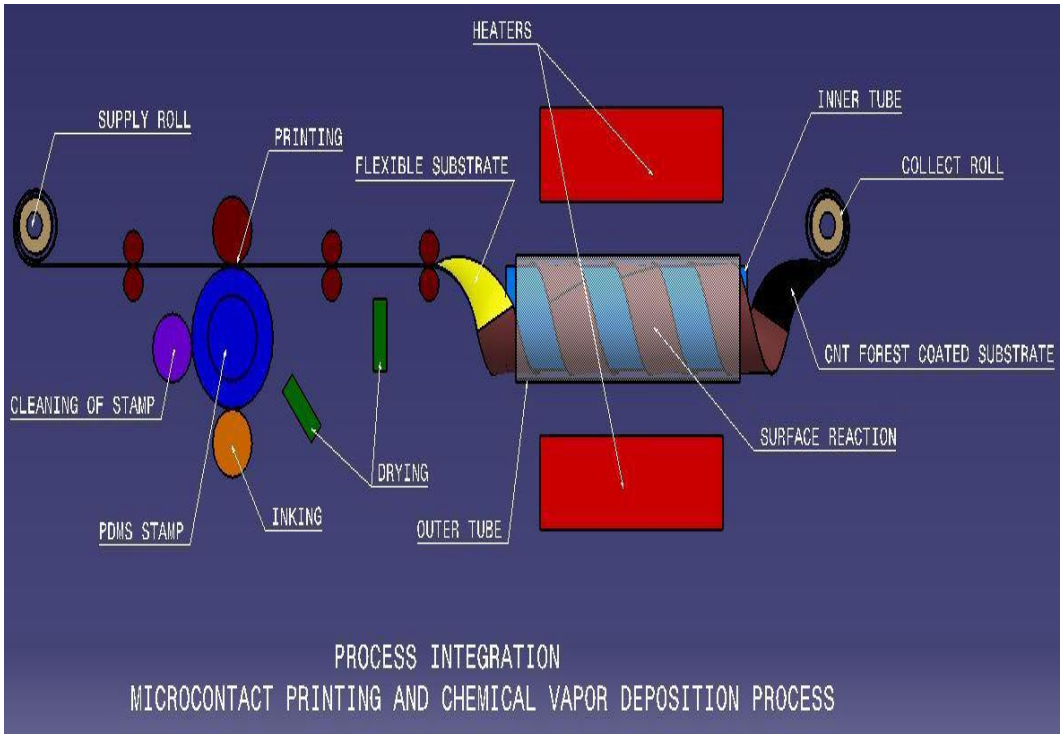

Figure 1.8 Schematic of process integration (CVD & µCP) [9]

(i) The continuous type plasma deposition process enables the deposition of a thin coating on all kinds of substrates which use electrical monomer discharges [10-11]. One major concern about this R2R process is the influence of geometrical errors in the R2R processing equipment. The misalignment of rolls, lateral disturbances, inaccurate speed and tension control, and a non-uniform web, can cause additional lateral dynamics of the web in the cross-machine direction [12]. (ii) In a roll-to-roll patterning system, axially moving flexible web (substrate) is fed from unwinding roll, passes through the contact region on the scanning stage, and is taken-up by the rewinding roll. In the event of external disturbance, residual transverse vibrations arise. Therefore, the printing process has to be stopped until the flexible substrate reaches an acceptable, negligible transverse fluctuation level [13]. (iii) Chemical vapor deposition (CVD) is a chemical process that has enabled low-cost and scalable synthesis of vertically aligned carbon nanotube forests. The roll-to-roll (R2R) CVD process is used to ensure continuous synthesis of CNTs. Whereas micro contact printing is a technique to fabricate patterns onto a substrate at both micro and nano scales. To achieve maximum productivity and quality an integrated system is proposed. This is a continuous process in which metal particle ink will be transferred onto the metal substrate using a stamping process. Once the catalyst is transferred onto the flexible substrate, it goes through the drying process and the metal strip is treated using the CVD process in a controlled atmosphere. The desired patterned carbon nanotube growth is achieved on the metal substrate and the final product is collected on the end roll [9]. The above proposed model has challenges that need to be addressed before it could be used on an industrial scale for large-scale manufacturing. The first major challenge is the fact that the process rates of the micro-contact printing process and the chemical vapor deposition process are

very different. The second major challenge is to reduce the degree of vibration in axially moving material.

The introduction of lithographic processes into R2R manufacturing schemes is an emerging technology for making flexible electronic devices in mass quantities. The recent trend towards micro patterning of thin film webs has enabled stricter manufacturing tolerances than the traditionally admissible vibration levels. Browsing the literature on the study of web vibrations, one can note that the problem has been treated in the context of axially moving material that is isolated from roll dynamics. This idealization has led to assuming "artificial" web tension and web speed profiles. In several cases, the ideal conditions of constant tension and constant speed have been assumed. In other cases, constant tension / variable speed or variable speed / constant tension were unjustifiably proposed.

1.2 Research Objectives

This thesis aims at developing a model for the dynamics of roll-to-roll systems designed for usage in microcontact printing. The focus is placed on transverse vibrations of axially moving webs, which travel between supporting rolls. The objectives of the dissertation are outlined as follows:

1. Using a string-based mathematical model for understanding web vibration characteristics.
2. Conducting experiments on the vibration of axially moving web to decide which structural element is the appropriate one for the analysis.

3. Development of roll-to-roll dynamic models for single span and multi span roll-to-roll systems. Analyzing the influence of a system's geometrical parameters on the roll-to-roll dynamics.
4. Studying the mutual influence of transverse vibration on the dynamics of roll-to-roll systems. Thus, establishing a coupled system of differential equations relating roll motion, web axial movement, and web transverse vibration.
5. Solving obtained coupled model in (4) numerically.
6. Developing a control methodology for mitigating transverse vibration of axially moving webs.

1.3 Dissertation Organization

We studied a part of the web travelling between the two supports. A web dynamic model for the web, which was based on a string like model, was developed before developing the roll-to-roll dynamic model. The developed web dynamic model was verified experimentally at the Manufacturing and Productivity Lab at MIT. The web dynamic model and roll-to-roll dynamic model were then coupled. At the end, using the coupled dynamic model of roll-to-system, a vibration suppression method was proposed for the vibration mitigation of the axially moving web. The details in every chapter of the dissertation are given below.

- **Chapter 1: Introduction:** This chapter provides an introduction to the research topic investigated in this dissertation.

- **Chapter 2: Literature review:** This chapter discusses the literature related to the dynamic of the axially moving materials and their transverse vibration suppression techniques.
- **Chapter 3: Web Vibration in a Single-Span Roll-to-Roll System:** In this chapter, the transverse vibration of an axially moving web and the dynamic behavior of a single-span roll-to-roll system is studied by considering the rotational motion of the rolls and the web velocity-tension coupling. The axially moving web is modeled as a string like model, which is mathematically represented by the hyperbolic partial differential equation (HPDE). The finite difference scheme, along with the state space technique, is used to transform the second-order HPDE into second-order ordinary differential equations (ODEs). To see the effect of the transport velocity on the vibration of the string-like model, dynamic responses at different axial velocities are compared. The effect of the external disturbance frequency on the dynamic response is investigated. Increasing the axial speed of the web decreases the response frequencies of the system, while decreasing the web speed increases them. The roll-to-roll dynamics is described by non-linear coupled first-order ordinary differential equations. It is found that the web-transmitted tension undergoes a short transient phase followed by a smooth nonlinear variation in the time. While transferring a certain amount of web material from the unwinding roll to the rewinding roll, the angular speed of both rolls varied nonlinearly. In case of varying web axial speed and the web-transmitted tension, based on the R2R system's dynamics, the transverse vibration of the axially moving web between the rolls is found to be non-periodic, with a higher frequency response to rapid changes

in the web axial speed and a lower frequency response to slow changes in the web axial speed.

- **Chapter 4: Web Vibration of Two-Span Roll-to-Roll System:** In this chapter, the transverse vibration of an axially moving web and the dynamic behavior of two-span roll-to-roll system is studied by considering the rotational motion of the rolls and the web velocity-tension coupling. The roll-to-roll dynamics is described by non-linear coupled first-order ordinary differential equations. It is found that the web-transmitted tension undergoes a short transient phase followed by a smooth nonlinear variation in the time. The effect of system geometrical parameters such as the length of the web, the inertia of the idler roll and the radius of the rewinding / unwinding roll on the angular speed and web transmitted tension have been studied.
- **Chapter 5: Multi-Span Roll-to-Roll Printing System:** In this chapter dynamic modelling of a multi-span roll-to-roll microcontact printing machine have been studied. Also details of the experiments performed at the Laboratory of Manufacturing and Productivity (MIT) to validate the web dynamic model is presented. Experiments are performed at different axial speeds of the web and at various web tensions.
- **Chapter 6: Web Vibration Suppression:** In this chapter, based on the developed coupled dynamic model of web, a web vibration methodology is proposed. Numerical results demonstrate that introducing a suitable boundary condition and control torques will cause the vibrational energy to dissipate and prevent the string from excessive vibrations. The effect of dimensionless speed shows a significant

decrease in the amplitude and the reduction is even more prominent as the dimensionless speed is increased. Numerical simulations are also backed by experiments.

- **Chapter 7: Conclusions and Recommendations:** Final concluding remarks are presented and further recommendations are suggested for possible future work in this chapter.

CHAPTER 2

LITERATURE REVIEW

In this section, previous studies focusing on roll-to-roll (R2R) web processing for high rate automated production are summarized. In covering the research, studies on axially moving materials and their vibration control are considered.

2.1 Literature Review

Micro contact printing is a technique developed by Xia and Whitesides [14-16] that uses small features on an "stamp" to transfer micron pattern to a substrate. When printing at micron level, the motion of the substrate (flexible web) is very important, and small fluctuations can result in low quality printing and in-process measurement problems [17-21]. Web tension regulation in roll-to-roll systems was considered for the first time in [22] and subsequently in [23-25]. The R2R dynamics model is based on the laws of physics: (i) Hooke's law allows for web elasticity, (ii) Coulomb's law explains the contact between the web and the roll, including friction, (iii) The mass conservation law allows for the coupling between the speed and the tension of the web, and (iv) The second fundamental relation of dynamics accounts for variations in the rotating speeds [26]. Many researchers over the years have applied this approach to develop the web tension-velocity model in a roll-to-roll system, [27-35].

2.1.1 Vibration of Axially Moving Webs

Because of their importance in the industrial processing of thin materials, axially moving webs are located at the heart of web dynamics studies. Axially moving webs are modeled as a string like system, a beam like system, a membrane like system and as a plate like system.

Researchers have been investigating the problem of the vibration of axially moving strings since the 1950s [36-38]. Since then, the subject has been under increasing investigation [39]. In all the published literature so far, one can observe that webs are modeled as either elastic or viscoelastic axially moving strings between the simply supported ends. To achieve a good understanding of what has been done so far, the published studies can be classified into five categories:

(i) Papers concerned with the vibrations of axially moving strings with constant axial velocity and constant transmitted tension [36-44], where special attention was placed on critical speeds and instabilities. The linear transverse vibration of an axially travelling string was studied in [36-38]. In the studies by Ulsoy and Mote [39] and Wickert and Mote [40], the out of plane dynamic axial characteristics of the travelling materials were investigated with the help of the string model and the stability of the systems was investigated by eigen frequency analyses. The effect of the longitudinal disturbance in the supports on the transverse vibration was investigated by Horssen [42]. Horssen and Ponomareva [43] used the Laplace transform technique to get the response for the transverse vibration in an axially moving string. It was shown by Wang et al. [44], that by applying Hamiltonian dynamics, transverse vibration can be studied by using the eigen value analysis.

(ii) Papers focusing on nonlinear oscillations of axially moving strings with constant axial velocity and varying transmitted tension [45-47]. Nonlinear stability of an axially moving string under parametric excitations were analyzed in [45]. Chen and Zhao [46] proposed a numerical algorithm for an axially moving viscoelastic string having varying axial tension. The non-linear transverse response for an axially moving string was investigated by Ghayesh and Mordian [47]. The Kelvin-Voight model was used for the viscoelastic elastic string under periodically varying tension.

(iii) Papers analyzing the periodic, quasi-periodic, chaotic, and transient motions of axially moving strings with axial acceleration and constant transmitted tension [48-49] were studied. Glerikin's method was applied by Chen and Zhao [48] to develop a differential-integral numerical approach for the out of plan dynamics of an accelerating string. The equation of motion was derived in two descriptions (Eulerian and Lagrangian) for an axially accelerating string by Zwier and Braun [49].

(iv) Papers presenting parametrically excited nonlinear responses of axially moving strings with harmonically-varying axial velocity and constant transmitted tension [50-54]. The effects of parameters such as mean web velocity, web stiffness and damping coefficients, and a middle support on frequency response curves and bifurcation points, were investigated. Fung et al. [50] discussed the dynamic behavior of an accelerating viscoelastic string. The finite element approach was used to solve the non-linear differential equations of motion. Shortly afterwards, the nonlinear problem of the transverse vibrations of a viscoelastic axially travelling string with variable speed under a uniform state of stress was studied by the same authors [51]. The non-linear transverse vibration of an axially accelerating string having geometric non-linearity was investigated by Chung et al. [54].

(v) Papers investigating the vibrations and instabilities in axially moving strings with axial acceleration and varying web-transmitted tension [55-57] were studied. The outcomes of these studies were quite valuable for analyzing the motion of axially moving strings in applications related to band and chain saws, power transmission belts and chains, and other devices involving pulley-supported conveyors.

Chen et al. [60] investigated the axially accelerating string to perform the chaotic-dynamics under the geometric nonlinearities. Through numerical solutions, chaotic behavior was presented by using the Poincare maps. For a multi-spring supported string, Yurddas et al. [61] performed a non-linear dynamic analysis. A stability analysis was performed using the method of multiple scales under non-ideal boundary conditions.

Like axially moving strings, axially moving beams constitute a very important field which contributes towards an understanding of nonlinear vibration in axially moving materials. Initially, researchers were only inspired by the band saw operation to investigate the axially moving beam [63]. In wood cutting or metal cutting operations using a band saw, the saw blade is under the influence of edge forces. Because of edge loading, torsional, as well as transverse vibration of the saw blade is generated which can cause the blade buckling. Torsional vibrations under the influence of an edge loaded force in an axially moving beam were investigated and the dependence of the frequency of the torsional vibration and edge loading was shown in [63]. However, later in [64] it was observed that ignoring the coupling between the transverse and the torsional vibration of a beam leads to a significant error. Analyzing the axially moving beam as an uncoupled system results in overestimated critical buckling load values, which in turns undermine the system stability. In first attempt to study the axially moving beam [63], the transverse oscillation in a Bernoulli beam was

investigated. Simpson [65-66] for the first time generated the equations of motion for an axially moving Timoshenko beam. Both the Timoshenko beam and the Bernoulli beam were compared, and the comparison showed that a good convergence exists, but only for lower speeds. The Timoshenko beam model shows a lower critical speed value as compared with the Bernoulli beam model.

An attempt to calculate the fundamental frequency of oscillation was made by Mote [67]. Hamilton's principle was used by Wickert [41] to derive the equation for both transverse and longitudinal motion. Modal analysis and the Green function method were used to study the dynamic characteristics of axially moving beam.

Behdinan and Tabarrok [68] used the Glerikin method to study the non-linear vibration of sliding beams. Lee et al. [69] used the exact dynamic stiffness matrix approach to formulate the axially moving beam under the application of a uniformly distributed tensile load. Lee and Hyungmi [70] studied a viscoelastic beam under uniform axial tension and developed a spectral element model for the stability and dynamic analysis. Cepon and Boltezar [71] solved the problem of pre-tensioned axially moving beams by applying the Glerikin finite-element method. It was shown that, at higher axial speeds, the Glerikin method poorly predicts the transverse response. Yang et al. [72] proposed an approximated solution for an axially moving viscoelastic beam under the application of multi-frequency excitation. Comparison showed that the approximated solution agrees with the numerical approach. For the dynamic analysis of an axially moving elastic beam, Wang et al. [73] introduced a radial basis collocation method. Numerical examples revealed the effectiveness of the developed method. A generalized integral transform technique (GITT) was developed by Chen and Jian [74] to study the out of plan vibration of an axially moving beam. For

dynamic analysis of pipes used to convey fluid, Zang et al. [75] developed a new semi-analytical method, called the differential transformation method (DTM). High accuracy with reduced computational time was shown by the DTM. Chen and Jian [76] used the generalized integral transform technique (GITT) for the forced vibration of an axially moving Timoshenko beam.

As the variation in the transport speed directly contributes to the system instability, Oz and Pakdemirli [77] studied the axially moving beam with harmonically varying speeds. Perturbation analysis was used to solve the equation of motion. It was found that the instability occurred, when the fluctuation in axial speed becomes equal to twice the fundamental frequency of the transverse vibration of the beam moving at a constant velocity. Shin and Fong [78] studied the dynamic stability of a harmonically moving beam. Using the Glerilkin method, it was shown through numerical results that the dynamic stability is directly influenced by the frequency of axial speed fluctuation. In a similar approach, Chen et al. [79-80] studied the dynamic stability of a pre-tensioned viscoelastic accelerating beam. The effect of beam material viscosity, transport speed variation and applied axial tension on the dynamic stability was demonstrated through numerical examples.

Non-linear free transverse vibration of an axially moving beam under non-uniform tension was studied by Chen and Yang [81]. Using the integro-partial-differential equation and the multiple scale method, different modes of free non-linear vibration of the axially moving beam under the non-uniform axial tensile load were calculated. The Timoshenko beam theory was used by Sui et al. [82] to investigate the dynamic characteristic of an axially

moving beam having variable axial tension comprised of functionally graded material. Natural frequencies and mode shapes were calculated using the complex mode approach.

It was shown by Haiwei et al. [83] that for an axially accelerating sandwich beam with harmonic axial tension, amplitude of the transverse vibration can be controlled by selecting an appropriate value for the initially applied tension. Qaio et al. [84] showed the transverse vibration of a cantilever beam connected with an axial base. The effect of axial speed on the dynamic stability was presented in detail. The effect of thermal heating on the dynamic response of a microbeam was thoroughly investigated by Ashraf et al. [85]. The ramp-type thermal heating effect on the strain energy density and dimensionless speed was discussed. A three-dimension numerical analysis of the thermo-mechanical dynamics of an axially moving beam was studied by Ghayesh and Farokhi [86]. Stability analysis was performed using the Glerikin approach. Mingwu et al. [87] had shown that for an underwater beam, where the transport speed exceeds the critical limit, buckling-instability will result.

As discussed so far, to make things simpler string theory, as well as beam theory, was used in various studies to avoid complexity in the mathematical formulation for two-dimensional axially moving systems. In many situations, this simplification can show acceptable results, but it still cannot be applied in many cases. In situations, where the load distribution changes along the width, or when the properties of the plate material are orthotropic, or the intermediate supports or composite plates are under consideration, one-dimensional linear string or beam theory is not applicable. To get reliable results all such cases call for the application of two-dimensional plate theory.

The first study to investigate the dynamic response of a band saw using two-dimensional plate theory was conducted by Ulsoy and Mote [88]. Governing equations were derived in

the form of partial differential equations and the Ritz method was used to discretize them. A mathematical model for an axially moving isotropic web using two-dimensional (2D) plate theory was developed by Lin and Mote [89]. The mathematical model was derived in the form of nonlinear partial differential equations.

For an axially travelling plate under the action of in-plan force and acceleration, dynamic stability was studied in [90]. The complexity of the mathematical formulation caused many researchers to apply the finite element method to study its dynamics. Wang in [91] developed a finite element description using the Mindlin–Reissner plate theory for an axially travelling plate. It was observed that, in addition to the critical web speed, the normal and shear stresses in the plate can be determined using the finite element approach. In-plane vibration of an axially moving plate was studied using the Rayleigh-Ritz method in [92]. Hatamai et al. [93] thoroughly studied the free transverse vibration of an axially moving plate in the context of the viscoelastic parameters, axial speed and external disturbances. Using Newton's second law, the equation of motion for the transverse displacement of an axially moving viscoelastic plate was derived by Yang et al. [94]. The instability and divergence of the system were studied using the finite difference method. It was shown that increasing the axial speed and decreasing the material viscosity will cause system instability.

The study of the vibration of an axially moving membrane is vital to ensure that the full spectrum of axially moving materials is covered. A numerical study on the dynamics of an axially moving membrane was performed by Koivurova and Pramila [95]. To add the effect of membrane viscosity, the finite strain model was used. The effect of the translating speed was investigated, along with the geometric non-linearity. Shin et al. [96] studied the effect

of axial transport speed on the in-plane dynamic response. Discretization of the equation of motion was done using Glerikin's approach. Results showed that the axial transport speed and the aspect ratio of the membrane significantly affect the in-plan dynamics of the membrane. After a short while, Shin et al. [97-98] investigated the dynamics of transverse vibration of an axially moving membrane.

A numerical investigation on the dynamics of an axially moving membrane was presented by Saksa et al. [99]. Modal analysis was used to study the dynamic and stability analysis of a moving panel. Through numerical results the effect of viscosity on the stability and critical axial speed of the moving panel was discussed. It was shown that low viscosity will cause divergent instability and, at higher viscosities, the magnitude of the critical speed is increased. The Laplace transform method was applied to study and determine both the dynamic and stability characteristics of an axially moving membrane by Wu et al. [100]. It was shown that increasing the axial tension of membrane, will increase the natural frequencies of vibration. Glerikin's meshless method was proposed to study the out-of-plane vibration of an axially moving membrane by Wu et al. [101].

2.1.2 Vibration Control of Axially Moving Webs

Many researchers have focused on finding a solution for the problem of web vibration by means of isolation. To achieve a good understanding of what have been done so far, published studies can be classified into two categories: (i) Studies focused on the passive vibration suppression by optimizing damping/stiffness in order to minimize the vibration amplitude, e.g., [102-109]. For an axially moving string, a vibration suppression technique by utilizing a hydraulic roll was presented in [102]. It was shown in [103] that that the

string displacement is bounded when a bounded distributed force is applied to it transversally. A passive nonlinear targeted energy transfer technique was demonstrated by Viguie et al. [104] to suppress the vibration. Foda [105] achieved vibration dissipation by placing some passive elements and actuators at selected positions along the string length. Nonlinear targeted energy transfer (TET) is applied to suppress the excessive vibration of an axially moving string with transverse wind loads [106]. A nonlinear energy sink (NES) was attached to the string to absorb vibrational energy. It was shown in [107] that by applying a distributed force vibration suppression can be achieved in a fast manner. Zhao et al. [108] developed a vibration suppression strategy via constructing a Lyapunov function to asymptotically stabilizes the string. Viscoelastic boundary control approach was utilized to suppress the transverse vibration in axially moving webs [109].

(ii) Papers adopting active vibration techniques to precisely tuning time varying conditions at high moving speeds, e.g., [110-119]. Sensors and actuators were applied along the length of an axially travelling string with the objective to avoid excessive transverse vibration in [110]. For an axially moving string, a vibration suppression technique based on the wave absorption or impedance matching through actuators and sensors placed on the web span was presented by Lin and Hu [111]. In an attempt to minimize the amplitude of transverse vibration in an axially moving string, actuators were installed at the web upstream and web downstream as controlling force generators [112]. Li et al. [113] introduced an active pivoting roll that adaptively decouples adjacent spans, thereby isolating a controlled span from bounded disturbances in an adjacent uncontrolled span. The proposed method in [113] was further verified experimentally. Web speed tracking and transverse vibration control was achieved by installing force actuators in web domain through a mechanical guide and

regulating the applied torques at the web boundaries in [114]. Yang et al. [115] proposed a control scheme for an axially moving string under the varying applied axial tension. A hydraulic actuator was used to divide the string into two spans, a controlled and uncontrolled span. Kim et al. [116] presented the transverse vibration control of an axially moving pre-tensioned string by introducing an electro-hydraulic. A tensioner was used as an actuator to design an adaptive controller for the vibration of an axially moving string by Chen and Zhang [117]. The Lyapunov analysis was used to derived the control law. An adaptive boundary control was developed for vibration suppression of an axially moving accelerated/decelerated belt system [118]. By utilizing Lyapunov-based back stepping method, a boundary control was proposed for vibration suppression of belt system. A disturbance observer is proposed to attenuate the effects of unknown boundary disturbance of axially moving belt system in [119].

R2R-based manufacturing is an efficient method for the achievement of high volume production. R2R manufacturing is a mature technology and has been applied to web printing in paper machines, textile fabrics, and film processors to make production cheaper in a short time. Recently, continuous R2R manufacturing enabled processes for patterning, coating, cutting, and linking different layers of flexible printed electronics at high speed and low cost have been proposed. When combined with the emerging microcontact printing (μCP) technology, R2R manufacturing is believed to have a broad impact on large-scale production. During the high-speed R2R unwinding / rewinding processes, it is critical to maintain the web tension within desired values. When employing soft lithography to print micro-features on a web, a small vibration can cause undesirable fluctuations and a precise

account for the dynamic behavior becomes vital for allowing sufficient control authority and ensuring product quality.

In light of the fact that a significant number of engineering applications involving axially moving strings occur in unwinding / rewinding (roll-to-roll, or R2R) systems, the authors feel that formulations that model the problem of an axially moving web in isolation from the roll dynamics limit the model utility. In this study, it is intended to rigorously consider the coupling between the roll-to-roll dynamics and the transverse vibration of the web between the rolls. In addition, one does not need to assume simply supported boundary conditions for the vibration problem since the unwinding and rewinding rolls enter the analysis as part of the overall model. This comprehensive approach couples the physics-based variations of axial web tension with angular roll velocities to the web vibration-imposed fluctuations. In order to study the coupled dynamics, the motion of the vibrating web while transferring from the unwinding roll to the rewinding roll is analyzed.

CHAPTER 3

WEB VIBRATION IN A SINGLE-SPAN ROLL-TO-ROLL SYTEM

3.1 Roll-to-Roll Dynamics

The simplest R2R system is that having two rolls with outer radii R_1 and R_2, and a single span web which has an under tension deformed length L as shown in Fig. 3.1.

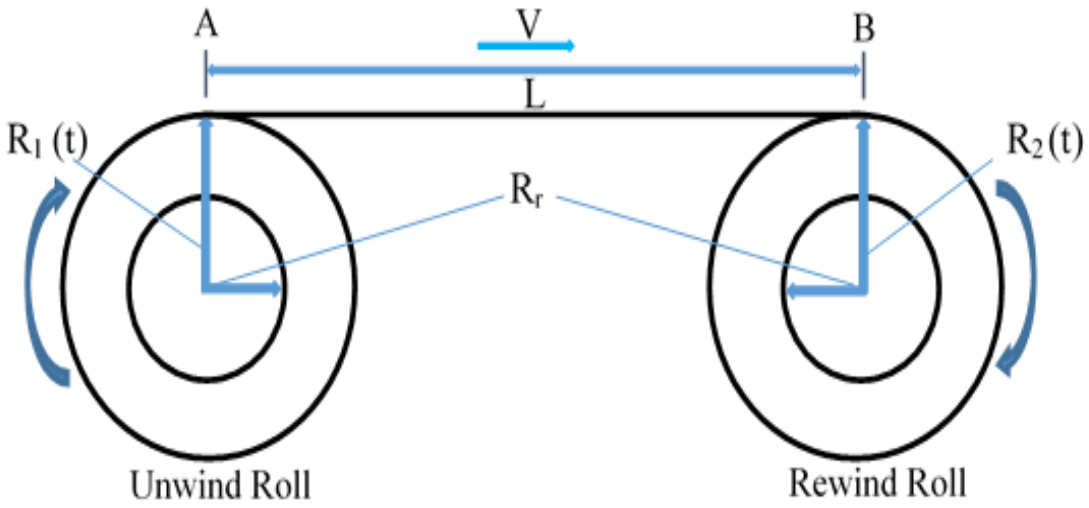

Figure 3.1 One Span R2R System

To study the dynamic behavior of this system, one needs to consider the rotational motion of the rolls and the web velocity-tension coupling.

3.1.1 Web Tension Velocity Relationship

To derive the mathematical equation for web tension, Hook' law, Coulomb's law and law of mass conservation are utilized. Assuming small width of the web in comparison to its length and considering small bending stiffness with no slip condition at the boundaries (rolls), let us consider the web span between points A and B as shown in Fig. 3.1. Then, Hooke's law can be written as

$$T = E\,A\,\frac{L - L_0}{L_0} \tag{3.1}$$

where T is the axial tension in the web, E is the modulus of elasticity of the elastic web, A is the cross-sectional area of the web, and L_0 is the un-deformed length. The conservation of mass requires that,

$$\rho AL = \rho_0 A L_0 \tag{3.2}$$

where ρ_0 and ρ are the web material density before and after deformation, respectively. If the deformed length of the web is assumed to be

$$L = L_0 + \varepsilon L_0 \tag{3.3}$$

where ε is elastic strain. Substituting equation (3.3) into equation (3.2) leads to,

$$\rho A\,(L_0 + \varepsilon L_0) = \rho_0 A L_0 \tag{3.4}$$

which is reduced to

$$\rho = \left(\frac{1}{1+\varepsilon}\right)\rho_0 \tag{3.5}$$

Substituting (3.5) into the continuity equation ($\frac{\partial \rho}{\partial t} + \frac{\partial(\rho V)}{\partial x} = 0$) and dividing the result by ρ_0 produces

$$\frac{\partial}{\partial t}\left(\frac{1}{1+\varepsilon}\right) = -\frac{\partial}{\partial x}\left(\frac{V}{1+\varepsilon}\right) \tag{3.6}$$

Integrating equation (3.6) over the web length specified from point A to point B (i.e., $\int_0^L \frac{\partial}{\partial t}\left(\frac{1}{1+\varepsilon}\right) dx = -\int_0^L \frac{\partial}{\partial x}\left(\frac{V}{1+\varepsilon}\right) dx$) leads to

$$\frac{\partial}{\partial t}\left[\left(\frac{x}{1+\varepsilon}\right)\right]_{x=0}^{x=L} = -\left[\left(\frac{V}{1+\varepsilon}\right)\right]_{x=0}^{x=L} \tag{3.7}$$

Defining

$$\left.\begin{array}{r} \varepsilon\,(0,t) = \varepsilon_1(t) \\ \varepsilon\,(L,t) = \varepsilon_2(t) \end{array}\right\} \tag{3.8}$$

$$\left.\begin{array}{r} V\,(0,t) = V_1(t) \\ V\,(L,t) = V_2(t) \end{array}\right\} \tag{3.9}$$

Transforms equation (3.7) into

$$\frac{\partial}{\partial t}\left[\frac{L}{1+\varepsilon_2}\right] = \left[\frac{V_1}{1+\varepsilon_1}\right] - \left[\frac{V_2}{1+\varepsilon_2}\right] \tag{3.10}$$

Differentiating the left-hand side of equation (3.10) with respect to time, and simplifying gives

$$(1+\varepsilon_2)(L\cdot) - L(\varepsilon_2\cdot) = V_1\left[\frac{(1+\varepsilon_2)^2}{1+\varepsilon_1}\right] - V_2(1+\varepsilon_2) \tag{3.11}$$

If the strains are assumed to be small (1.e., $\varepsilon_1(t) \ll 1$ & $\varepsilon_2(t) \ll 1$), then

$$\left.\begin{array}{r} \frac{1}{(1+\varepsilon_1)} \approx (1-\varepsilon_1) \\ (1+\varepsilon_2)^2 \approx (1+2\varepsilon_2) \end{array}\right\} \tag{3.12}$$

Which leads to

$$(1+\varepsilon_2)(L\cdot) - L(\varepsilon_2\cdot) \approx V_1(1-\varepsilon_1+2\varepsilon_2) - V_2(1+\varepsilon_2) \tag{3.13}$$

Knowing that $\varepsilon_1 = \frac{T_1}{EA}$ and $\varepsilon_2 = \frac{T_2}{EA}$, equation (3.13)

$$L\frac{dT_2}{dt} \approx EA\left(V_2 - V_1 + \frac{dL}{dt}\right) + T_1V_1 - T_2\left(2V_2 - V_1 - \frac{dL}{dt}\right) \tag{3.14}$$

Assuming the web to be inextensible ($\frac{dL}{dt} = 0$), then the web tension-velocity relationship becomes

$$L\frac{dT_2}{dt} \approx EA(V_2 - V_1) + T_1V_1 - T_2(2V_2 - V_1) \tag{3.15}$$

Knowing that $V_1 = R_1\ \Omega_1$ and $V_2 = R_2\ \Omega_2$, equation (3.15) can be written in terms of rolls angular velocities as

$$\frac{dT_2}{dt} \approx \left[\frac{R_1}{L_2}T_1 - \frac{2R_1}{L_2}T_2 - \frac{EAR_1}{L_2}\right]\Omega_1 + \left[\frac{R_2}{L_2}T_2 + \frac{EAR_2}{L_2}\right]\Omega_2 \tag{3.16}$$

3.1.2 Equation of Motion of the Roll

Let us then focus on the forces acting on a roll, one has to consider (i) the inertial torque, (ii) the torque caused by the web tension, (iii) the motor torque, and (iv) the friction torque, as shown in Fig. 3.2.

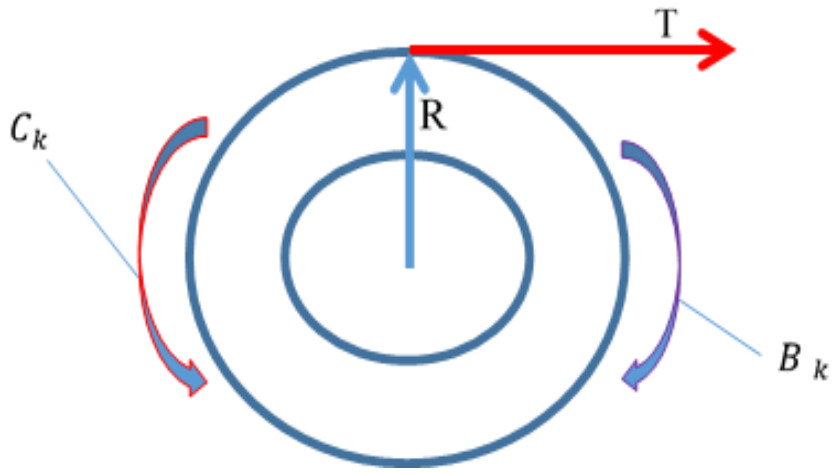

Figure 3.2 Free Body Diagram of the Roll (Torques acting on a roll)

Assuming slowly varying roll inertia and radii, the dynamic equilibrium equation of a roll can then be written as

$$\frac{d(J_k\,\Omega_k)}{dt} = R_k(t)(T_{k+1} - T_k) + B_k\Omega_k - C_k \tag{3.17}$$

where Ω_k is the rotational velocity of the roll "*k*", J_k is the rotational moment of inertia, B_k is the motor torque constant, and C_k is the torque due to friction. Using equation (3.17), equations of motion for individual rolls are given as

For first roll

$$\frac{\mathrm{d}}{\mathrm{d}t}(J_1 * \Omega_1) = R_1 * T_2 + B_1 * \Omega_1 - C_1 \tag{3.17a}$$

For second roll

$$\frac{\mathrm{d}}{\mathrm{d}t}(J_2 * \Omega_2) = -R_2 * T_3 + B_2 * \Omega_2 - C_2 \tag{3.17b}$$

The system of equations (3.16) and (3.17) consists of coupled equations that describe the R2R system's dynamics. These differential equations will be numerically solved to find the time-domain description of R2R system's motion.

3.1.3 Roll Radius and Moment of Inertia

In light of the fact that the unwinding roll radius decreases and the rewinding roll radius increases by the same amount at the same time, Equation (3.17) needs to be supplemented with the following equations:

$$R_1(t) = R_{01} - \frac{\theta_1}{2\pi}h \tag{3.18}$$

$$R_2(t) = R_{02} + \frac{\theta_2}{2\pi}h \tag{3.19}$$

where R_{01} and R_{02} are the initial radii of unwinding and rewinding rolls, respectively. h is the web thickness. θ_1 and θ_2 are the angular displacements of unwinding and rewinding rolls, respectively, as shown in Fig. 3.3. Note that in every turn, the radius of unwinding roll decreases by an amount that is equal to the thickness of the web and in the same time the radius of the rewinding roll increases by the same amount.

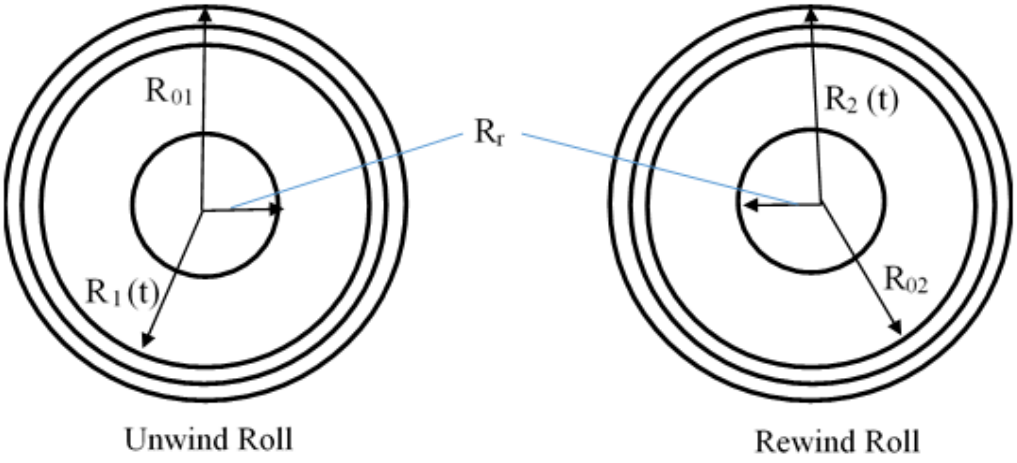

Figure 3.3 Geometry of unwinding and rewinding rolls

The time rates of change of angular displacements of the rolls are

$$\frac{d\theta_1}{dt} = \Omega_1 \tag{3.20}$$

$$\frac{d\theta_2}{dt} = \Omega_2 \tag{3.21}$$

Due to changing the radii of rolls with time, moments of inertia also change with time as

$$J_1(t) = J_r + J_{W1}(t) \tag{3.22}$$

$$J_2(t) = J_r + J_{W2}(t) \tag{3.23}$$

Where J_r is the moment of inertia of the roll material, $J_{W1}(t)$ is the moment of inertia of web material on unwinding roll and $J_{W2}(t)$ is the moment of inertia of web material on rewinding roll. Moment of inertia of the roll material is given by

$$J_r = \frac{1}{2} m_r R_r^2$$

Using,

$$m_r = \rho_r \pi R_r^2 W$$

Hence,

$$J_r = \frac{1}{2}\,\rho_r \pi R_r^4 W \tag{3.24}$$

where ρ_r is the density of roll, R_r is the radius of roll and W is the width of each roll's, as clarified in Fig. 3.3. For wrapped web material

$$J_{W1}(t) = \frac{1}{2}\,m_{w1}\,R_1^2 - \frac{1}{2}\,m_{w1}\,R_r^2$$

$$J_{W1}(t) = \frac{1}{2}\,\rho_w \pi R_1^2 W\,R_1^2 - \frac{1}{2}\,\rho_w \pi R_r^2 W\,R_r^2$$

$$J_{W1}(t) = \frac{1}{2}\pi W\,(\rho_w\,R_1^4 - \,\rho_w\,R_r^4) \tag{3.25}$$

Similarly,

$$J_{W2}(t) = \frac{1}{2}\pi W\,(\rho_w\,R_2^4 - \,\rho_w\,R_r^4) \tag{3.26}$$

Substituting equations (3.24) – (3.26) in equations (3.22) and (3.23) gives

$$J_1(t) = \frac{1}{2}\pi W\,[R_r^4(\rho_r - \,\rho_w) + \,\rho_w[R_1(t)]^4] \tag{3.27}$$

$$J_2(t) = \frac{1}{2}\pi W\,[R_r^4(\rho_r - \,\rho_w) + \,\rho_w[R_2(t)]^4] \tag{3.28}$$

Time derivatives of roll's moment of inertia can be calculated by differentiating the equations (3.27) and (3.28) and utilizing following equations:

$$\frac{\mathrm{d}\big(R_1(t)\big)}{\mathrm{d}t} = -\frac{\Omega_1}{2\pi}h \tag{3.29}$$

$$\frac{\mathrm{d}\big(R_2(t)\big)}{\mathrm{d}t} = \frac{\Omega_2}{2\pi}h \tag{3.30}$$

Hence,

$$\frac{\mathrm{d}(J_1(t))}{\mathrm{d}t} = -\rho_w * W * h\,[\,[R_1(t)]^3 * \Omega_1] \tag{3.31}$$

$$\frac{\mathrm{d}(J_2(t))}{\mathrm{d}t} = \rho_w * W * h\,[\,[R_2(t)]^3 * \Omega_2] \tag{3.32}$$

To this end, the tension-angular velocities equation (3.16) becomes

$$\frac{\mathrm{d}T}{\mathrm{d}t} = \frac{EA}{L}(R_2\ \Omega_2 - R_1\ \Omega_1) - \frac{1}{L}R_2\ \Omega_2\ T \tag{3.33}$$

where

$$\frac{\mathrm{d}\Omega_1}{\mathrm{d}t} = \frac{1}{\frac{1}{2}\pi W\,[R_r^4(\rho_r - \rho_w) + \rho_w R_1^4]}\Big[(R_1 T + B_1\Omega_1 - C_1) + \Omega_1\left(\rho_w * W * h\,\left(\left(R_1(t)\right)^3 * \Omega_1\right)\right)\Big] \tag{3.34}$$

$$\frac{\mathrm{d}\Omega_2}{\mathrm{d}t} = \frac{1}{\frac{1}{2}\pi W\,[R_r^4(\rho_r - \rho_w) + \rho_w R_2^4]}\Big[(-R_2 T + B_2\Omega_2 - C_2) + \Omega_2\left(\rho_w * W * h\,\left(\left(R_2(t)\right)^3 * \Omega_2\right)\right)\Big] \tag{3.35}$$

3.1.4 Numerical Solution of Roll-to-Roll Dynamics

A numerical simulation for describing the transfer of a certain amount of web material from the unwinding roll to the rewinding roll is performed. The variation of web axial velocity and transmitted tension with time are calculated, using the parameters presented in Table 3.1, [2].

A step input torque of 1.0 N.m is applied at both the unwinding and rewinding motors. Thus, the angular velocity and angular displacement of unwinding and rewinding rolls vary with time as shown in Figs. 3.4 and 3.5.

Table 3.1 Parameters of the roll-to-roll R2R System

S. No.	Parameter	Value
1	Density of Web Material	8190 kg/m^3
2	Density of the Roll Material	8050 kg/m^3
3	Thickness of the Web	0.000275 m
4	Width of the Web	0.1 m
5	Modulus of Elasticity of Web	117 GPa
6	Radius of the Roll (Both)	0.04 m
7	Initial Radius of Unwinding Roll	0.15 m
8	Initial Radius of Rewinding Roll	0.04 m
9	Frictional Torque at Unwinding Roll	0.004 N.m
10	Frictional Torque at Rewinding Roll	0.002 N.m

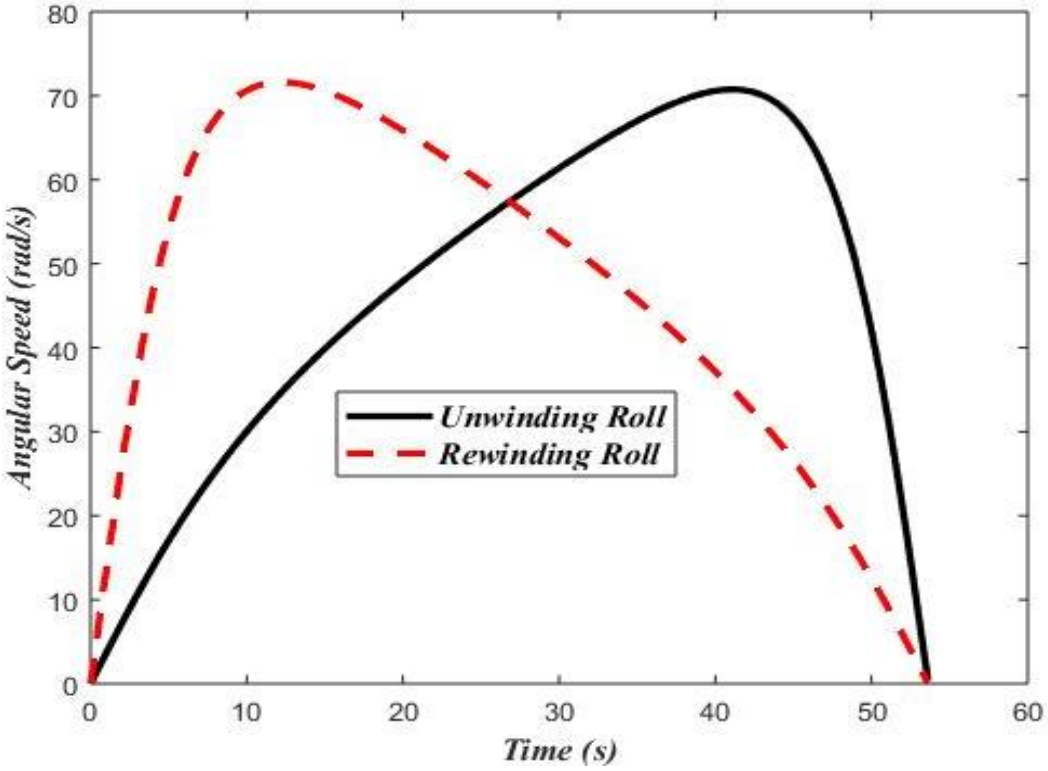

Figure 3.4 Angular speed variation of rolls

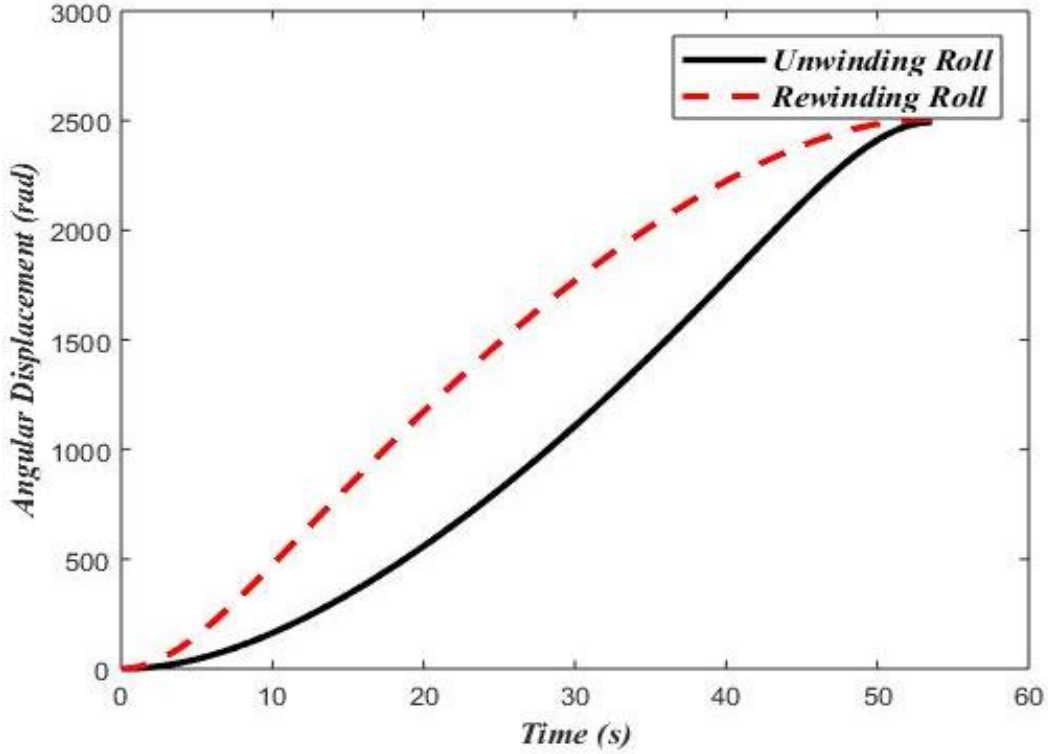

Figure 3.5 Angular displacement variation of rolls

In Fig. 3.4, angular velocity of the rewinding roll increases with a faster rate than the unwinding roll. This is because the rewinding roll has initially a lower moment of inertia than the unwinding roll. The opposite effect occurs after the two rolls reach the same angular velocity. In order to transfer the web material from the unwinding roll to the rewinding roll, both rolls attain same maximum angular displacement within the same time, as shown in Fig. 3.5.

The variation of the radii of unwinding and rewinding rolls with time is shown in Fig. 3.6. As it might be intuitively expected, the variations of the radii will be such that the unwinding roll radius shrinks to the value of the initial radius of the rewinding roll and the rewinding roll radius grows to the value of the initial radius of unwinding roll within the same time.

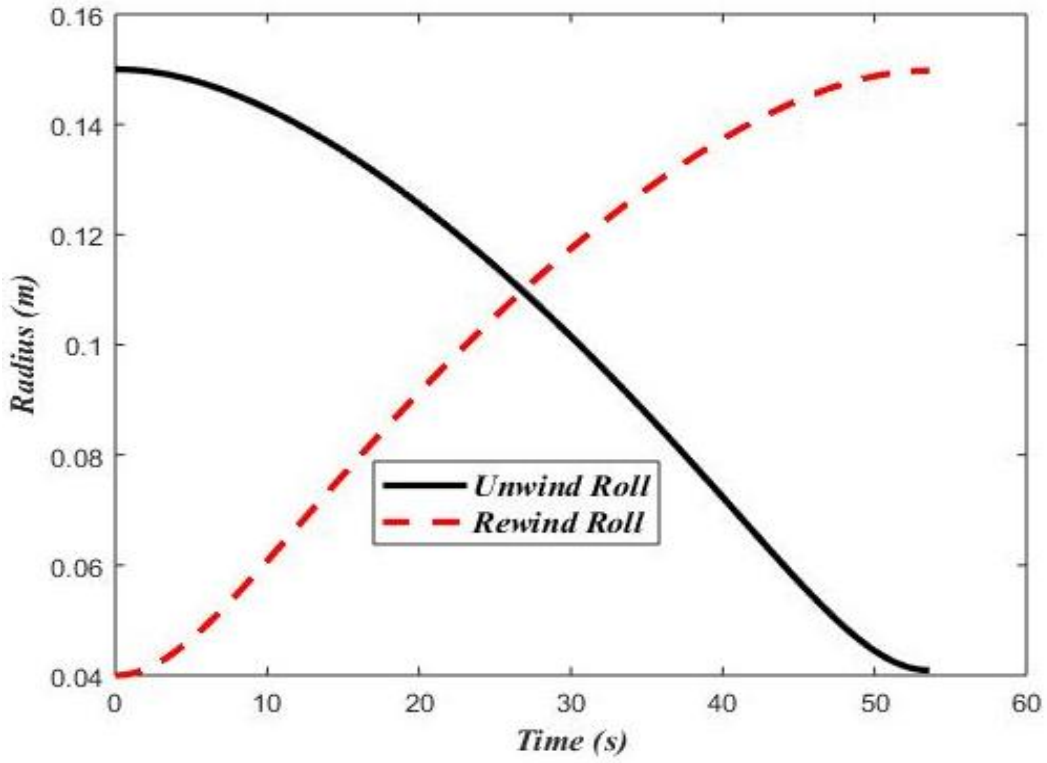

Figure 3.6 Radii variation of rolls with time

Axial velocity and tension in the web between the two rolls are shown in Figs. 3.7 and 3.8, respectively.

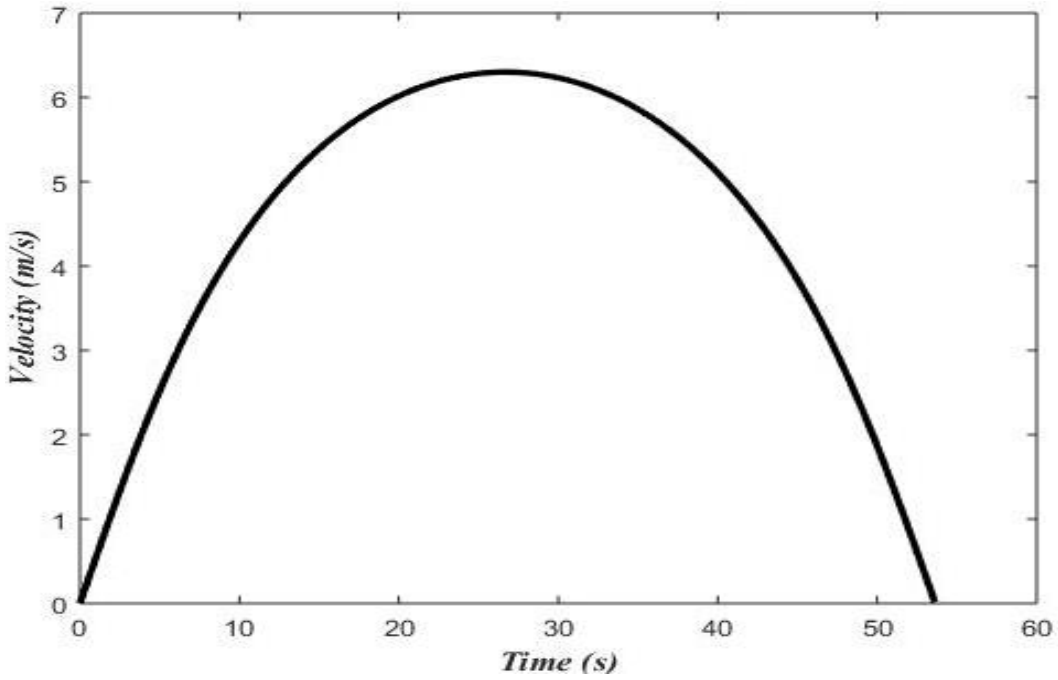

Figure 3.7 Axial web velocity variation with time

As a result of the input torques at the unwinding and rewinding rolls, the axial transport speed of the web starts from zero, reaches a maximum value, and decreases to reach zero by the end of material complete transfer from the unwinding roll to the rewinding roll.

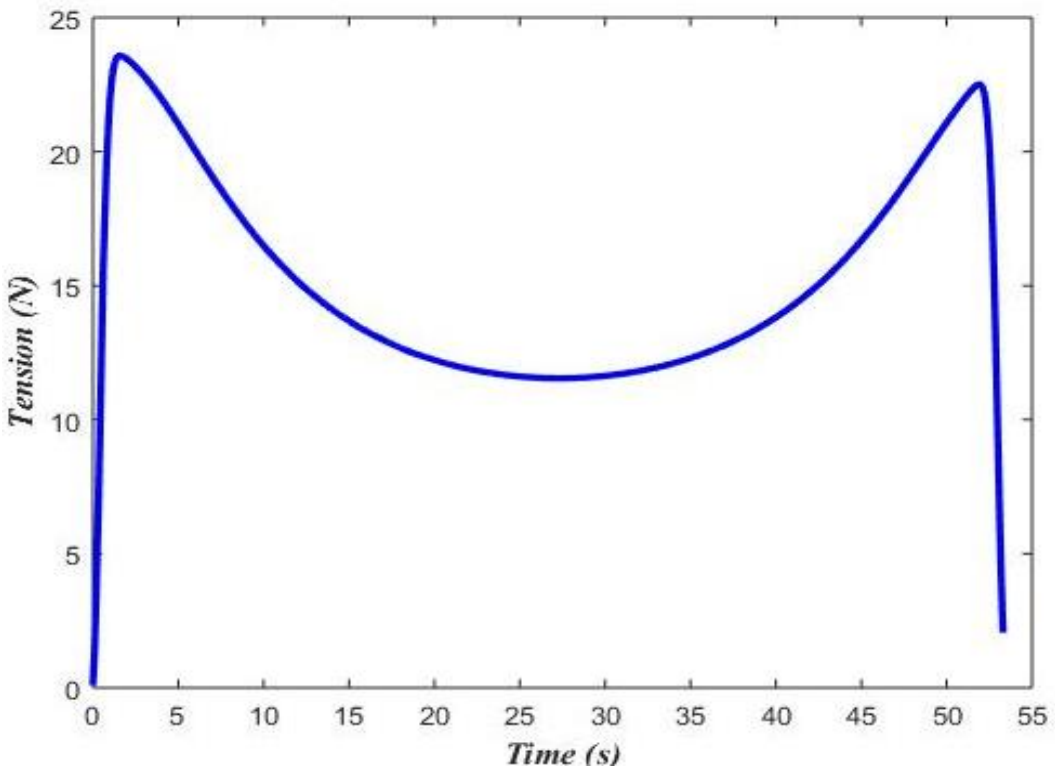

Figure 3.8 Web-transmitted tension variation with time

The variation of the tension transmitted in the web with time, shown in Fig. 3.8, starts with a sharp increase with time, and then becomes smooth and nonlinear before sharply decreasing at the end of material transfer period. For consistent production, an industrial process should not be implemented on the web during the transient phase.

3.2 Web Vibration Model

In many web processing cases, manufacturing steps are done in an intermittent fashion. Due to this the web vibrates while it is axially moving. Mechanical vibrations in R2R systems can originate at the rolls if their round shape is distorted, or they are out of balance, misaligned, or if they accelerate, decelerate or stop. Web vibrations can also be caused by an intermittent processing style that typically characterizes material deposition, ink printing, and physical and chemical curing. Webs are traditionally modeled as strings,

beams, or membranes. In the following, let us model the web as a string. Using the Hamilton's Principle was used to derive the equation of vibrational motion for a string travelling between two ends

$$\delta \int_{t1}^{t2} [\tau - (U + W^{NC})] dt = 0 \tag{3.36}$$

where τ is kinetic energy, U is potential energy and W^{NC} is work done by non-conservative forces in axially moving string representing an axially moving web.

Kinetic energy of the string is described as:

$$\tau = \int_0^l \frac{1}{2} (\rho A) v^2 dx = 0 \tag{3.37}$$

where ρ is the density and A is the area of string. Since the web is vibrating longitudinally and transversally while travelling axially, let us calculate the total velocity of the web. By considering the velocity diagram shown in Fig. 3.9.

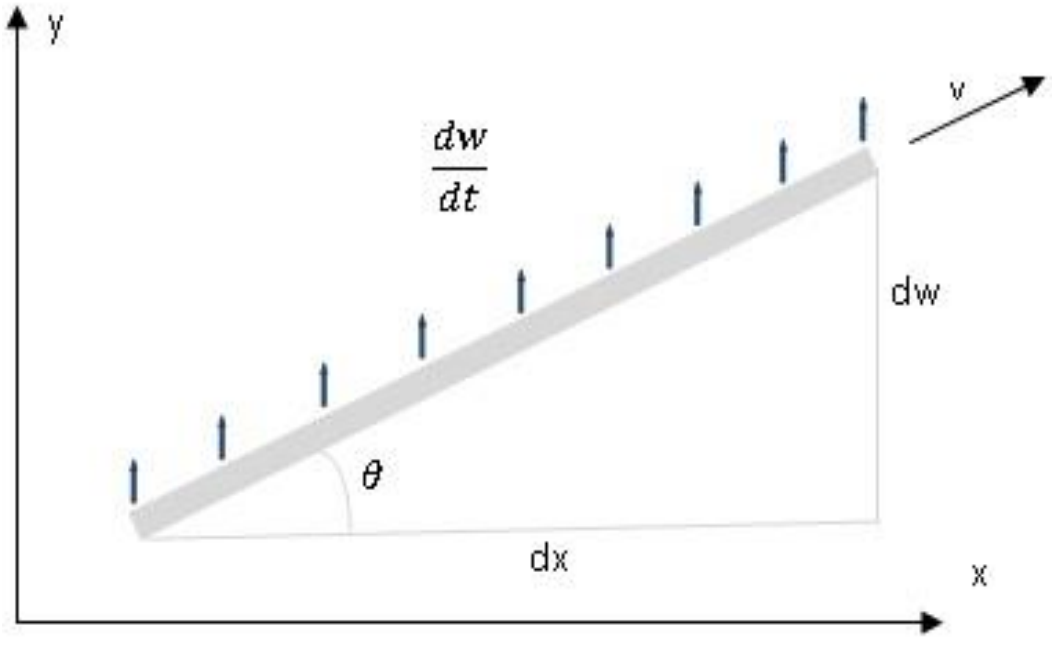

Figure 3.9 Deformation / Velocity diagram

Considering small angle approximation

$$cos\theta \approx 1$$

$$cos\theta \approx \frac{1}{\sqrt{1 + tan^2\theta}} \approx \frac{1}{\sqrt{1 + \frac{\partial^2 w}{\partial x^2}}}$$

$$sin\theta \approx tan\theta$$

Therefore, the velocity in transverse direction is

$$v_y = \frac{\partial w}{\partial t} + v\, sin\theta = \frac{\partial w}{\partial t} + v\, tan\theta$$

$$v_y = \frac{\partial w}{\partial t} + v\, \frac{\partial w}{\partial x}$$

The velocity in longitudinal direction is

$$v_x = v\, cos\theta, \text{ as } cos\theta \approx 1, v_x = v$$

Magnitude of the string velocity can be found using Pythagorean Theorem

$$v = \sqrt{v_y^2 + v_x^2}$$

$$v = \sqrt{\left[\left(\frac{\partial w}{\partial t} + v\, \frac{\partial w}{\partial x}\right)^2 + v^2\right]} \qquad (3.38)$$

Kinetic energy can be calculated from

$$\tau = \int_0^l \frac{1}{2}\rho A \left[\left(\frac{\partial w}{\partial t} + v\, \frac{\partial w}{\partial x}\right)^2 + v^2\right] dx = 0 \qquad (3.39$$

Potential energy of the string is

$$U = \int_0^l T\, dS + \frac{1}{8}\left(\frac{\partial w}{\partial x}\right)^4 \qquad (3.40)$$

where T is the tension along the string and

$$S = \sqrt{\left(\frac{\partial w}{\partial x}dx\right)^2 + dx^2}$$

Therefore,

$$dS = \sqrt{\left(\frac{\partial w}{\partial x}dx\right)^2 + dx^2} - dx$$

Using Tyler series expansion

$$dS = dx\left[1 + \frac{1}{2}\left(\frac{\partial w}{\partial x}\right)^2 - 1\right] = \frac{1}{2}\left(\frac{\partial w}{\partial x}\right)^2 dx$$

Hence,

$$U = \frac{1}{2}\int_0^l \left[T\left(\frac{\partial w}{\partial x}\right)^2 + \frac{1}{4}EA\left(\frac{\partial w}{\partial x}\right)^4\right]dx \tag{3.41}$$

assume that

$$W^{NC} = 0 \tag{3.42}$$

Substituting equations (3.39), (3.41) and (3.42) in equation (3.36) gives

$$\delta \int_{t1}^{t2}\int_0^l \left\{\frac{1}{2}\rho A\left[\left(\frac{\partial w}{\partial t}\right)^2 + 2\left(v\frac{\partial w}{\partial t}\frac{\partial w}{\partial x}\right) + v^2\left(\frac{\partial w}{\partial x}\right)^2 + v^2\right] - \left[\frac{1}{2}T\left(\frac{\partial w}{\partial x}\right)^2\right]$$

$$- \left[\frac{1}{8}EA\left(\frac{\partial w}{\partial x}\right)^4\right]\right\} dxdt = 0$$

Applying the variation (δ) on the previous equation leads to

$$\int_{t1}^{t2}\int_0^l \left\{\rho A\left[\left(\frac{\partial w}{\partial t}\right)\delta\left(\frac{\partial w}{\partial t}\right) + v\left(\frac{\partial w}{\partial t}\right)\delta\left(\frac{\partial w}{\partial x}\right) + v\left(\frac{\partial w}{\partial x}\right)\delta\left(\frac{\partial w}{\partial t}\right) + v^2\left(\frac{\partial w}{\partial x}\right)\delta\left(\frac{\partial w}{\partial x}\right)\right.\right.$$

$$\left.\left. + 0\right] - \left[T\left(\frac{\partial w}{\partial x}\right)\delta\left(\frac{\partial w}{\partial x}\right)\right] - \left[\frac{1}{2}EA\left(\frac{\partial w}{\partial x}\right)^3\delta\left(\frac{\partial w}{\partial x}\right)\right]\right\} dxdt$$

$$= 0 \tag{3.43}$$

Simplifying (3.43) term by term, noting that $\delta w|_{t1}^{t2} = 0$, then

1st Term

$$\int_{t1}^{t2}\int_{0}^{l} \rho A \left(\frac{\partial w}{\partial t}\right) \delta \left(\frac{\partial w}{\partial t}\right) dxdt = \int_{0}^{l} \rho A \left(\frac{\partial w}{\partial t}\right) \delta w|_{t1}^{t2} dx - \int_{t1}^{t2}\int_{0}^{l} \rho A \frac{\partial^2 w}{\partial t^2} \delta w dxdt$$

$$\int_{t1}^{t2}\int_{0}^{l} \rho A \left(\frac{\partial w}{\partial t}\right) \delta \left(\frac{\partial w}{\partial t}\right) dxdt = -\int_{t1}^{t2}\int_{0}^{l} \rho A \frac{\partial^2 w}{\partial t^2} \delta w dxdt$$

2nd Term

$$\int_{t1}^{t2}\int_{0}^{l} \rho A\, v \left(\frac{\partial w}{\partial t}\right) \delta \left(\frac{\partial w}{\partial x}\right) dxdt$$

$$= \int_{t1}^{t2} \rho A\, v \left(\frac{\partial w}{\partial t}\right) \delta w|_{0}^{l}\, dt - \int_{t1}^{t2}\int_{0}^{l} \rho A\, v \frac{\partial^2 w}{\partial t \partial x} \delta w dxdt$$

3rd Term

$$\int_{t1}^{t2}\int_{0}^{l} \rho A\, v \left(\frac{\partial w}{\partial x}\right) \delta \left(\frac{\partial w}{\partial t}\right) dxdt$$

$$= \int_{0}^{l} \rho A\, v \left(\frac{\partial w}{\partial x}\right) \delta w|_{t1}^{t2} dx - \int_{t1}^{t2}\int_{0}^{l} \rho A \left(\frac{\partial v}{\partial t}\frac{\partial w}{\partial x} + v \frac{\partial^2 w}{\partial t^2}\right) \delta w dxdt$$

$$\int_{t1}^{t2}\int_{0}^{l} \rho A\, v \left(\frac{\partial w}{\partial x}\right) \delta \left(\frac{\partial w}{\partial t}\right) dxdt = -\int_{t1}^{t2}\int_{0}^{l} \rho A \left(\frac{\partial v}{\partial t}\frac{\partial w}{\partial x} + v \frac{\partial^2 w}{\partial t^2}\right) \delta w dxdt$$

4th Term

$$\int_{t1}^{t2}\int_{0}^{l} \rho A\, v^2 \left(\frac{\partial w}{\partial x}\right) \delta \left(\frac{\partial w}{\partial x}\right) dxdt$$

$$= \int_{t1}^{t2} \rho A\, v^2 \left(\frac{\partial w}{\partial x}\right) \delta w|_{0}^{l}\, dt - \int_{t1}^{t2}\int_{0}^{l} \rho A\, v^2 \frac{\partial^2 w}{\partial x^2} \delta w dxdt$$

5th Term

$$\int_{t1}^{t2}\int_{0}^{l} T\ \left(\frac{\partial w}{\partial x}\right)\ \delta\ \left(\frac{\partial w}{\partial x}\right) dxdt = \int_{t1}^{t2} T\ \left(\frac{\partial w}{\partial x}\right)\delta w|_{0}^{l}\, dt - \int_{t1}^{t2}\int_{0}^{l} T\ \frac{\partial^2 w}{\partial x^2}\ \delta w dxdt$$

6th Term

$$\int_{t1}^{t2}\int_{0}^{l} \frac{1}{2} EA\ \left(\frac{\partial w}{\partial x}\right)^3\ \delta\ \left(\frac{\partial w}{\partial x}\right) dxdt$$

$$= \int_{t1}^{t2} \frac{1}{2} EA \left(\frac{\partial w}{\partial x}\right)^3 \delta w|_{0}^{l}\, dt - \int_{t1}^{t2}\int_{0}^{l} \frac{3}{2} EA \left(\frac{\partial w}{\partial x}\right)^2 \frac{\partial^2 w}{\partial x^2}\ \delta w dxdt$$

Equation (3.43) becomes

$$\frac{\partial^2 w}{\partial t^2} + 2\ v\ \frac{\partial^2 w}{\partial t \partial x} + \left(\frac{\rho A\ v^2 - T}{\rho A}\right)\frac{\partial^2 w}{\partial x^2} + \frac{\partial v}{\partial t}\frac{\partial w}{\partial x} - \frac{3}{2}\frac{EA}{A\rho}\left(\frac{\partial w}{\partial x}\right)^2 \frac{\partial^2 w}{\partial x^2} = 0$$

Ignoring the non-linear term

$$\frac{\partial^2 w}{\partial t^2} + 2\ v\ \frac{\partial^2 w}{\partial t \partial x} + \left(\frac{\rho A\ v^2 - T}{\rho A}\right)\frac{\partial^2 w}{\partial x^2} + \frac{\partial v}{\partial t}\frac{\partial w}{\partial x} = 0 \qquad (3.44)$$

Equation (3.44) is the equation of motion in the transverse direction of the axially moving string. This equation can be normalized by introducing the following dimensionless variables:

$$w_* = \frac{w}{L}$$

$$x_* = \frac{x}{L}$$

$$t_* = t\ \sqrt{\frac{T}{\rho A L^2}}$$

$$v_* = v\sqrt{\frac{\rho A}{T}}$$

$$\frac{\partial^2 w_*}{\partial t_*^2} + 2\,v_*\frac{\partial^2 w_*}{\partial t_* \partial x_*} + (v_*^2 - 1)\frac{\partial^2 w_*}{\partial x_*^2} + \frac{\partial v_*}{\partial t_*}\frac{\partial w_*}{\partial x_*} = 0 \tag{3.45}$$

Here v_* is the dimensionless axial speed of the string, representing the ratio of web axial speed to wave speed in the web material.

Equation (3.45) is a second-order linear hyperbolic partial differential equation (HPDE) for the transverse vibration of the axially moving string.

A Finite difference technique is used to transform the second-order HPDE in to second-order ordinary differential equations (ODEs). For this purpose, central difference scheme is used for spatial discretization as follows,

$$\left.\frac{\partial w_*}{\partial x_*}\right|_{x_{*i}} = \frac{w_{*(i+1)} - w_{*(i-1)}}{2 * dx_*} \tag{3.46}$$

$$\left.\frac{\partial^2 w_*}{\partial {x_*}^2}\right|_{x_{*i}} = \frac{w_{*(i+1)} - 2 * w_{*i} + w_{*(i-1)}}{d{x_*}^2} \tag{3.47}$$

Applying equations (3.46) and (3.47) to equation (3.45) results in $n-1$ second-order ODEs, where n is the total number of spatial points and dx_* is the step size. i.e.,

$$\left.\begin{aligned}
&\frac{\mathrm{d}^2 w_{*1}}{dt_*^2} + 2\,\frac{v_*}{\mathrm{d}x_*}\,\frac{\mathrm{d}w_{*2}}{\mathrm{d}t_*} + \frac{(v_*^2 - 1)}{{\mathrm{d}x_*}^2}\,(-2 * w_{*1} + w_{*2}) + \frac{v_*}{\mathrm{d}x_*} * w_{*2} = 0 \\
&\frac{\mathrm{d}^2 w_{*2}}{dt_*^2} + 2\,\frac{v_*}{\mathrm{d}x_*}\left(-\frac{\mathrm{d}w_{*1}}{\mathrm{d}t_*} + \frac{\mathrm{d}w_{*3}}{\mathrm{d}t_*}\right) + \frac{(v_*^2 - 1)}{{\mathrm{d}x_*}^2}\,(w_{*1} - 2 * w_{*2} + w_{*3}) + \frac{v_*}{\mathrm{d}x_*}(-w_{*1} + w_{*3}) = 0 \\
&\qquad\qquad\qquad

In matrix form (3.48) becomes

$$\frac{\mathrm{d}^2 w_*}{\mathrm{d}t_*^2} + 2\, v_* G\, \frac{\mathrm{d}w_*}{\mathrm{d}t_*} + \{(v_*^2 - 1)K + v_* * G\} w_* = 0 \tag{3.49}$$

where G and K are $(n-\ 1) * \ (n-1)$ matrices given bellow

$$G = \frac{1}{dx_*} \begin{bmatrix} 0 & 1 & 0 & \dots & 0 \\ -1 & 0 & 1 & 0 & \vdots \\ 0 & -1 & \ddots & \ddots & 0 \\ \vdots & 0 & \ddots & \ddots & 1 \\ 0 & \dots & 0 & -1 & 0 \end{bmatrix}$$

$$K = \frac{1}{dx_*{}^2} \begin{bmatrix} -2 & 1 & 0 & \dots & 0 \\ 1 & -2 & 1 & 0 & \vdots \\ 0 & 1 & \ddots & \ddots & 0 \\ \vdots & 0 & \ddots & \ddots & 1 \\ 0 & \dots & 0 & 1 & -2 \end{bmatrix}$$

To solve the $n-1$ second-order ODEs of equation (3.48), a state space representation is used to convert them into $2 * (n-1)$ first-order ODE's, which are given by

$$w_{*1} = \ y_1, w_{*2} = \ y_3, w_{*3} = \ y_5, \dots, w_{*(n-1)} = \ y_{2*(n-1)-1} \tag{3.50}$$

$$\left.\begin{aligned} \frac{dy_1}{dt_*} &= \ y_2 \\ \frac{\mathrm{d}y_2}{\mathrm{d}t_*} = \frac{\mathrm{d}^2 w_{*1}}{\mathrm{d}t_*^2} &= -2\, \frac{v_*}{\mathrm{d}x_*}\, y_4 + \frac{(v_*^2 - 1)}{\mathrm{d}x_*{}^2}\, (2 * y_1 - \ y_3) - \frac{v_*^{\cdot}}{\mathrm{d}x_*} * y_4 \\ \frac{\mathrm{d}y_2}{\mathrm{d}t_*} = \frac{\mathrm{d}^2 w_{*1}}{\mathrm{d}t_*^2} &= -2\, \frac{v_*}{\mathrm{d}x_*}\, y_4 + \frac{(v_*^2 - 1)}{\mathrm{d}x_*{}^2}\, (2 * y_1 - \ y_3) - \frac{v_*^{\cdot}}{\mathrm{d}x_*} * y_4 \\ \frac{\mathrm{d}y_3}{\mathrm{d}t_*} &= \ y_4 \\ \frac{\mathrm{d}y_4}{\mathrm{d}t_*} = \frac{\mathrm{d}^2 w_{*2}}{\mathrm{d}t_*^2} &= -2\, \frac{v_*}{\mathrm{d}x_*}\, (y_2 - y_6) + \frac{(v_*^2 - 1)}{\mathrm{d}x_*{}^2}\, (-y_1 + 2 * \ y_3 - y_5) - \frac{v_*^{\cdot}}{\mathrm{d}x_*} (y_2 - y_6) \\ &\vdots \\ \frac{\mathrm{d}y_{2*(n-1)-1}}{\mathrm{d}t_*} &= \ y_{2*(n-1)} \\ \frac{\mathrm{d}y_{2*(n-1)}}{\mathrm{d}t_*} = -2\, \frac{v_*}{\mathrm{d}x_*}\, y_{2*(n-1)-2} &+ \frac{(v_*^2 - 1)}{\mathrm{d}x_*{}^2} \left(-y_{2*(n-1)-3} + 2 * y_{2*(n-1)-1}\right) - \frac{v_*^{\cdot}}{\mathrm{d}x_*}\, y_{2*(n-1)-2} \end{aligned}\right\} \tag{3.51}$$

Transverse vibration of the axially moving string can be calculated using the coupled system of first-order ODEs given in equations (3.50) and (3.51) using the following initial conditions:

$$y_1(0) = \ y_3(0) = \ y_5(0) = \cdots = \ y_{2*(n-1)-1}(0) = a(x_*) \tag{3.52}$$

$$y_2(0) = \ y_4(0) = \ y_4(0) = \cdots = \ y_{2*(n-1)}(0) = b(x_*) \tag{3.53}$$

where $a(x_*)$ and $b(x_*)$ are the initial transverse displacements and initial transverse speeds, respectively. Simple supporting conditions are assumed at the end of the axially moving web.

3.2.1 Model Validation

To verify the numerical modal developed for the transverse vibration of the axially moving string, equation (3.45), the study of Mote et al. [40] was considered for comparison. In [40] solution of HPDE was obtained using state space and modal analysis approach as follows:

$$w_*(x_*t_*) = \sum_{n=1}^{\infty} [g_n^R(t_*) \ \sin(n\pi x_*) \cos(n\pi v_* x_*)$$

$$+ \ \ g_n^I(t_*) \ \sin(n\pi x_*) \sin(n\pi v_* x_*) \ ] \tag{3.54}$$

where $g_n^R(t_*)$ and $g_n^I(t_*)$ are the real and imaginary components of the generalized coordinates, respectively, which can be calculated using

$$g_n^R(t_*) = \ g_n^R(0) \ \cos(w_n t_*) + \ g_n^I(0) \ \sin(w_n t_*) \tag{3.55}$$

$$g_n^R(t_*) = \ g_n^I(0) \ \cos(w_n t_*) - \ g_n^R(0) \ \sin(w_n t_*) \tag{3.56}$$

where $g_n^R(0)$ and $g_n^I(0)$ are initial values of the real and imaginary components of the generalized coordinates, respectively. Hence,

$$g_n^R(0) = n\,\pi\sqrt{2(1-v_*^2)}\int_0^1 \Big[a(x_*)\big((1+v_*^2)\sin(n\pi x_*)\cos(n\pi v_* x_*) + 2v_*\cos(n\pi x_*)\sin(n\pi v_* x_*)\big)\Big]dx - \sqrt{2(1-v_*^2)}\int_0^1 [b(x_*)(\sin(n\pi x_*)\sin(n\pi v_* x_*)\ )]dx \quad (3.57)$$

$$g_n^l(0) = n\,\pi\sqrt{2(1-v_*^2)}\int_0^1 \Big[a(x_*)\big((1+v_*^2)\sin(n\pi x_*)\sin(n\pi v_* x_*) - 2v_*\cos(n\pi x_*)\cos(n\pi v_* x_*)\big)\Big]dx + \sqrt{2(1-v_*^2)}\int_0^1 [b(x_*)(\sin(n\pi x_*)\cos(n\pi v_* x_*)\ )]dx \quad (3.58)$$

Comparison was made in Fig 3.10 for the case of the dimensionless transport velocity of 0.1 at the location $x_* = 0.5$, using the following the initial conditions:

$$a(x_*) = 0 \quad (3.59)$$

$$b(x_*)\ = 0.01 * \exp(x_*)\ *\ \sin(\mathrm{pi} * x_*) \quad (3.60)$$

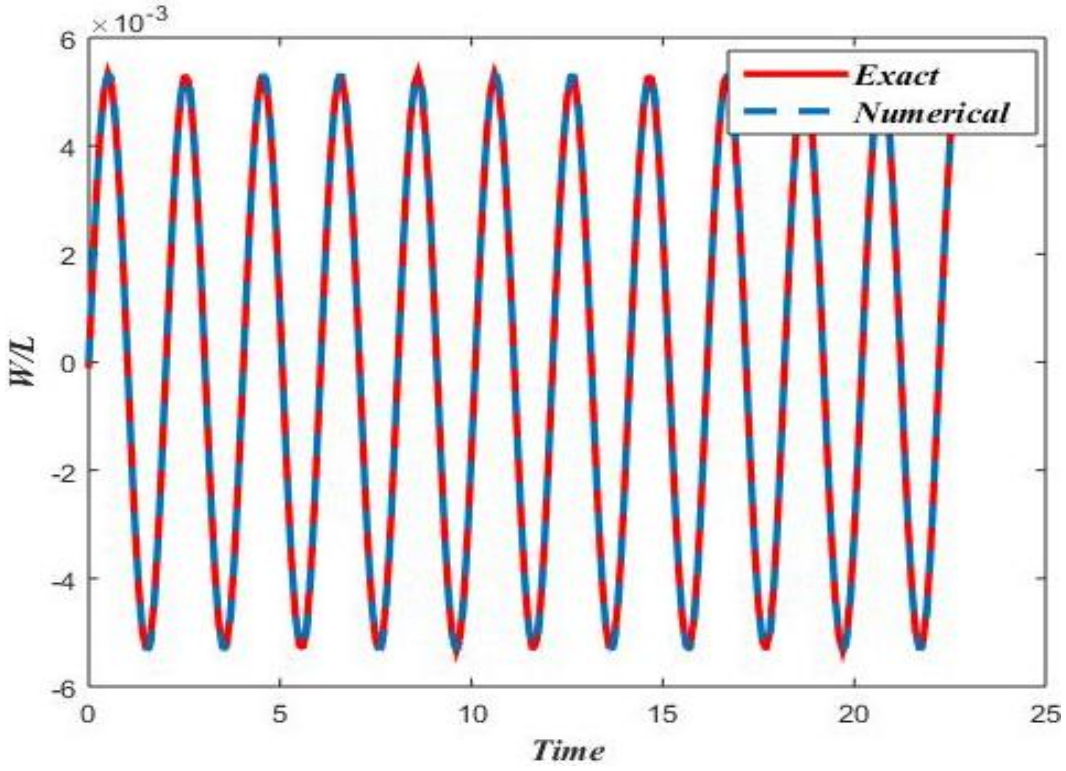

Figure 3.10 Transverse Response Comparison at $v_* = 0.1$ & $x_* = 0.5$

The finite difference model utilized in this thesis is in good agreement with the state space model analysis-based solution, when retaining the first four terms.

3.2.2 Effect of Axial Speed on Web Vibration Response

Figs. 3.11-3.13 show transverse displacement time history (in terms of normalized displacements) monitored at the three representative locations x_*= 0.25, 0.50 and 0.75, respectively. The string has axial speeds of $v_* = 0.3, 0.5$ and 0.7.

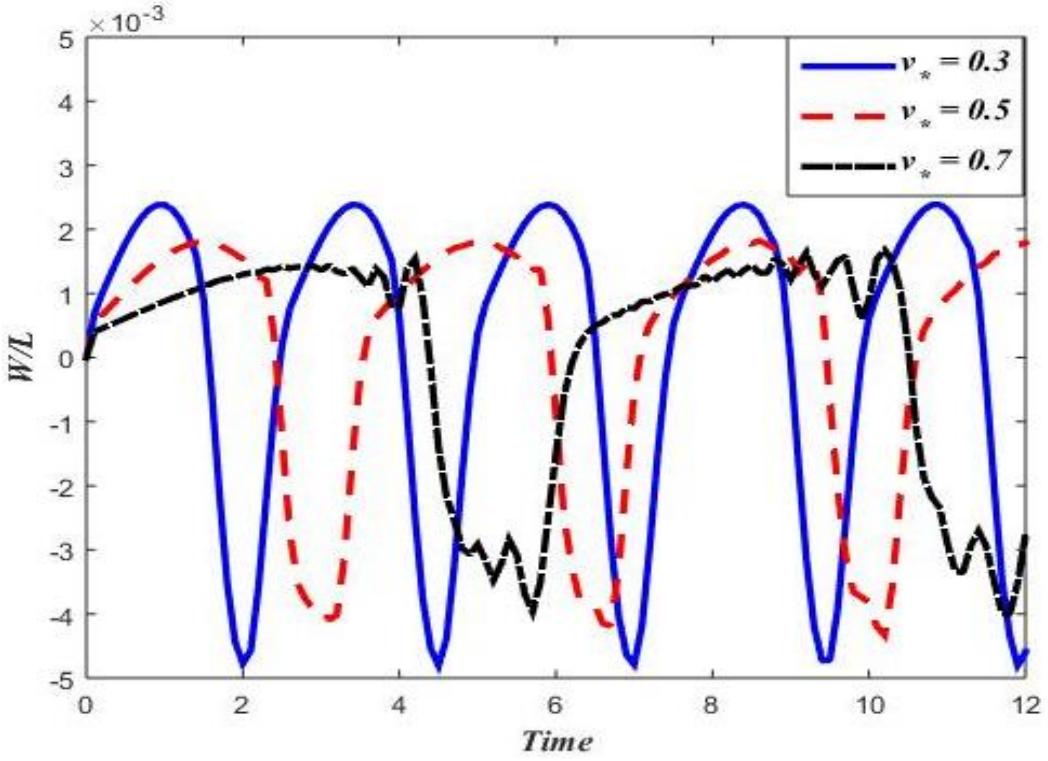

Figure 3.11 Transverse displacement at $x_* = 0.25$ for webs having different speeds

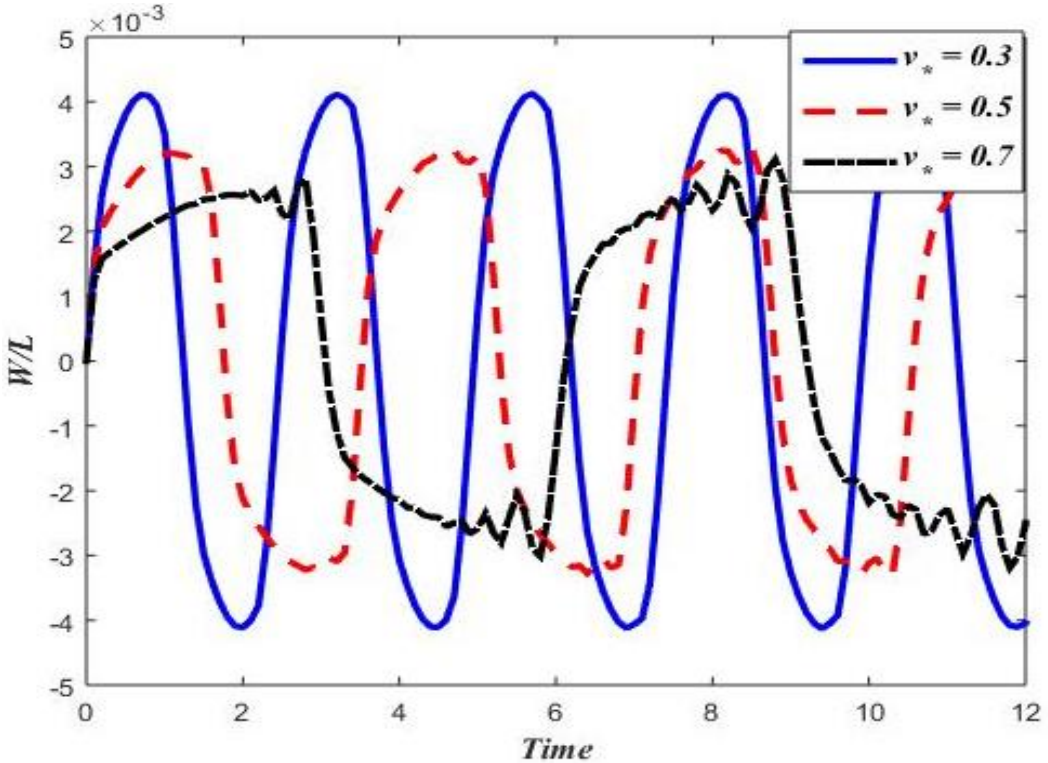

Figure 3.12 Transverse displacement at $x_* = 0.5$ for webs having different speeds

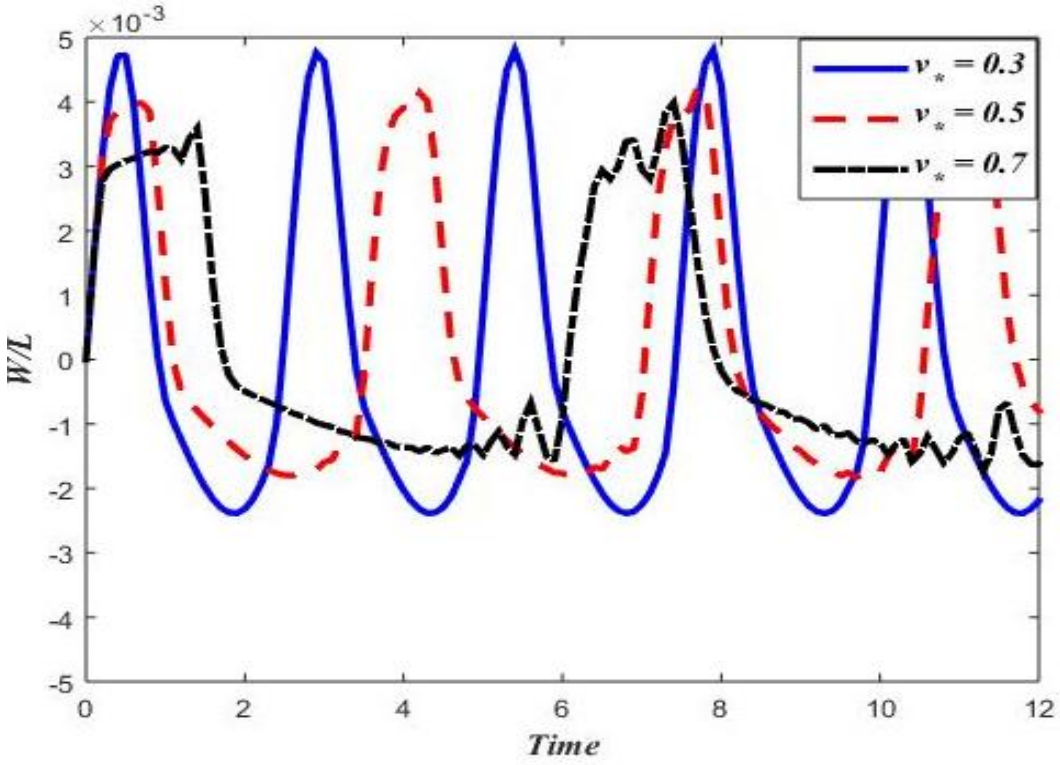

Figure 3.13 Transverse displacement at $x_* = 0.75$ for webs having different speeds

Comparing the responses in Figs. 3.11-3.13 indicates that increasing the axial web speed leads to a reduced displacement amplitude as well as a reduced vibration frequency. The frequency responses, obtained by applying Fast Fourier Transform, are shown in Figure 3.14. It is noted that the webs with non-dimensional speeds of 0.0 (stationary web), 0.3, 0.5, and 0.7 have their lower vibration frequencies at 49.55, 39.26, 27.48, and 17.12 Hz, respectively. Note that as the axial web speed increases, more modes are excited. An analysis of the non-dimensional frequencies in the range of non-dimensional speed indicates that divergent instability of the string will occur when the non-dimensional speed reaches unity as shown in Fig 3.15. Mode shapes are strongly dependent on the axial speed of the string. The dependence of the first three mode shapes on the axial speed is shown in Fig. 3.16.

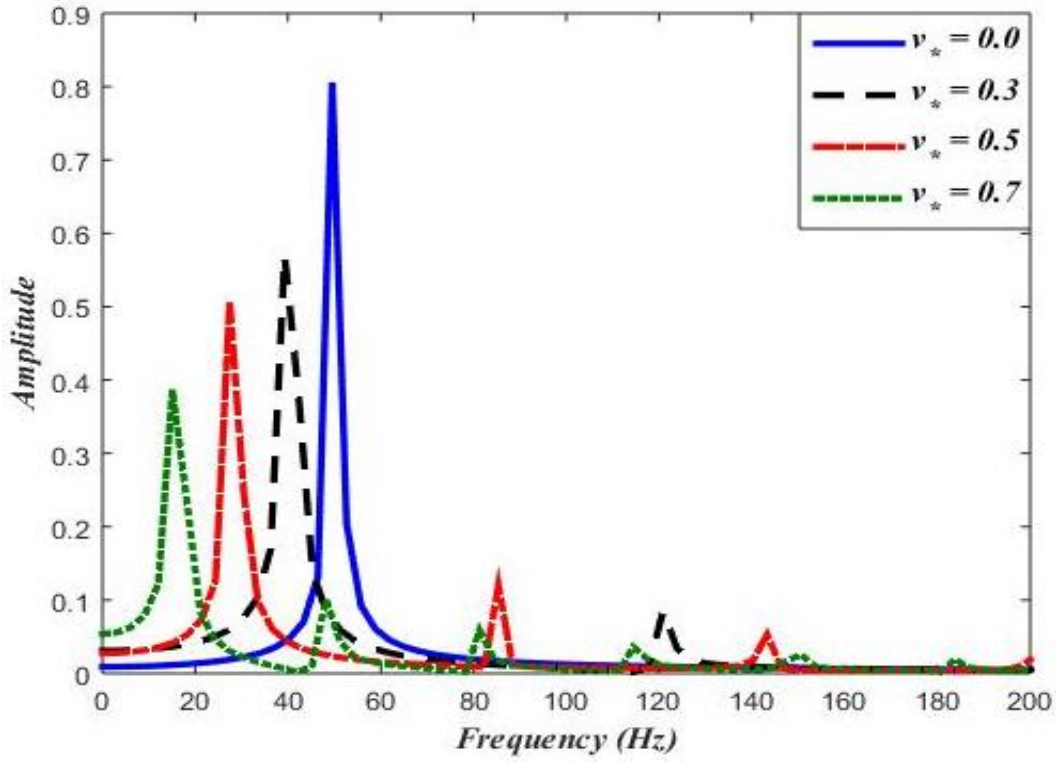

Figure 3.14 Frequency of response at $x_* = 0.5$ for webs having different speeds

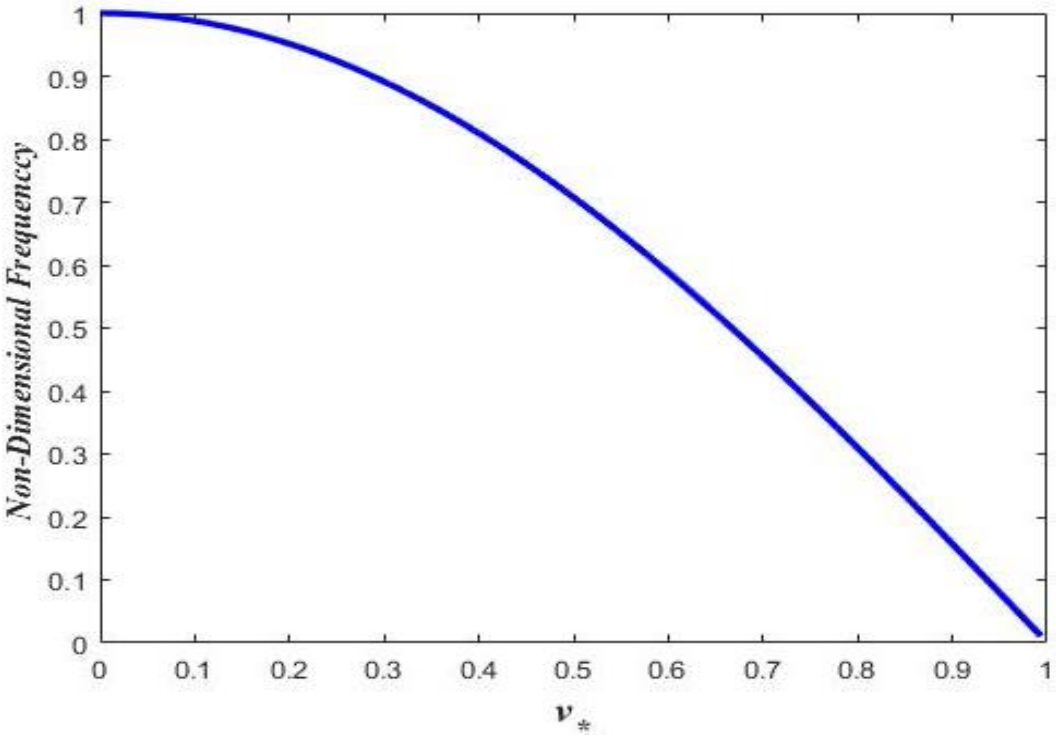

Figure 3.15 Frequency vs axial speed

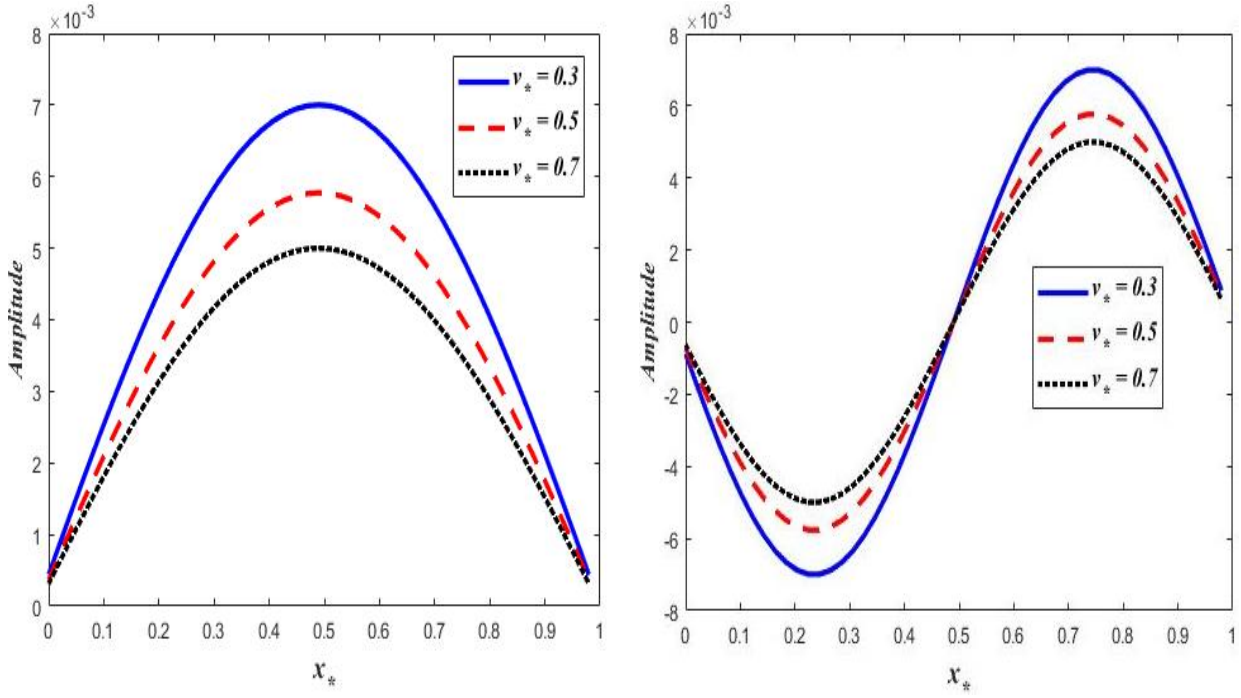

(a) (b)

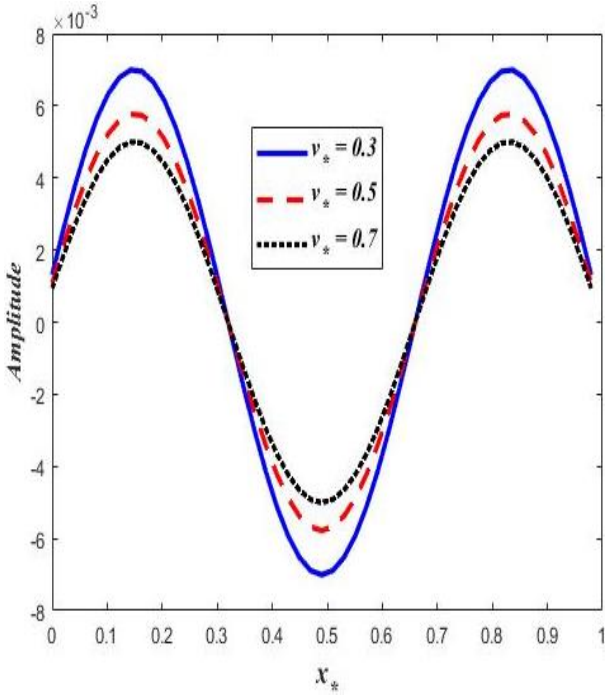

(c)

Figure 3.16 Comparison of first three mode shapes at different velocities

3.2.3 Effect of Roll-Borne Disturbances on Web Vibration Response

Transverse vibration of an axially moving web can be excited by transverse displacements at one of the rolls. This happens when the roll is out of round geometry. The displacement at the roll may cause parametric resonance phenomena, affecting the system response and causing instability. Resonant vibrations in mechanical structures occur when the excitation frequency and system natural frequencies coincide. The boundary conditions for the equation of motion are given as

$$\left.\begin{matrix} w_*(0,t_*) = 0.01 * \sin(\Omega * t_*) \\ w_*(l,t_*) = 0 \end{matrix}\right\} \tag{3.61}$$

For these boundary conditions, the finite difference method is applied to transform the second-order HPDE into second-order ordinary differential equations (ODEs). Applying the central difference scheme to discretize the equation of motion results in n second-order ODEs, where n is the total number of spatial points and dx_* is the step size.

$$\left.\begin{matrix} \dfrac{\mathrm{d}^2 w_{*0}}{dt_*^2} = 0.01 * \Omega * cos(\Omega * t) \\ \dfrac{\mathrm{d}^2 w_{*1}}{dt_*^2} + \dfrac{v_*}{\mathrm{d}x_*}\left(\dfrac{\mathrm{d}w_{*2}}{\mathrm{d}t_*} - \dfrac{\mathrm{d}w_{*0}}{\mathrm{d}t_*}\right) + \dfrac{(v_*^2 - 1)}{{dx_*}^2}\left(w_{*0} - 2 * w_{*1} + w_{*2}\right) + \dfrac{v_*}{2 * \mathrm{d}x_*}(w_{*2} - w_{*0}) = 0 \\ \dfrac{\mathrm{d}^2 w_{*2}}{dt_*^2} + \dfrac{v_*}{\mathrm{d}x_*}\left(-\dfrac{\mathrm{d}w_{*1}}{\mathrm{d}t_*} + \dfrac{\mathrm{d}w_{*3}}{\mathrm{d}t_*}\right) + \dfrac{(v_*^2 - 1)}{{\mathrm{d}x_*}^2}\left(w_{*1} - 2 * w_{*2} + w_{*3}\right) + \dfrac{v_*}{2 * \mathrm{d}x_*}(-w_{*1} + w_{*3}) = 0 \\ \vdots \\ \dfrac{\mathrm{d}^2 w_{*(n-1)}}{\mathrm{d}t_*^2} + \dfrac{v_*}{\mathrm{d}x_*}\dfrac{\mathrm{d}w_{*(n-2)}}{\mathrm{d}t_*} + \dfrac{(v_*^2 - 1)}{{\mathrm{d}x_*}^2}\left(w_{*(n-2)} - 2 * w_{*(n-1)}\right) + \dfrac{v_*}{2 * \mathrm{d}x_*} * w_{*(n-2)} = 0 \end{matrix}\right\} \tag{3.62}$$

System of equations (3.62) are numerically integrated to find the time-domain response of an axially moving web.

3.2.3.1 Parametric Analysis

In this section, the effects of system's parameters on its response are investigated. Figs. 3.17-3.21 depicts the dynamic response of the system when excited with external disturbance of frequency, Ω. Response of the system is monitored at mid web span (x_*= 0.50) and three different web speeds have been considered i.e., $v_* = 0.3, 0.5$ and 0.7.

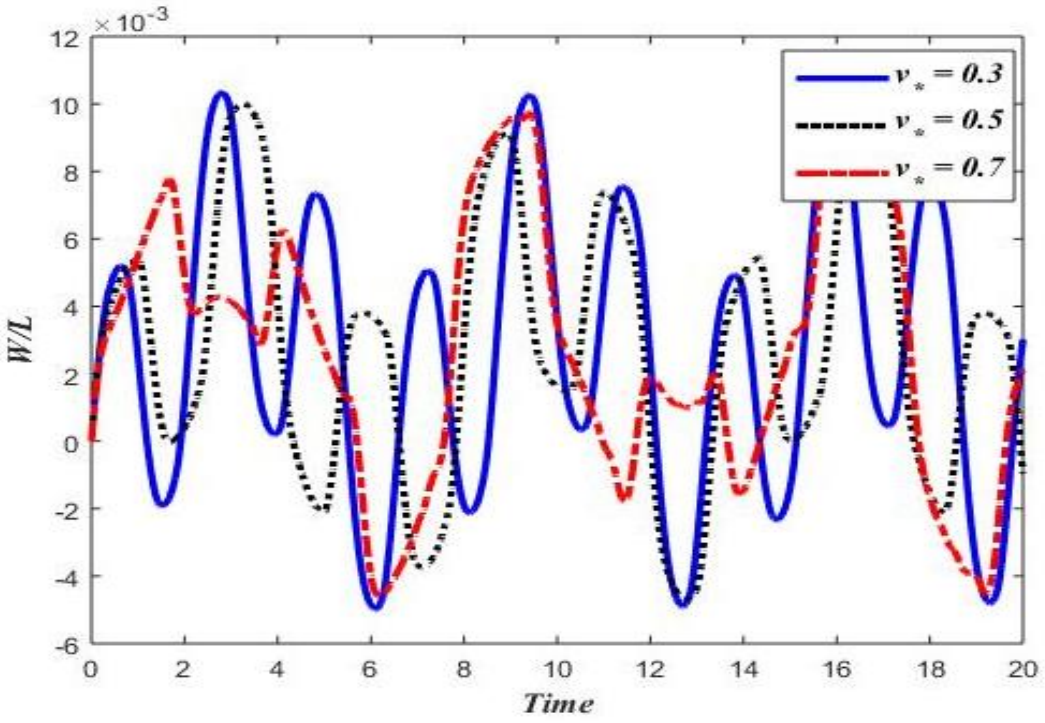

Figure 3.17 Transverse displacement at $x_* = 0.5$ & Ω = 0.6 for webs having different speeds

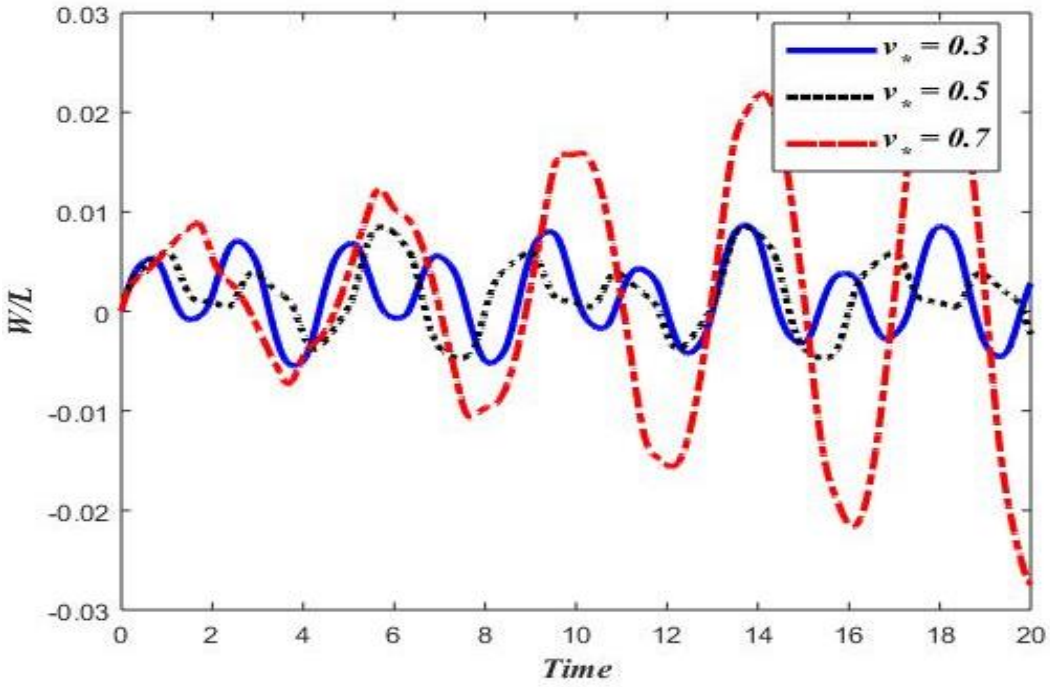

Figure 3.18 Transverse displacement at $x_* = 0.5$ & Ω = 1.2 for webs having different speeds

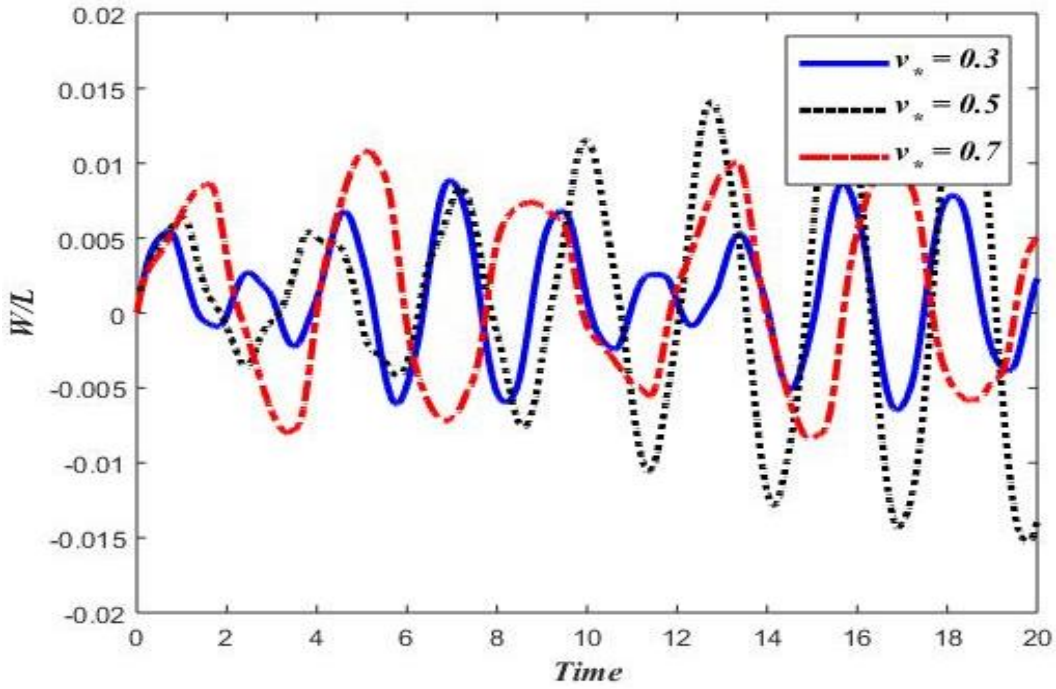

Figure 3.19 Transverse displacement at $x_* = 0.5$ & Ω = 1.4 for webs having different speeds

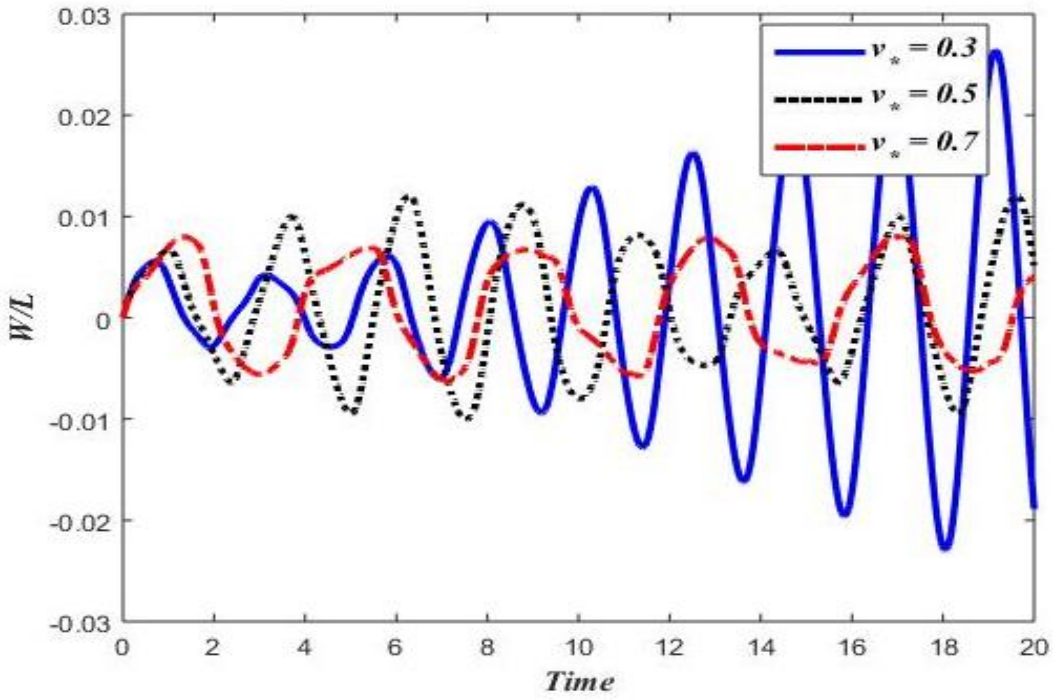

Figure 3.20 Transverse displacement at $x_* = 0.5$ & Ω = 1.7 for webs having different speeds

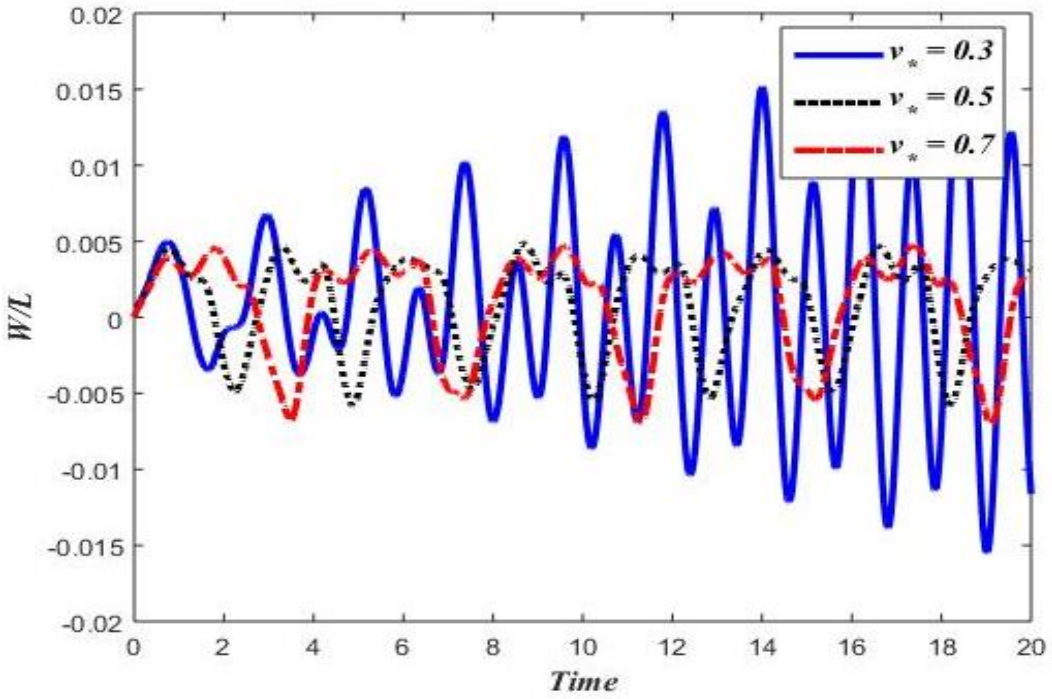

Figure 3.21 Transverse displacement at $x_* = 0.5$ & Ω = 3.4 for webs having different speeds

Figure 3.17 depicts the dynamic response of the web at a lower excitation frequency. At a lower frequency, the response is stable for the given web axial speed. As we increase the excitation frequency, the response moves towards the resonance. When excitation frequency is 1.2 the response of the system for axial speed of 0.7 becomes unstable while system stability is retained for other two speeds, shown in Fig. 3.18. As excitation frequency is increased to 1.4 and 1.7 the response becomes unstable at a web speeds of 0.5 and 0.3 respectively while the other two responses remain stable for each case, shown in Figs. 3.19 and 3.20.

The frequency-domain responses, obtained by applying Fast Fourier Transform, are shown in Figs. 3.22-3.26.

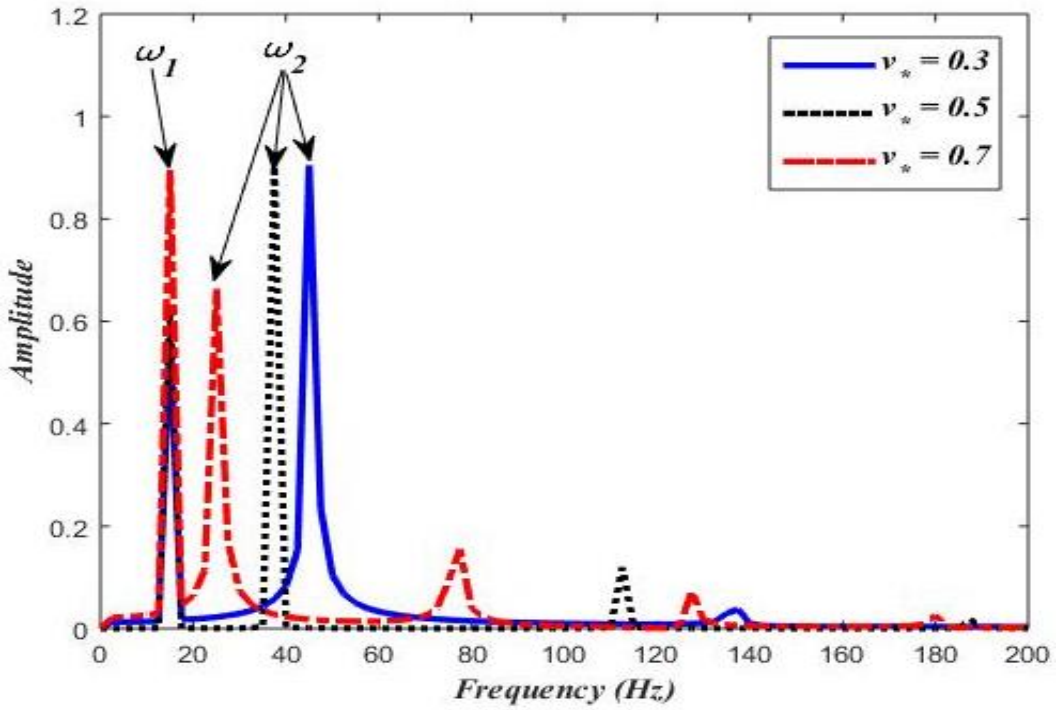

Figure 3.22 Frequency-domain response of displacement at $x_* = 0.5$ & Ω = 0.6 for webs having different speeds

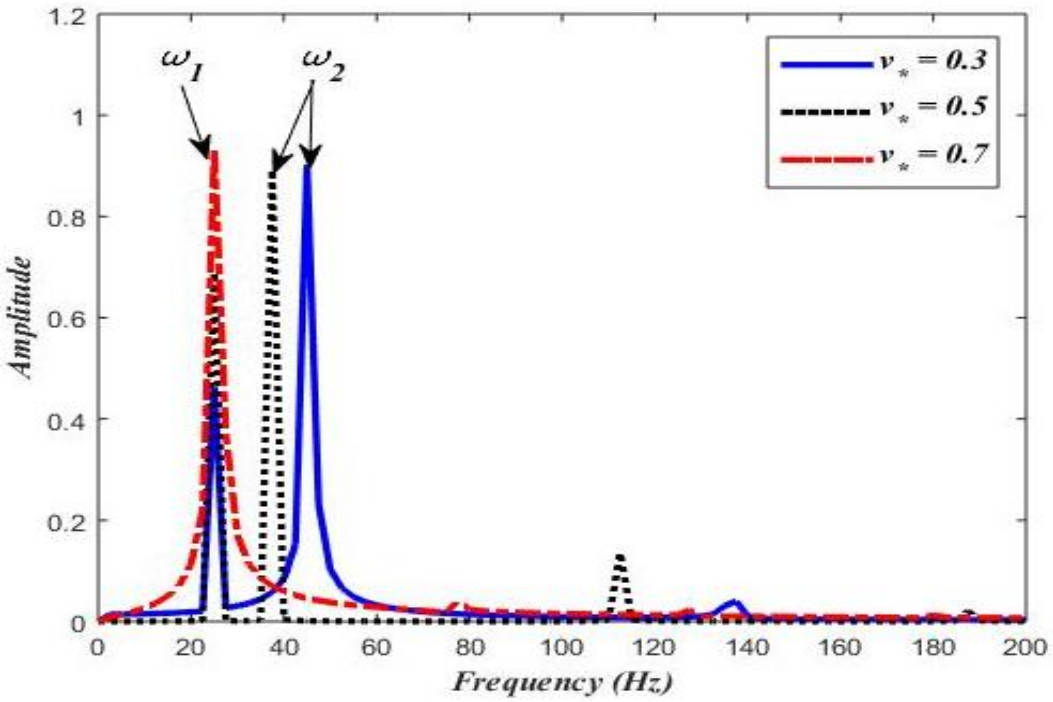

Figure 3.23 Frequency-domain response of displacement at $x_* = 0.5$ & Ω = 1.2 for webs having different speeds

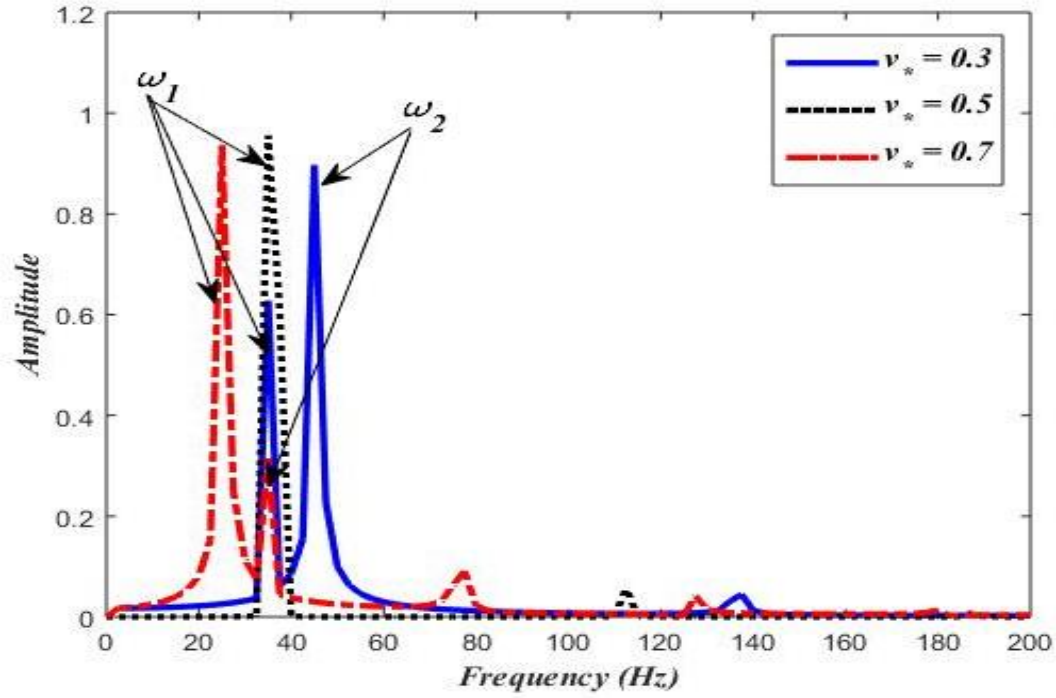

Figure 3.24 Frequency-domain response of displacement at $x_* = 0.5$ & Ω = 1.4 for webs having different speeds

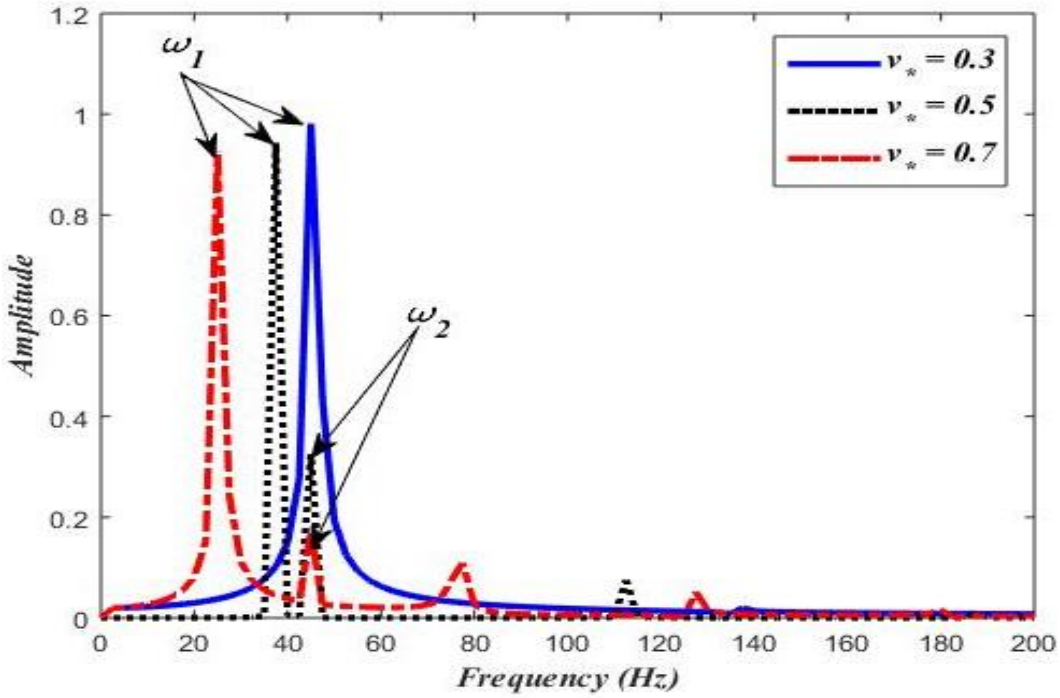

Figure 3.25 Frequency-domain response of displacement at $x_* = 0.5$ & Ω = 1.7 for webs having different speeds

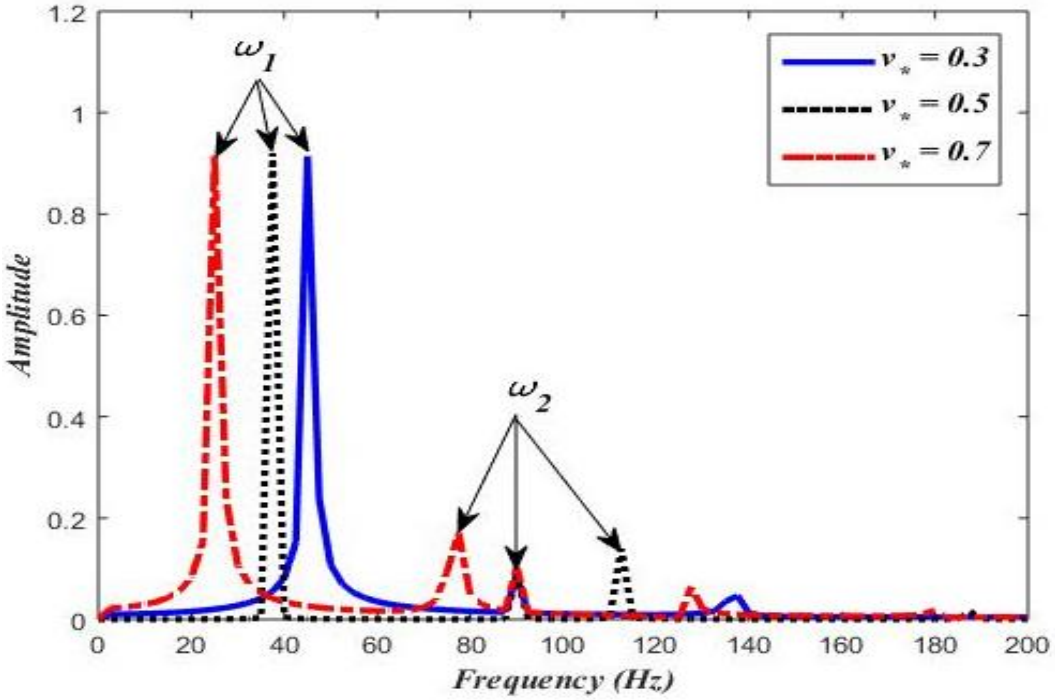

Figure 3.26 Frequency-domain response of displacement at $x_* = 0.5$ & Ω = 3.4 for webs having different speeds

The first and second frequencies of transverse vibration of the system at different axial speed of the web and the external excitation frequency are shown. Response frequency is highest at lowest speed and as web speed is increased frequency response is shifted to lower values. It is noted that the instability in the transverse response will occur when the first and second frequency of the oscillation converge to same value, shown in Figs. 3.22-3.25.

3.3 The Coupled Web Vibration

In this section, equation (3.45) is solved together with the system of equations (3.33)-(3.35), as a coupled system that describes the transverse vibration of the axially moving web between the unwinding and the rewinding rolls. The numerical finite difference approach utilized in the previous section is used here. Equation (3.45) is replaced with equations (3.50) and (3.51), equations (3.33) - (3.35) are augmented with the equations (3.18) - (3.19), and the initial conditions (3.59) and (3.60) are used for solving the coupled system for the time-domain response with the input torque shown in Fig. 3.27, is applied at both the unwinding and rewinding motors.

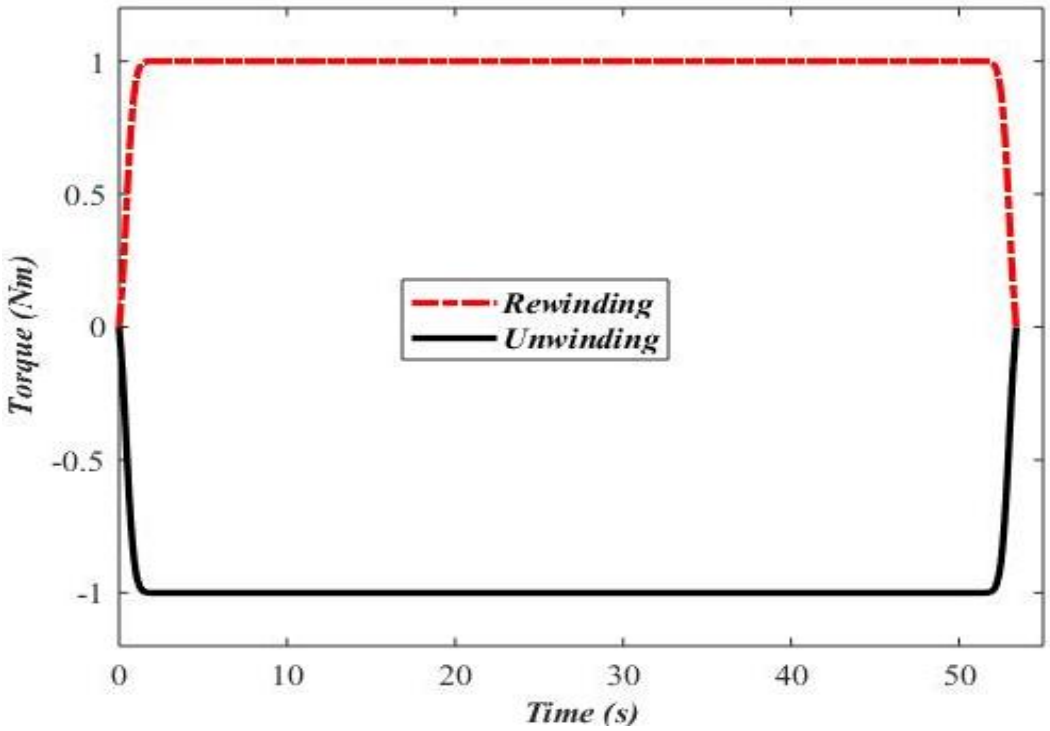

Figure 3.27 Web-transmitted tension variation with time

Figs. 3.28-3.30 show dynamic responses (in terms of normalized displacements) monitored at the three representative locations (x_*= 0.25, 0.50 and 0.75), respectively.

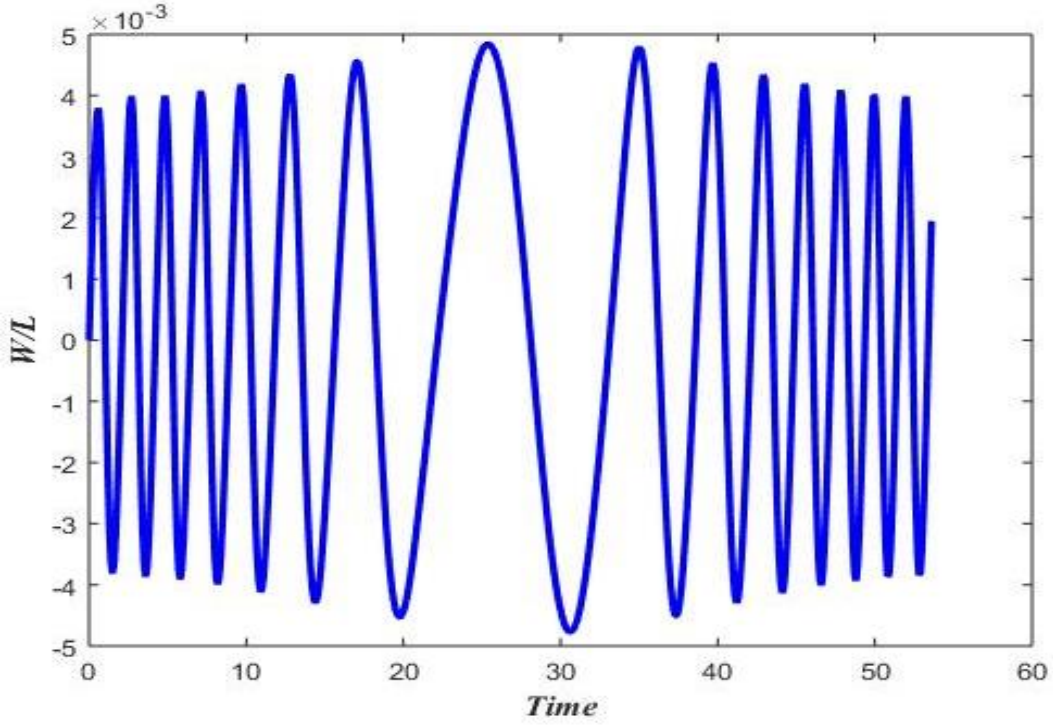

Figure 3.28 Transverse displacement at $x_* = 0.25$ for the axially moving web

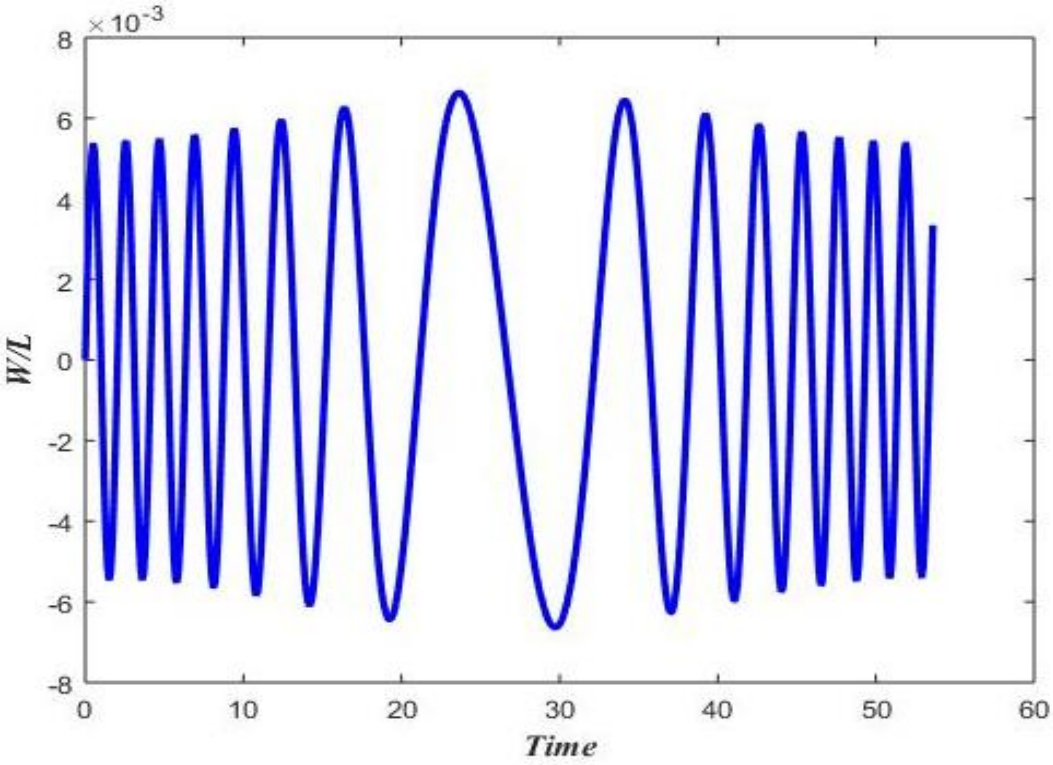

Figure 3.29 Transverse displacement at $x_* = 0.50$ for the axially moving web

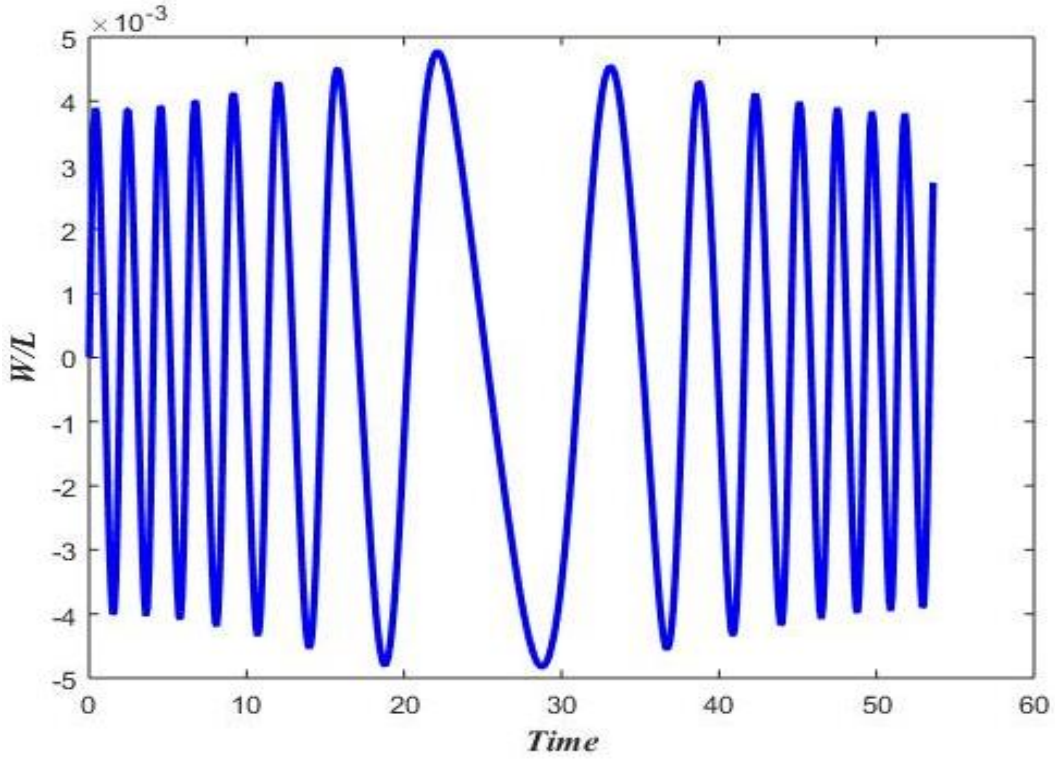

Figure 3.30 Transverse displacement at $x_* = 0.75$ for the axially moving web

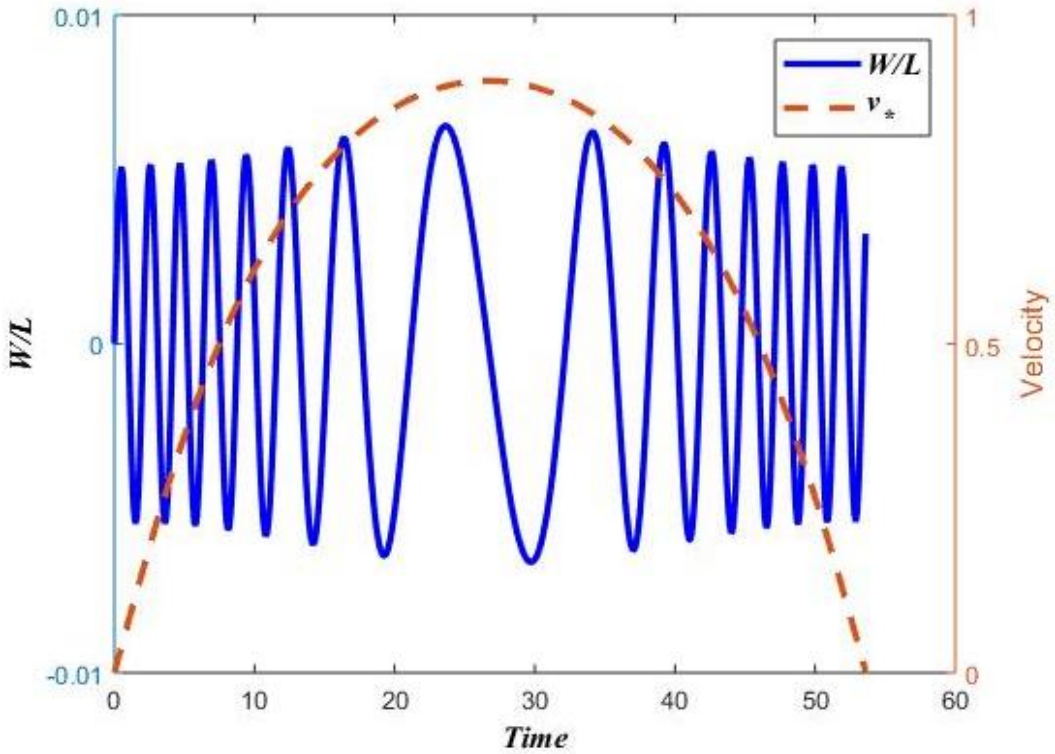

Figure 3.31 Transverse displacement (at $x_* = 0.5$) and web speed (dimensionless)

In light of varying axial web speed with time, as in Fig. 3.7, responses presented in Figs. 3.28-3.30 indicate non-periodic oscillations. To see the effect of varying speed on the response, dimensionless web speed is plotted alongside with the web response at '$x_* = 0.5$' as shown in Fig. 3.31. At the early and late phases of material transfer from the unwinding roll to the rewinding roll, the axial web speed changes rapidly with time leading to high frequency fluctuations in the dynamic response. Low frequency response is noted in the middle of the web material transfer time interval, due to the slow change in axial web speed with time. The frequency-domain responses, obtained by applying Fast Fourier Transform, are shown in Figure 3.32. It is noted that the web has multiple frequencies with highest amplitude at the web center.

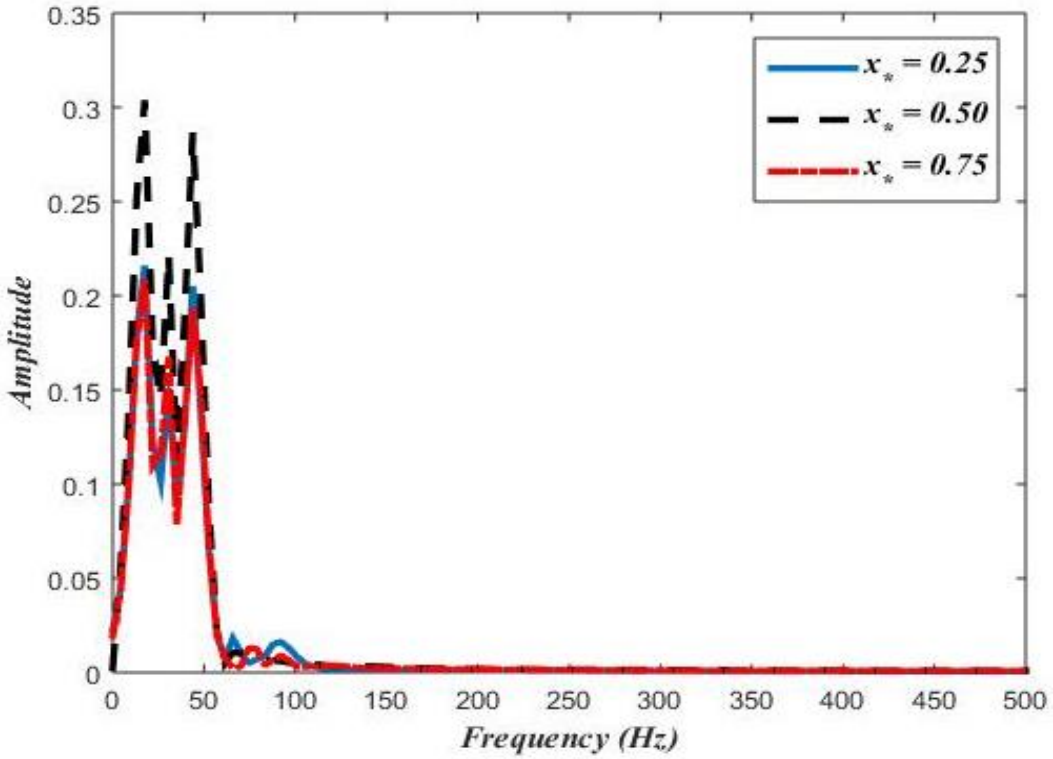

Figure 3.32 Frequency-domain response of displacement at different points on the web

From the above analysis, one can observe that the vibration characteristics of an axially moving string coupled with a roll-to-roll dynamic are significantly different from those obtained by considering the vibration of an axially moving string between two simple supports, in isolation from the web hosting system. In addition, vibrations of an axially moving web are more influenced by the R2R dynamics than the R2R dynamics affects by the vibrations of the axially moving web. In other words, a dominantly “one way” coupling is observed.

.

CHAPTER 4

WEB VIBRATION IN A TWO-SPAN ROLL-TO-ROLL SYTEM

4.1 Roll-to-Roll Dynamics

This section covers web dynamics and roll-to-roll dynamic modelling for the simplest printing system (three-roll one-span), as shown in Fig. 4.1.

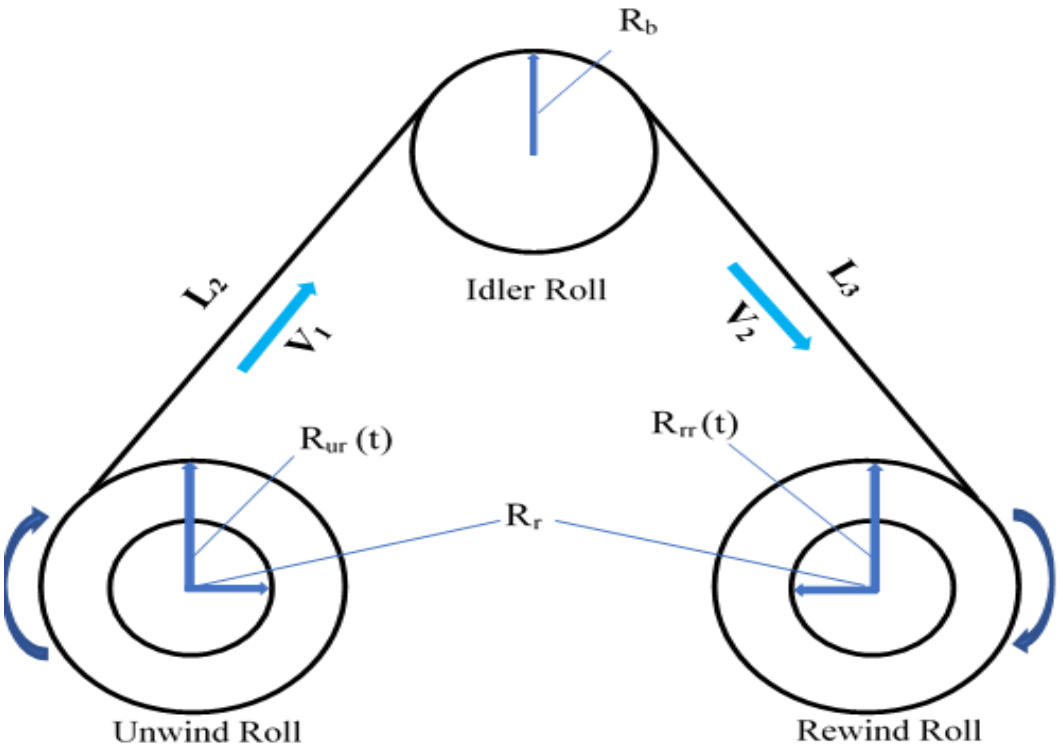

Figure 4.1 Two-Span R2R System

4.1.1 Web Tension Velocity Relationship

Following the mathematical model of single-span R2R systems, assuming small width of the web in comparison to its length and considering no slip condition at the boundaries (rolls), web tension-velocity relation for each span is given by

$$\frac{dT_2}{dt} \approx \left[\frac{R_{ur}}{L_2}T_1 - \frac{2R_{ur}}{L_2}T_2 - \frac{EAR_{ur}}{L_2}\right]\Omega_{ur} + \left[\frac{R_b}{L_2}T_2 + \frac{EAR_b}{L_2}\right]\Omega_b \qquad (4.1)$$

$$\frac{dT_3}{dt} \approx \left[\frac{R_b}{L_3}T_2 - \frac{2R_b}{L_3}T_3 - \frac{EAR_b}{L_3}\right]\Omega_b + \left[\frac{R_{rr}}{L_3}T_3 + \frac{EAR_{rr}}{L_3}\right]\Omega_{rr} \qquad (4.2)$$

where Ω_{ur}, Ω_b, Ω_{rr} are the angular speed and R_{ur}, R_b, R_{rr} are radii of unwinding, idler and rewinding roll respectively.

4.1.2 Equation of Motion of the Roll

Adopting the methodology used in section 3.1.2 and considering (i) the inertial torque, (ii) the torque caused by the web tension, (iii) the motor torque, and (iv) the friction torque, the equation of motion for individual rolls are given as

$$\frac{\mathrm{d}}{\mathrm{d}t}(J_{ur} * \Omega_{ur}) = R_{ur} * T_2 + B_1 * \Omega_{ur} - C_1 \qquad (4.3)$$

$$\frac{\mathrm{d}}{\mathrm{d}t}(J_b * \Omega_b) = R_b * (T_3 - T_2) + B_2 * \Omega_b - C_2 \qquad (4.4)$$

$$\frac{\mathrm{d}}{\mathrm{d}t}(J_{rr} * \Omega_{rr}) = -R_{rr} * T_3 + B_3 * \Omega_{rr} - C_3 \qquad (4.5)$$

Moment of inertia of idler roll is constant, whereas moment of inertia variation of unwinding and rewinding roll is given by

$$J_{ur}(t) = \frac{1}{2}\pi W\ [R_r^4(\rho_r - \rho_w) + \rho_w[R_{ur}(t)]^4] \tag{4.6}$$

$$J_{rr}(t) = \frac{1}{2}\pi W\ [R_r^4(\rho_r - \rho_w) + \rho_w[R_{rr}(t)]^4] \tag{4.7}$$

where ρ_r is the density of roll, R_r is the radius of roll and W is the width of the roll.

4.1.3 Numerical Solution of Two-Span Roll-to-Roll System

A numerical simulation for describing the transfer of a certain amount of web material from the unwinding roll to the rewinding roll in a two-span configuration is performed. Equations (4.1) - (4.5) are numerically integrated to find the time-domain description of the R2R system's motion. The parameters of the system used in the simulation are given in Table 4.1.

Table 4.1 Parameters of Two-Span R2R configuration

S. No.	Parameter	Value
1	Density of the Web Material	8190 kg/m^3
2	Density of the Roll Material	8050 kg/m^3
3	Thickness of the Web	0.000275 m
4	Width of the Web	0.1 m
5	Modulus of Elasticity of Web	117 GPa
6	Radius of the Unwinding and Rewinding Rolls	0.04 m
7	Initial Radius of Unwinding Roll	0.15 m
8	Initial Radius of Rewinding Roll	0.04 m
11	Frictional Torque at Rolls	0.004 N.m
14	Moment of Inertia of Side Idler Roll (J_b)	0.001 kg.m^2

The angular velocity of unwinding, idler and rewinding rolls vary with time as shown in Figs. 4.2.

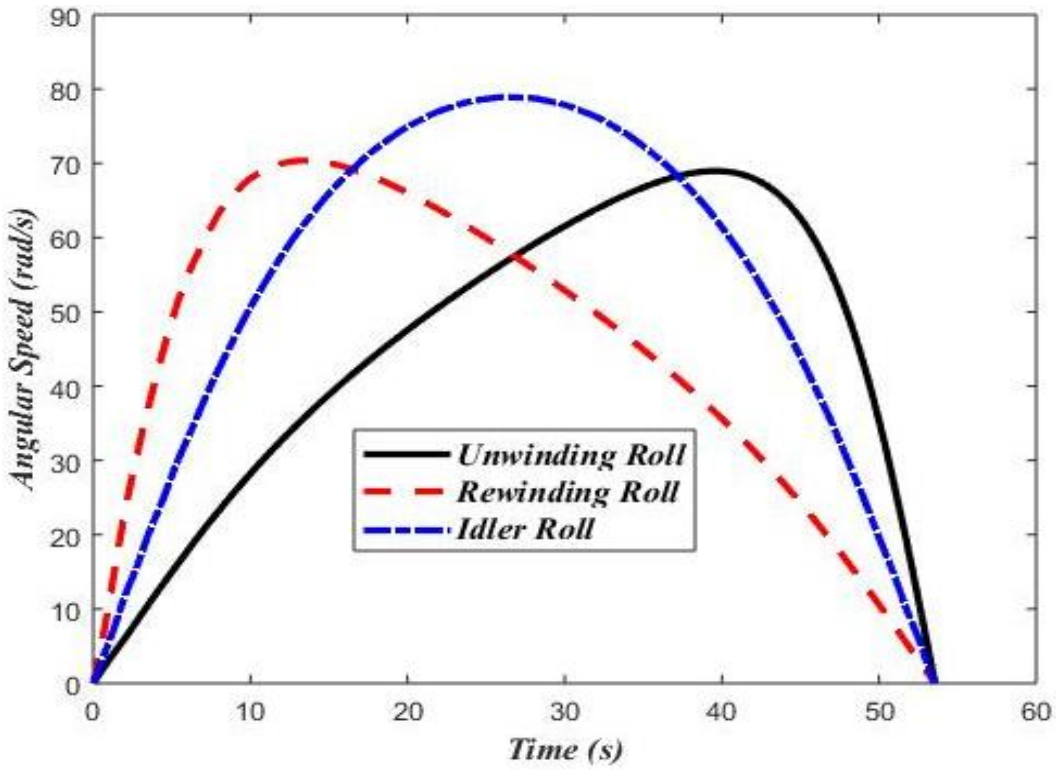

Figure 4.2 Angular velocity variation of rolls

The angular velocity of the rewinding roll increases at a faster rate than the unwinding roll. This is because the rewinding roll initially has a lower moment of inertia than the unwinding roll. The opposite effect occurs after the two rolls reach the same angular velocity. The radii variations will be such that the unwinding roll radius shrinks to the value of the initial radius of the rewinding roll and the rewinding roll radius grows to the value of the initial radius of the unwinding roll within the same time.

Axial tension in the web between two rolls in the first and the second span are shown in Figs. 4.3 and 4.4.

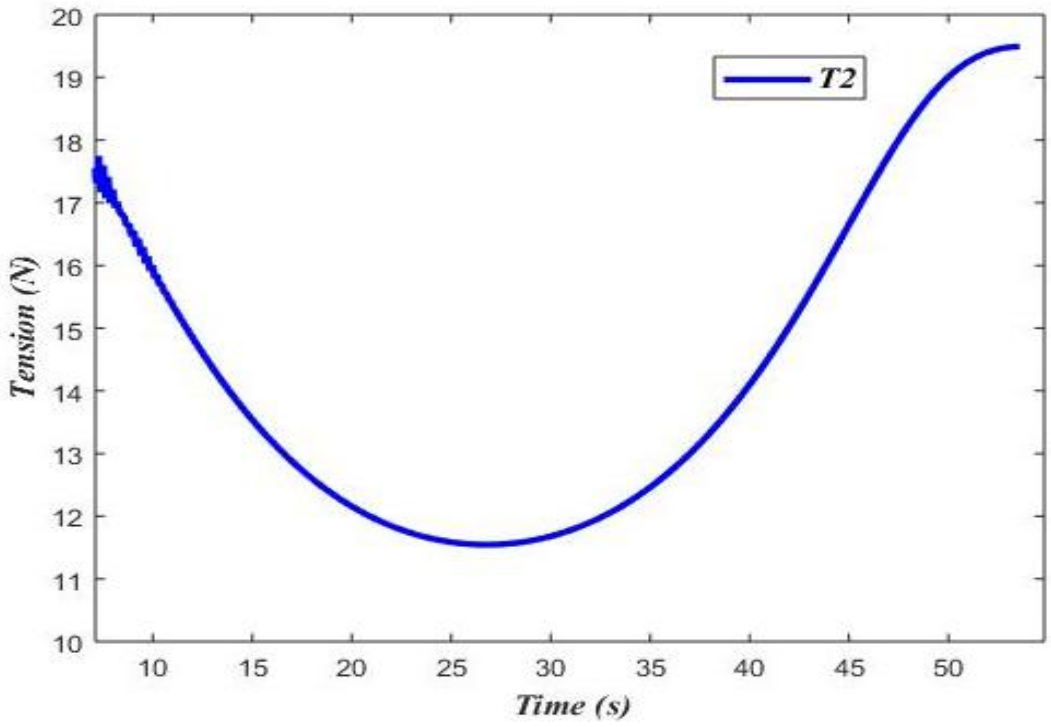

Figure 4.3 Web-transmitted tension (T_2) variation with time

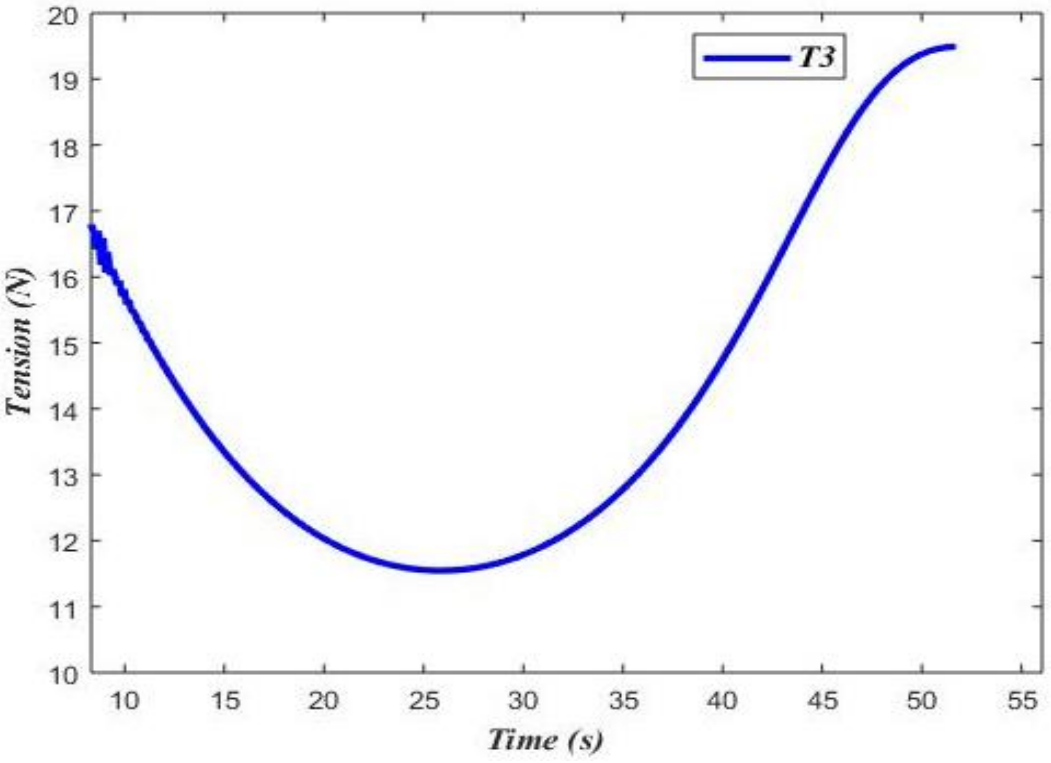

Figure 4.4 Web-transmitted tension (T_3) variation with time

The variation of the web-transmitted tension with time in both spans, shown in Figs. 4.3 and 4.4, is initially transient, and then becomes nonlinear.

4.1.4 Roll-to-Roll System Parameters

The geometry of the roll-to-roll system has an influence on the end-product and must be taken into account for understanding the complete dynamics of the system. So, the effects of system parameters such as the length of the web, moment of inertia of the idler roll and the radius of the rewinding / unwinding rolls on the angular speed and the web transmitted tension are analyzed. The details of this analysis are presented in the sequel.

The effect of idler roll moment of inertia (J_b) on angular speed of each roll is presented in Fig. 4.5. Three different J_b values i.e. $J_b = 0.0001, 0.001$ and 0.01, are considered.

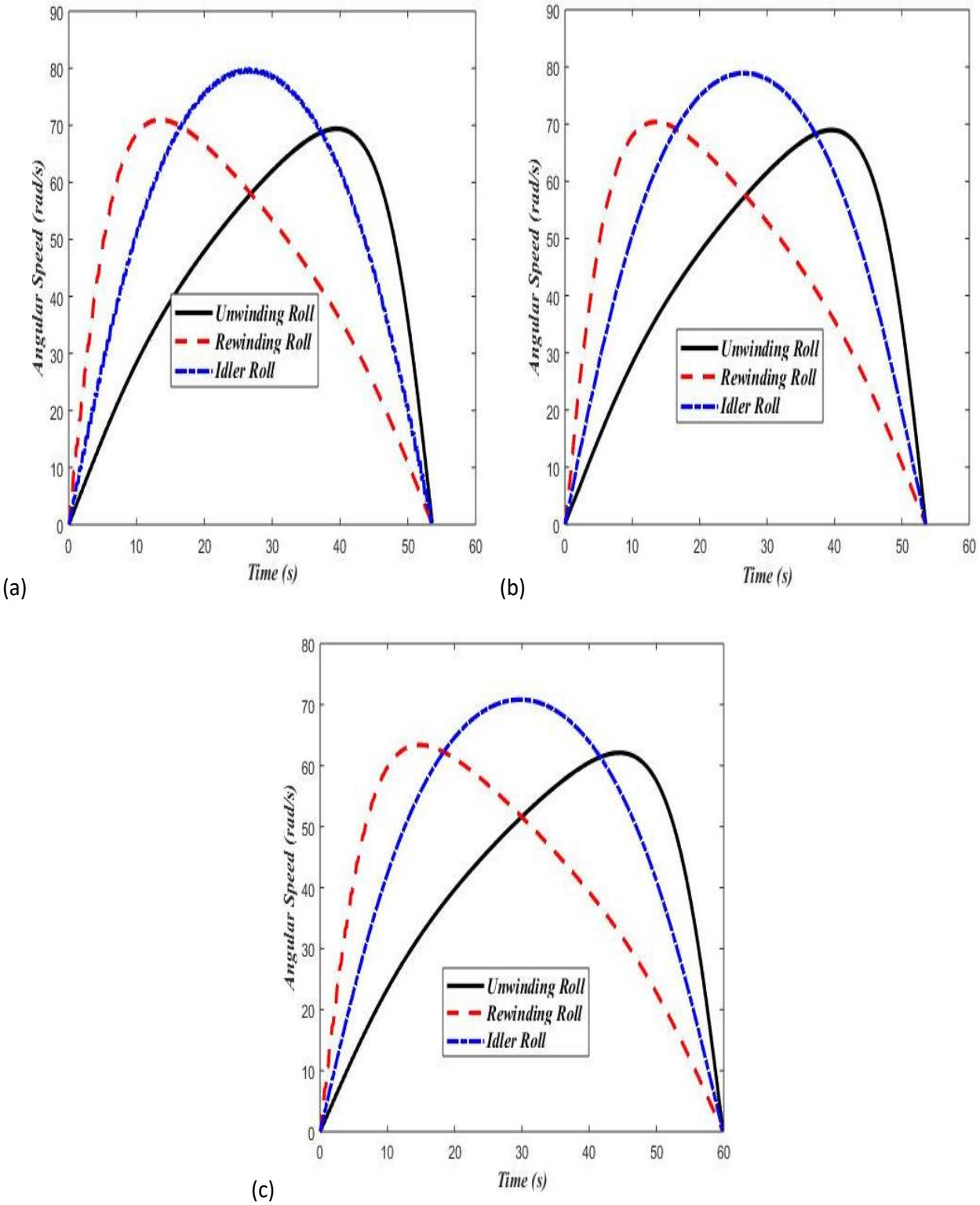

Figure 4.5 Angular velocity variation of rolls, (a) J_b = 0.0001, (b) J_b = 0.001 & (c) J_b = 0.01

Comparing the angular speeds in Fig. 4.5 indicates, that increasing the idler roll moment of inertia leads to a reduced amplitude of the roll angular speed at the expense of the increased time required to transfer the web material from the unwinding roll to the rewinding roll.

Axial web tension in the first and second web spans at different idler roll moment of inertia is shown in Fig. 4.6 and 4.7.

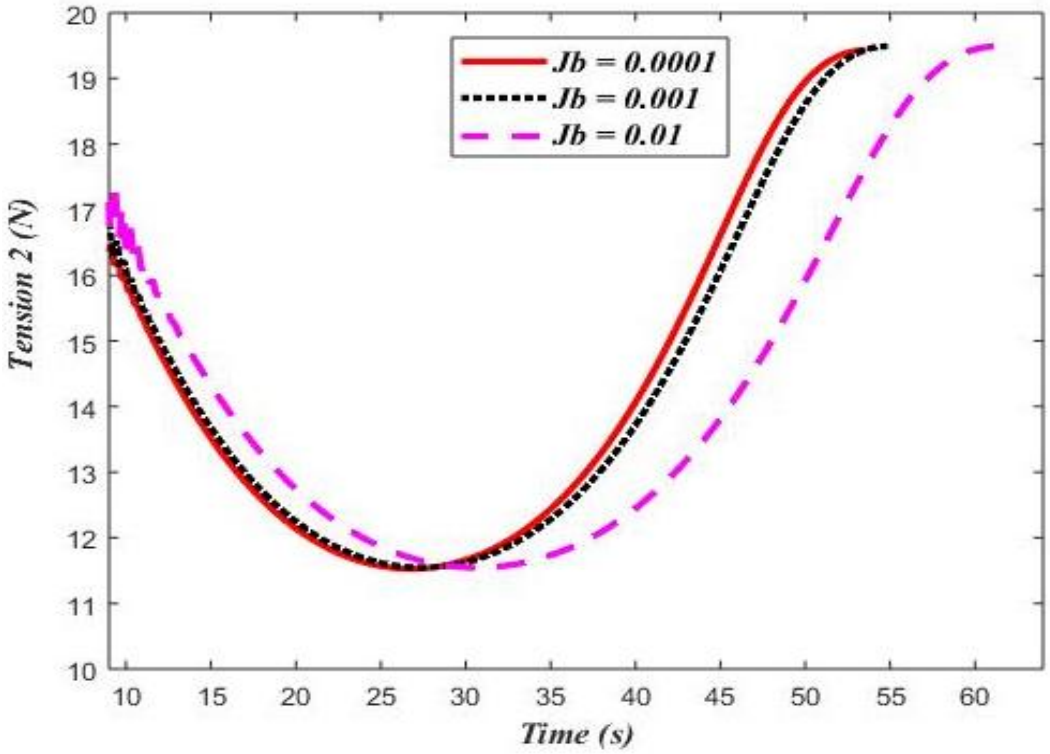

Figure 4.6 Comparing the web-transmitted tension (T_2) at different idler roll inertia

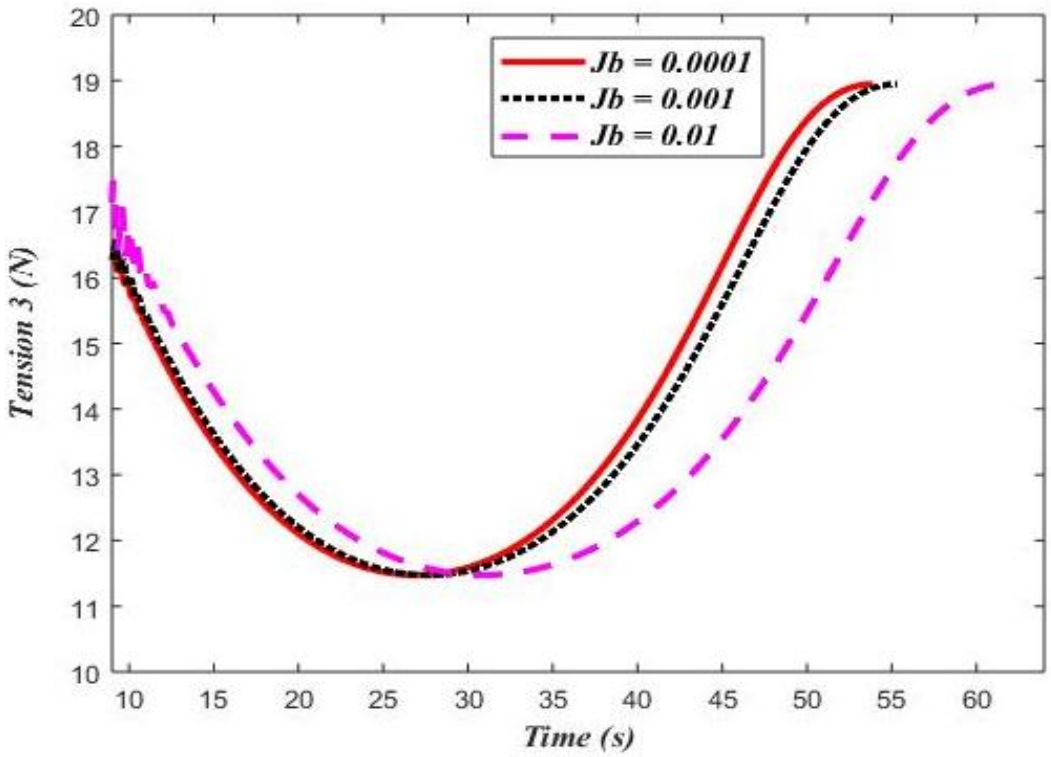

Figure 4.7 Comparing the web-transmitted tension (T_3) at different idler roll inertia

Comparison of the variation in web-transmitted tension with time in both spans indicates that, the magnitude of the tension is affected by the idler roll moment of inertia and time span increases as we increase the idler roll moment of inertia.

The effect of web length on the web transmitted axial tension was studied. Comparison of web tension at the different web lengths, $L = 1.9\ m, 1.5\ m, 1.2\ m, 0.95\ m$ and $0.475\ m$, is shown in Figs. 4.8 and 4.9.

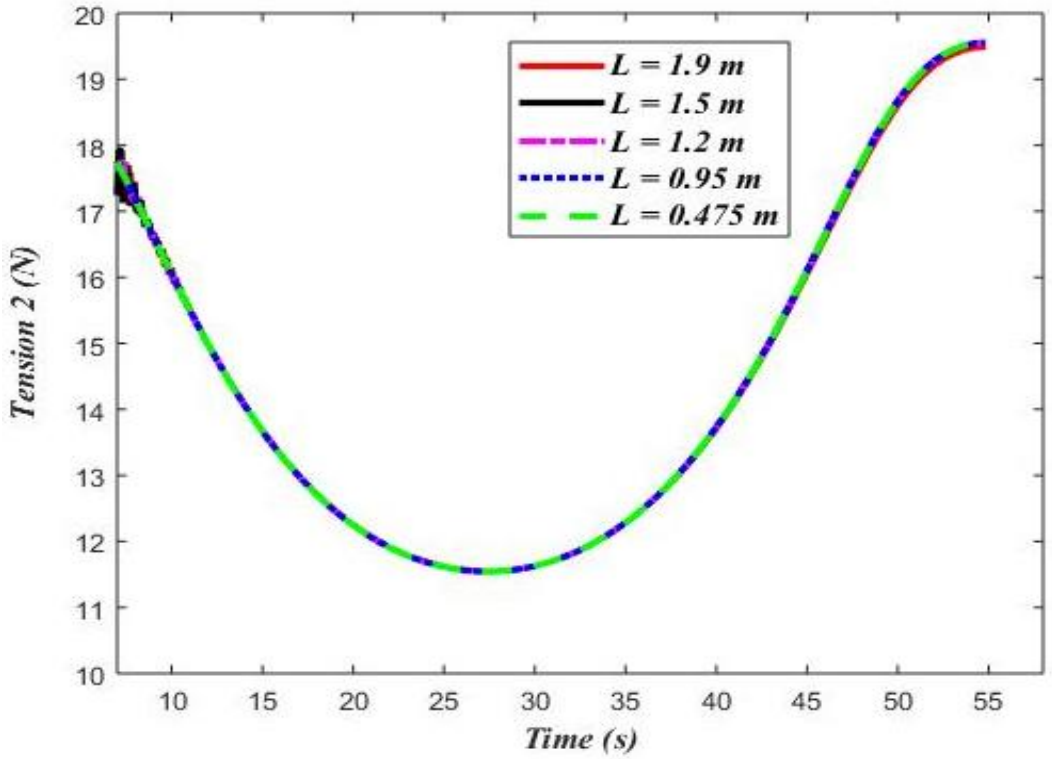

Figure 4.8 Web transmitted tension, T_2

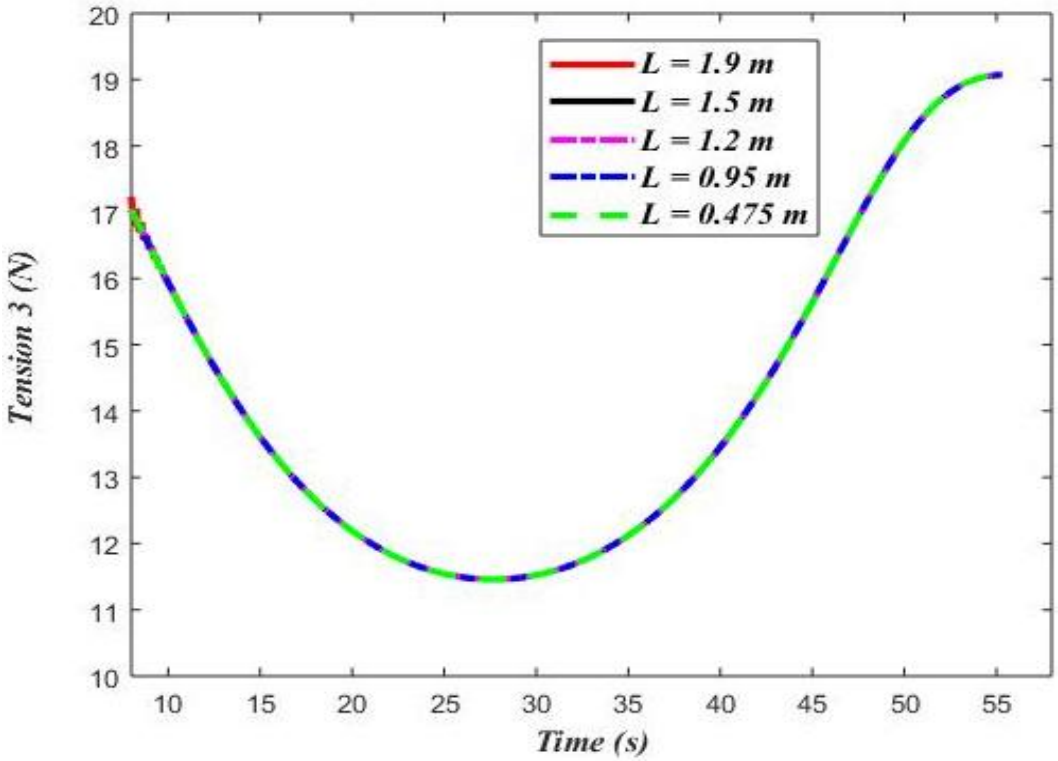

Figure 4.9 Web transmitted tension, T_3

Comparative study shows that changing the web length does not affect the web transmitted-tension in both spans.

The effect of the rewinding roll radius on the angular speed and the web transmitted tension was also studied. The angular speed of each roll is presented in Fig. 4.10.

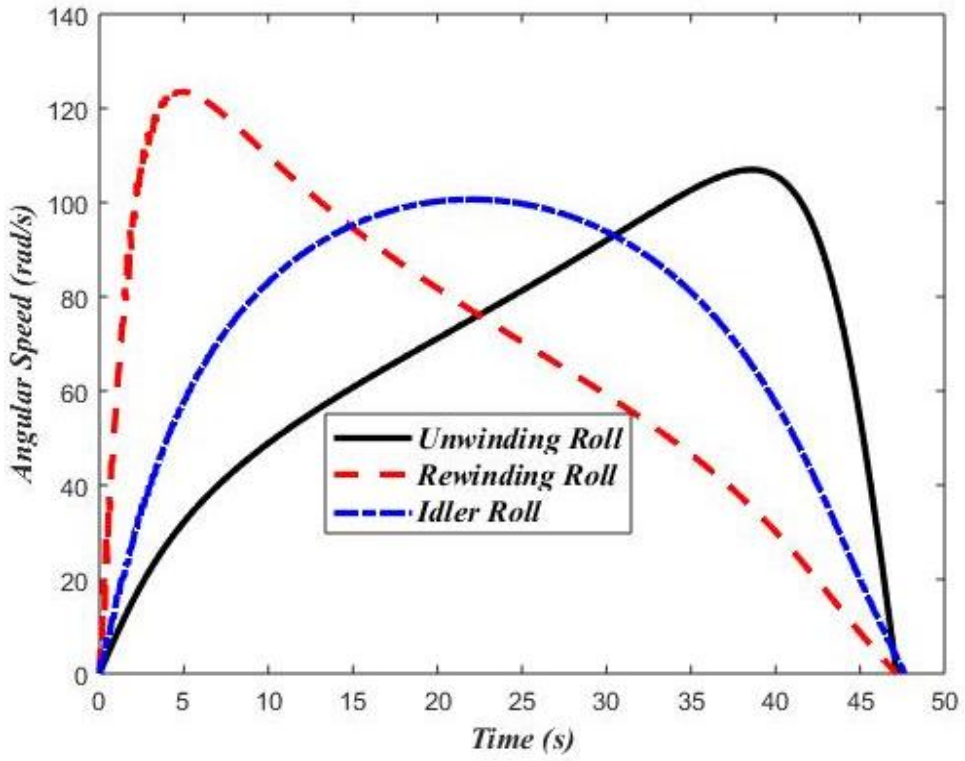

Figure 4.10 Time history of angular speed (R_{ur} = 0.04 m & R_{rr} = 0.02 m)

By reducing the rewinder roll radius, the angular velocity of the rewinding roll increases at a faster rate than the unwinding roll. This is because the rewinding roll initially has a lower moment of inertia than the unwinding roll. Furthermore, comparison of angular speeds in Fig. 4.10, indicates that reducing the rewinding roll radius leads to an increased amplitude in the roll angular speed and reduces the time required to transfer the web material from the unwinding roll to the rewinding roll.

Axial tension in the web between the two rolls in the first and second span are shown in Figs. 4.11 and 4.12.

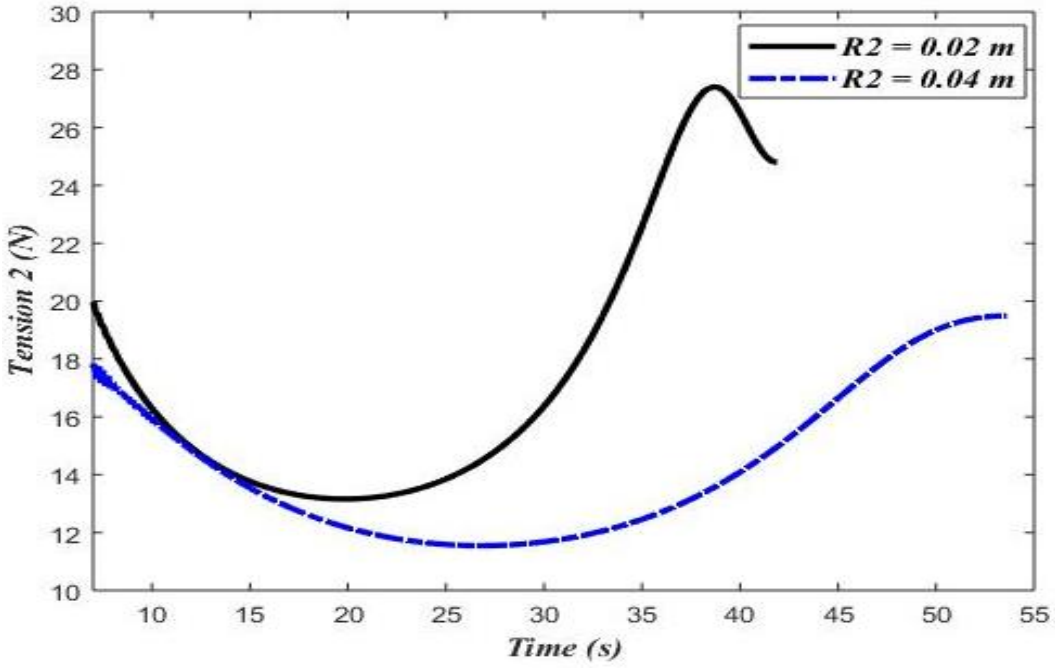

Figure 4.11 (a) Web transmitted tension, T_2 (R_{rr} = 0.02 m & 0.04 m)

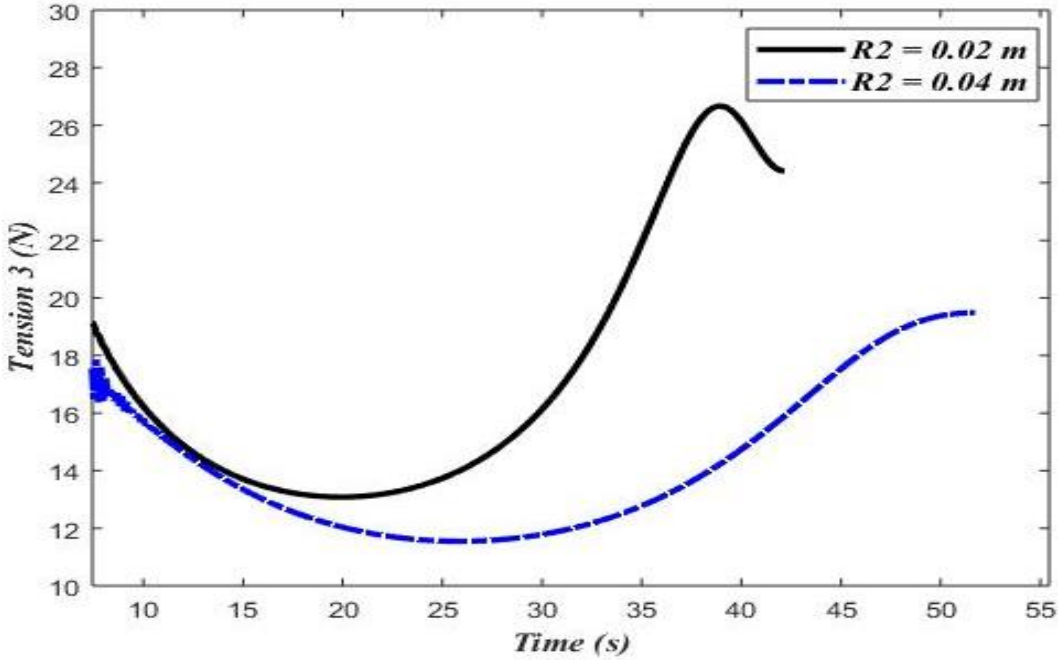

Figure 4.12 Web transmitted tension, T_3 (R_{rr} = 0.02 m & 0.04 m)

Comparison shows that reducing the rewinder radius not only reduces the time span, it also increases the magnitude of the variation in axial tension. A closer look at the axial tension, reveals that the magnitude of the web tension is increased by reducing the rewinding roll radius.

4.2 The Coupled Web Vibration

In a multi-span roll-to-roll system boundary conditions are different for each span. In the unwinding span, the radius of the idler roll will remain constant, whereas the radius of the unwinding roll will decrease (starting from the outer radius) with time, i.e. at the left boundary there is a varying transverse displacement. For these boundary conditions, the finite difference approach is used to discretize the equation (3.45). The discretized second-order ODEs representing the equation of motion for web transverse vibration in the unwinding span are given by

$$\left.\begin{aligned}
&\frac{d^2w_{*0}}{dt_*^2} = -\frac{\dot{\Omega}_u}{2\pi}h \\
&\frac{d^2w_{*1}}{dt_*^2}+\frac{v_*}{dx_*}\frac{dw_{*2}}{dt_*}-\frac{v_*}{dx_*}\frac{dw_{*0}}{dt_*}+\frac{(v_*^2-1)}{{dx_*}^2}(w_{*0}-2*w_{*1}+w_{*2})+\frac{\dot{v_*}}{2*\mathrm{d}x_*}(w_{*2}-w_{*0}) = 0 \\
&\frac{d^2w_{*2}}{dt_*^2}+\frac{v_*}{dx_*}\left(-\frac{dw_{*1}}{dt_*}+\frac{dw_{*3}}{dt_*}\right)+\frac{(v_*^2-1)}{{dx_*}^2}(w_{*1}-2*w_{*2}+w_{*3})+\frac{\dot{v_*}}{2*\mathrm{d}x_*}(-w_{*1}+w_{*3}) = 0 \\
&\qquad\vdots \\
&\frac{d^2w_{*(n-1)}}{dt_*^2}+\frac{v_*}{dx_*}\frac{dw_{*(n-2)}}{dt_*}+\frac{(v_*^2-1)}{{dx_*}^2}\left(w_{*(n-2)}-2*w_{*(n-1)}\right)+\frac{\dot{v_*}}{2*\mathrm{d}x_*}(w_{*(n-2)}) = 0
\end{aligned}\right\} \quad (4.8)$$

Note that n and $\mathrm{d}x_*$ represent the total number of spatial points and the step size, respectively.

In contrast to the unwinding span, in the rewinding span the radius of the idler roll will remain constant, whereas the radius of the rewinding roll will increase with time, i.e. at the right boundary there is a varying transverse displacement. The discretized second-order ODEs representing the equation of motion for the web transverse vibration in the rewinding span are given by

$$\left.\begin{aligned}
&\frac{d^2w_{*1}}{dt_*^2}+\frac{v_*}{dx_*}\frac{dw_{*2}}{dt_*}+\frac{(v_*^2-1)}{{dx_*}^2}(-2*w_{*1}+w_{*2})+\frac{\dot{v_*}}{2*\mathrm{d}x_*}*w_{*2}=0\\
&\frac{d^2w_{*2}}{dt_*^2}+\frac{v_*}{dx_*}\left(-\frac{dw_{*1}}{dt_*}+\frac{dw_{*3}}{dt_*}\right)+\frac{(v_*^2-1)}{{dx_*}^2}(w_{*1}-2*w_{*2}+w_{*3})+\frac{\dot{v_*}}{2*\mathrm{d}x_*}(-w_{*1}+w_{*3})=0\\
&\qquad\vdots\\
&\frac{d^2w_{*(n-1)}}{dt_*^2}+\frac{v_*}{dx_*}\left(\frac{dw_{*(n-2)}}{dt_*}-\frac{dw_{*(n)}}{dt_*}\right)+\frac{(v_*^2-1)}{{dx_*}^2}\left(w_{*(n-2)}-2*w_{*(n-1)}+w_{*(n)}\right)+\\
&\qquad+\frac{\dot{v_*}}{2*\mathrm{d}x_*}(w_{*(n-2)}-w_{*(n)})=0\\
&\frac{d^2w_{*n}}{dt_*^2}=\frac{\dot{\Omega}_r}{2\pi}h
\end{aligned}\right\}\quad(4.9)$$

Equations (4.8) and (4.9) describing the transverse vibration in the unwinding and rewinding span, are solved together as a coupled system of equations (4.1) - (4.5). The initial conditions (3.59) and (3.60) are used for solving the coupled system for the time-domain response. Figs. 4.14 - 4.15 show the dynamic responses monitored at the three representative locations (x_*= 0.25, 0.50 and 0.75), for the unwinding span.

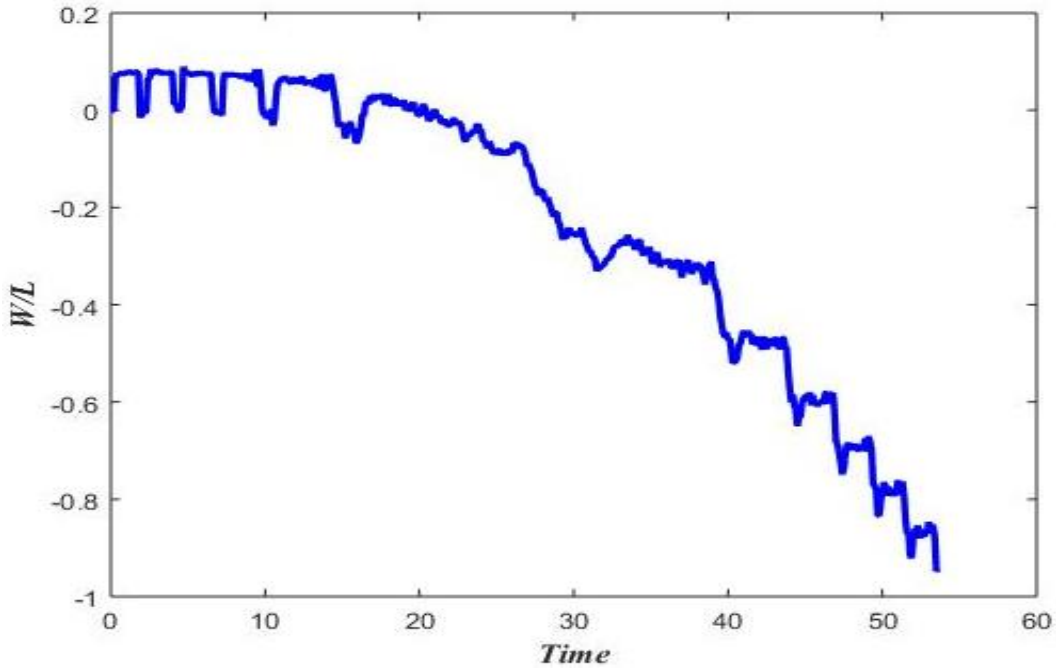

Figure 4.13 Transverse displacement at $x_* = 0.25$ (Unwinding Span)

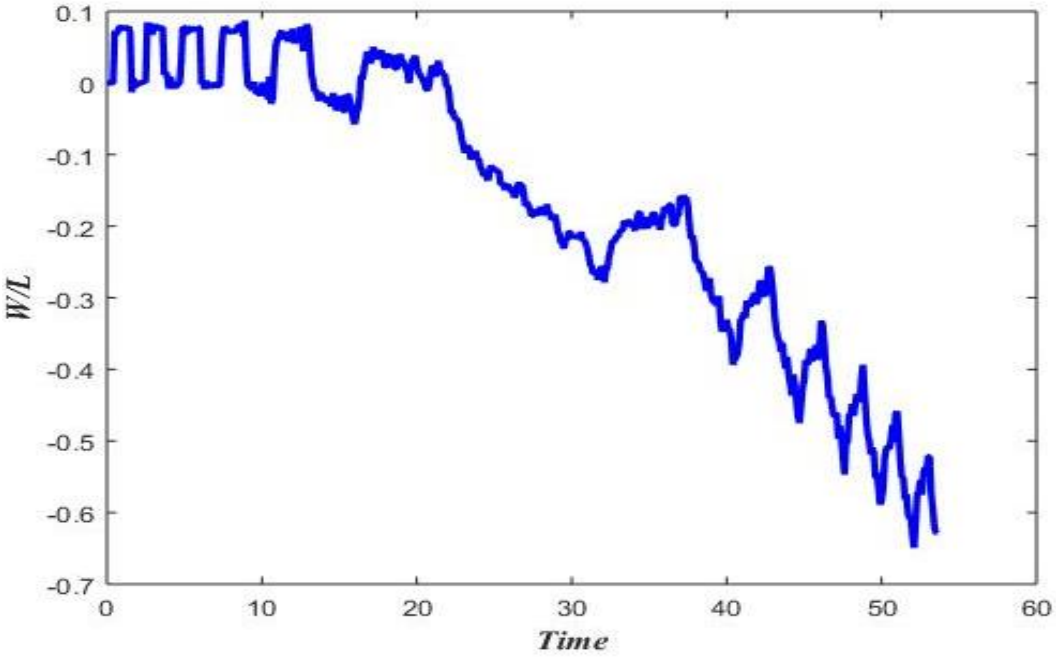

Figure 4.14 Transverse displacement at $x_* = 0.50$ (Unwinding Span)

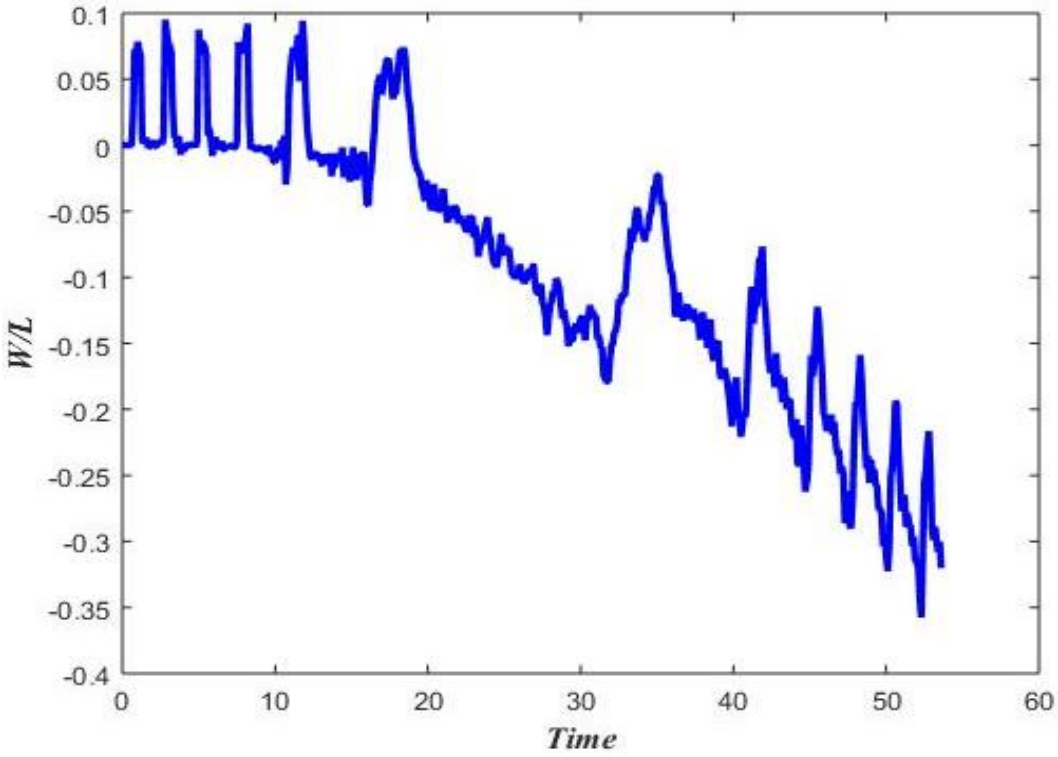

Figure 4.15 Transverse displacement at $x_* = 0.75$ (Unwinding Span)

The responses presented in Figs. 4.13 – 4.15 indicate non-periodic oscillations. It's worth noting that the magnitude of the response constantly decreases as the displacement at the left boundary decreases. At the early and late phases of material transfer from the unwinding roll to the rewinding roll, the axial web speed changes rapidly with time, leading to high levels of frequency fluctuation in the dynamic response.

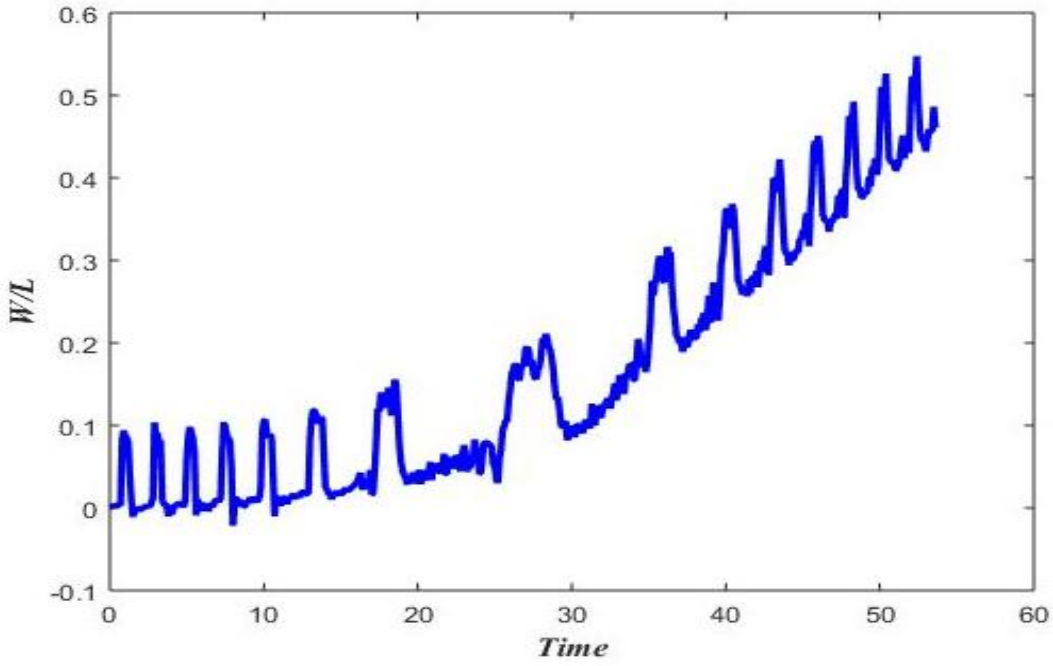

Figure 4.16 Transverse displacement at $x_* = 0.25$ (Rewinding Span)

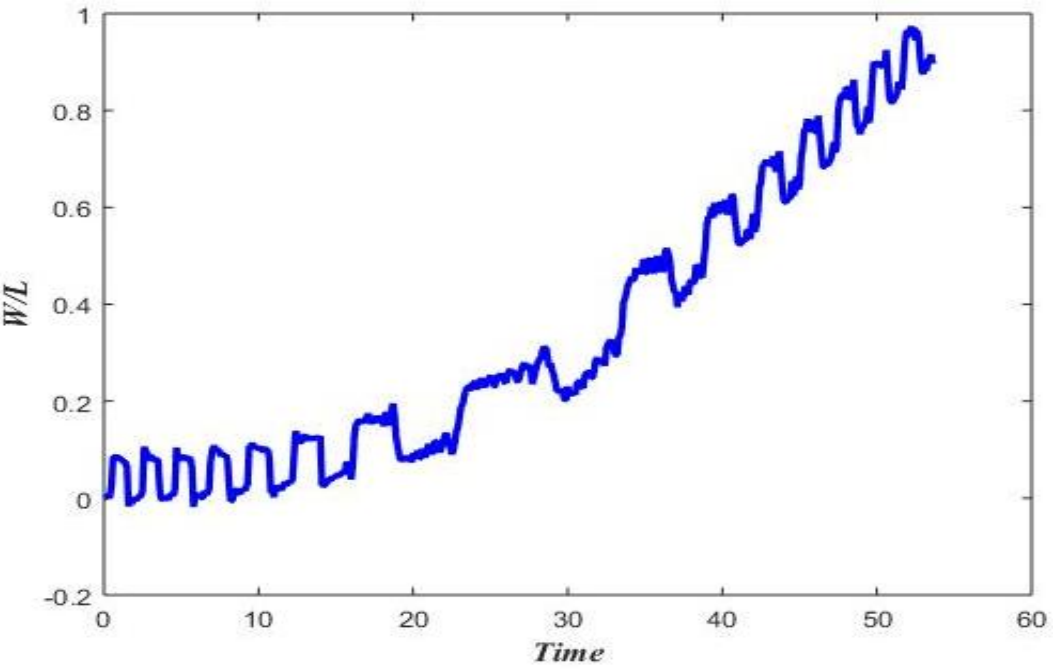

Figure 4.17 Transverse displacement at $x_* = 0.50$ (Rewinding Span)

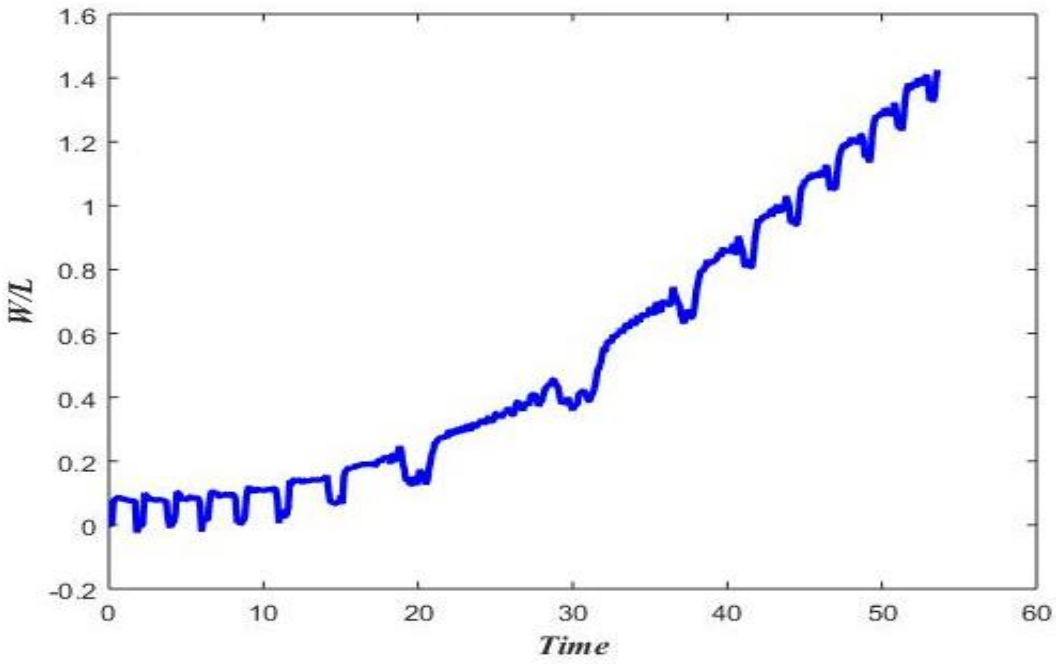

Figure 4.18 Transverse displacement at $x_* = 0.75$ (Rewinding Span)

Like the unwinding span, in rewinding span, the axial web speed will vary with time. The responses presented in Figs. 4.16 - 4.18 indicate non-periodic oscillations. The magnitude of the response constantly increases as the displacement at the right boundary increases. A low frequency response is noted in the middle of the web material transfer time interval, due to the slow change in the axial web speed with time.

CHAPTER 5

MULTI-SPAN ROLL-TO-ROLL PRINTING SYSTEM

5.1 Roll-to-Roll Dynamic

The methodology used for the single-span R2R system is applied to the five-roll and four-span μFLEX machine developed at MIT, shown in Fig. 1.3. Utilizing equation (3.16), the web tension-velocity relation for each span of the roll-to-roll system, represented in Fig. 5.1, is given by

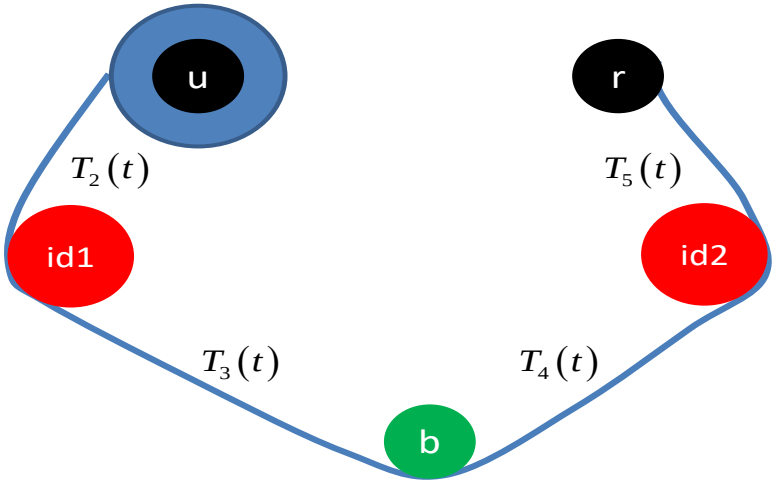

Figure 5.1 Four Span Roll-to-Roll System

$$\frac{dT_2}{dt} \approx \left[-\frac{EAR_u}{L_1}\right]\Omega_u + \left[\frac{EAR_{id1}}{L_1} + \frac{T_2\ R_{id1}}{L_1}\right]\Omega_{id1} \tag{5.1}$$

$$\frac{dT_3}{dt} \approx \left[\frac{EAR_b}{L_2} - \frac{T_3\,R_b}{L_2}\right]\Omega_b + \left[\frac{T_2\ R_{id1}}{L_2} - \frac{EAR_{id1}}{L_2}\right]\Omega_{id1} \tag{5.2}$$

$$\frac{dT_4}{dt} \approx \left[\frac{T_3\,R_b}{L_3} - \frac{EAR_b}{L_3}\right]\Omega_b - \left[\frac{T_4\ R_{id2}}{L_3} - \frac{EAR_{id2}}{L_3}\right]\Omega_{id2} \tag{5.3}$$

$$\frac{dT_5}{dt} \approx -\left[\frac{T_5\,R_r}{L_4} - \frac{EAR_r}{L_4}\right]\Omega_r + \left[\frac{T_4\ R_{id2}}{L_4} - \frac{EAR_{id2}}{L_4}\right]\Omega_{id2} \tag{5.4}$$

Utilizing equation (3.17), the equation of motion for individual roll is given by

$$\frac{\mathrm{d}\Omega_u}{\mathrm{d}t} = \frac{1}{\frac{1}{2}\pi W\,[R_{rr}^4(\rho_r - \rho_w) + \rho_w R_u^4]}\Big[(R_u T_2 + B_u\Omega_u - C_u) + \Omega_u\left(\rho_w * W * h\,\left(\left(R_u(t)\right)^3 * \Omega_u\right)\right)\Big] \tag{5.5}$$

$$\frac{d\Omega_{id1}}{dt} = \left[\frac{T_3}{J_{id1}} - \frac{T_2}{J_{id1}}\right]R_{id1} - \frac{1}{J_{id1}}\,C_{id1} \tag{5.6}$$

$$\frac{d\Omega_b}{dt} = \left[\frac{T_4}{J_b} - \frac{T_3}{J_b}\right]R_b - \frac{1}{J_b}\,C_b \tag{5.7}$$

$$\frac{d\Omega_{id2}}{dt} = \left[\frac{T_5}{J_{id2}} - \frac{T_4}{J_{id2}}\right]R_{id2} - \frac{1}{J_{id2}}\,C_{id2} \tag{5.8}$$

$$\frac{\mathrm{d}\Omega_r}{\mathrm{d}t} = \frac{1}{\frac{1}{2}\pi W\,[R_{rr}^4(\rho_r - \rho_w) + \rho_w R_r^4]}\Big[(-R_r T_5 + B_r\Omega_r - C_r) + \Omega_r\left(\rho_w * W * h\,\left(\left(R_r(t)\right)^3 * \Omega_r\right)\right)\Big] \tag{5.9}$$

Equations (5.1) - (5.9) are numerically integrated to find the time-domain description of R2R system's motion. Parameters of the system used in the simulation are given in Table 5.1.

Table 5.1 Parameters of Four-Span R2R configuration

S. No.	Parameter	Value
1	Density of the Web Material	8190 kg/m^3
2	Density of the Roll Material	8050 kg/m^3
3	Thickness of the Web	0.000275 m
4	Width of the Web	0.1 m
5	Modulus of Elasticity of Web	117 GPa
6	Radius of the Unwinding and Rewinding Rolls	0.04 m
7	Initial Radius of Unwinding Roll	0.15 m
8	Initial Radius of Rewinding Roll	0.04 m
9	Radius of the Side Idler Roll (R_{id1} & R_{id2})	0.038 m
10	Radius of the Central Idler Roll (R_b)	0.076 m
11	Frictional Torque at Rolls	0.004 N.m
12	Length of each Span (L_1, L_2, L_3 & L_4)	0.3 m
13	Moment of Inertia of Idler Roll (J_{id1} & J_{id2})	0.001 kg.m^2
14	Moment of Inertia of Idler Roll (J_b)	0.02443 kg.m^2

The angular velocity variation of the unwinding, rewinding, idler and impression rolls with time is shown in Fig. 5.2.

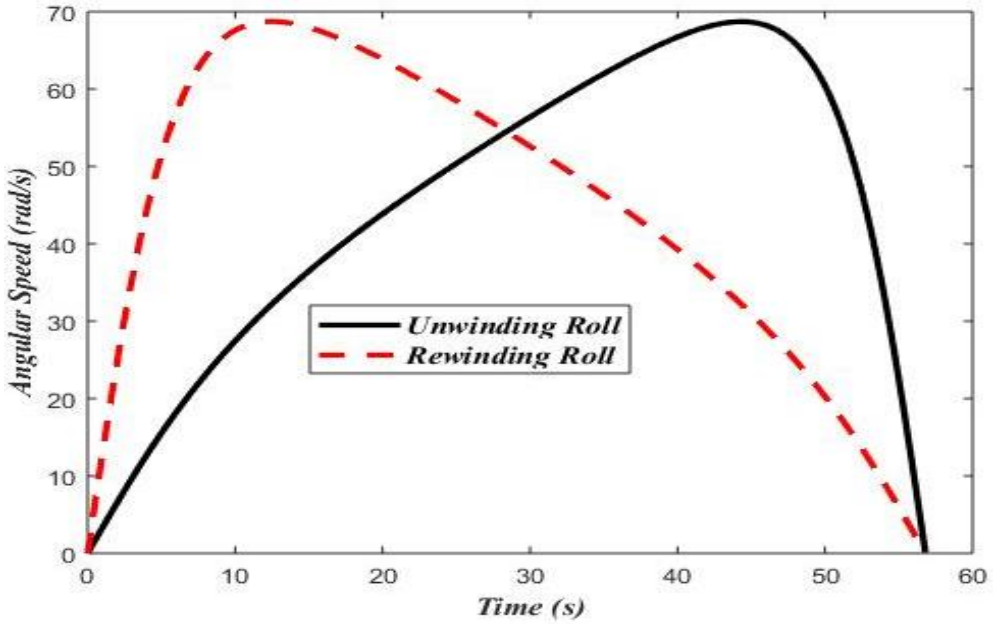

(a)

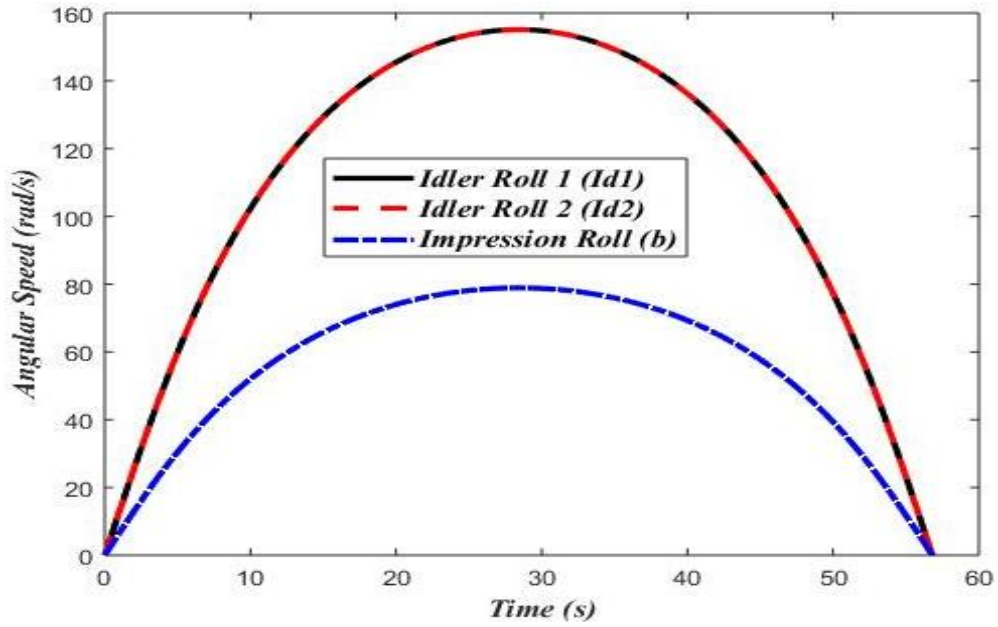

(b)

Figure 5.2 Angular velocity variation of (a) Unwinding & Rewinding rolls, and (b) Idler & Impression rolls

Comparing the angular speeds in Fig. 5.2, the impression roll with the maximum inertia will attain the minimum magnitude of angular speed.

The angular displacement and radii variation of the unwinding and rewinding rolls with time is shown in Fig. 5.3. Both rolls attain the same maximum angular displacement within the same time frame.

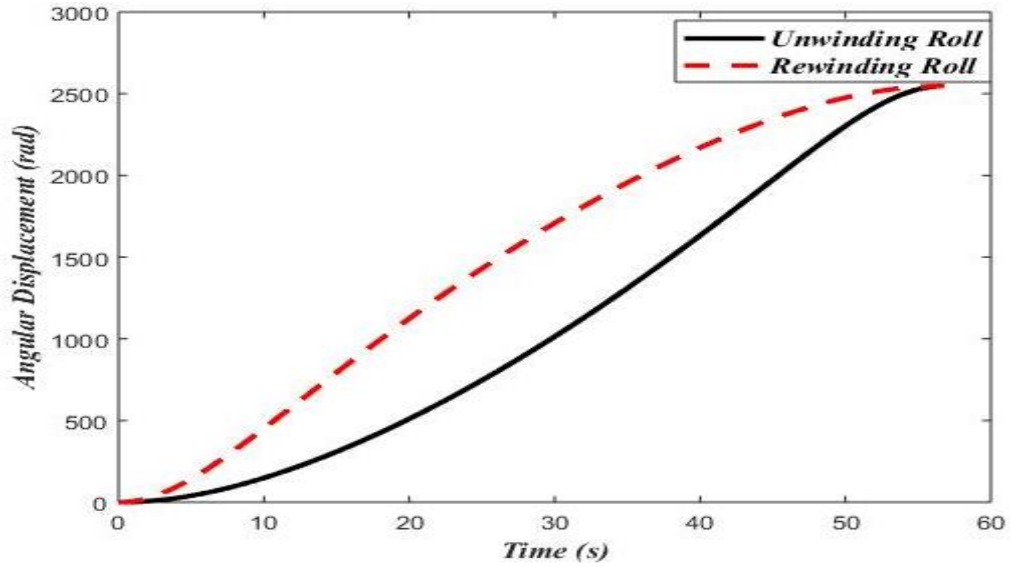

(a)

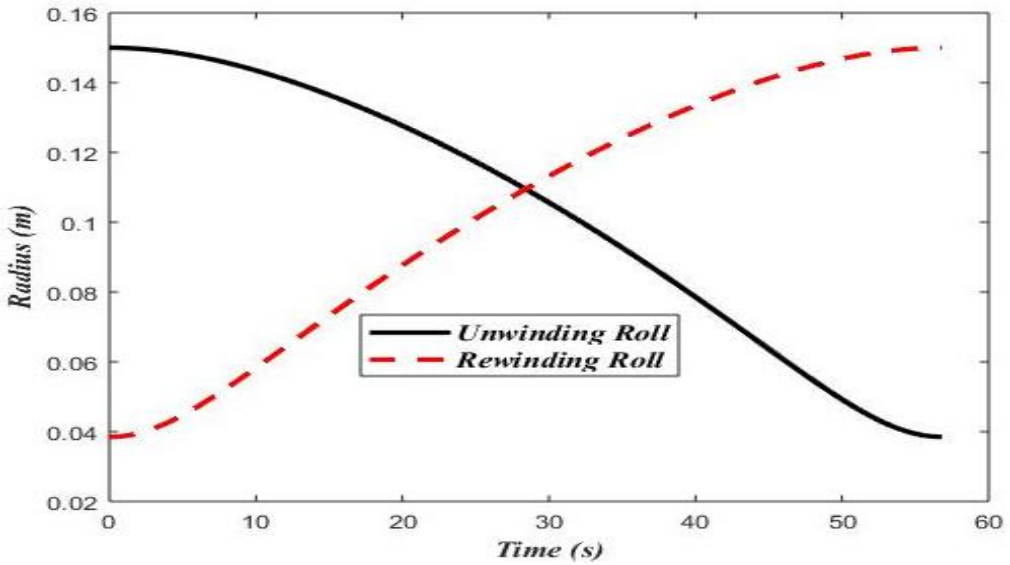

(b)

Figure 5.3 (a) Angular displacement variation and (a) Radii variation of Unwinding & Rewinding rolls

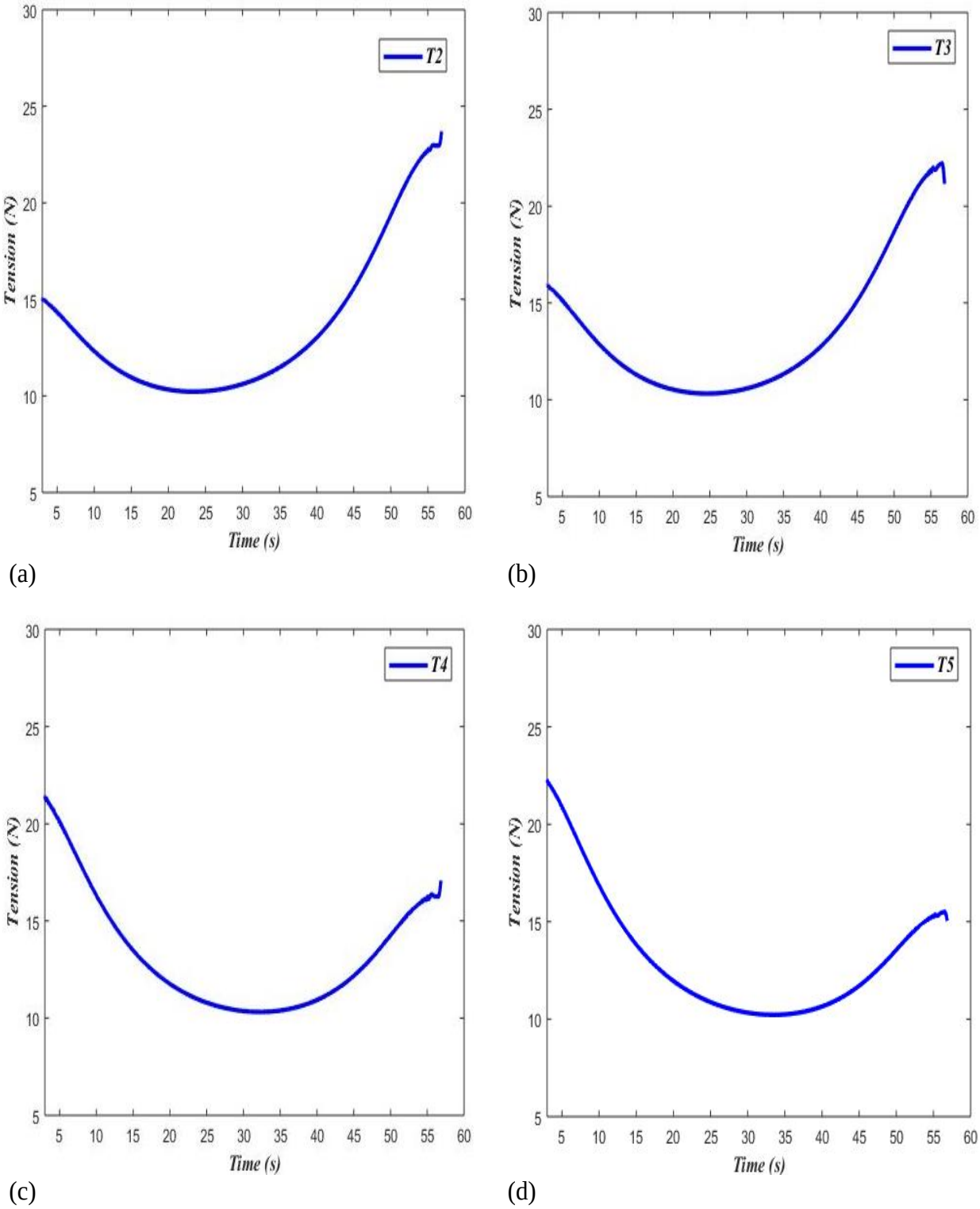

Figure 5.4 Web transmitted-tension variation with time (a) T_2, (b) T_3, (c) T_4 and (d) T_5

The variation of the web-transmitted tension with time in each span, shown in Fig. 5.4, is initially transient, and then becomes nonlinear.

5.2 Validation of Web Dynamic Model

To verify the mathematical model developed for the web dynamics, experiments were performed in the Laboratory of Manufacturing and Productivity at Massachusetts Institute of Technology (MIT). A roll-to-roll micro-contact printing machine built by the MIT team was used in these experiments, shown in Figs. 5.5 and 5.6.

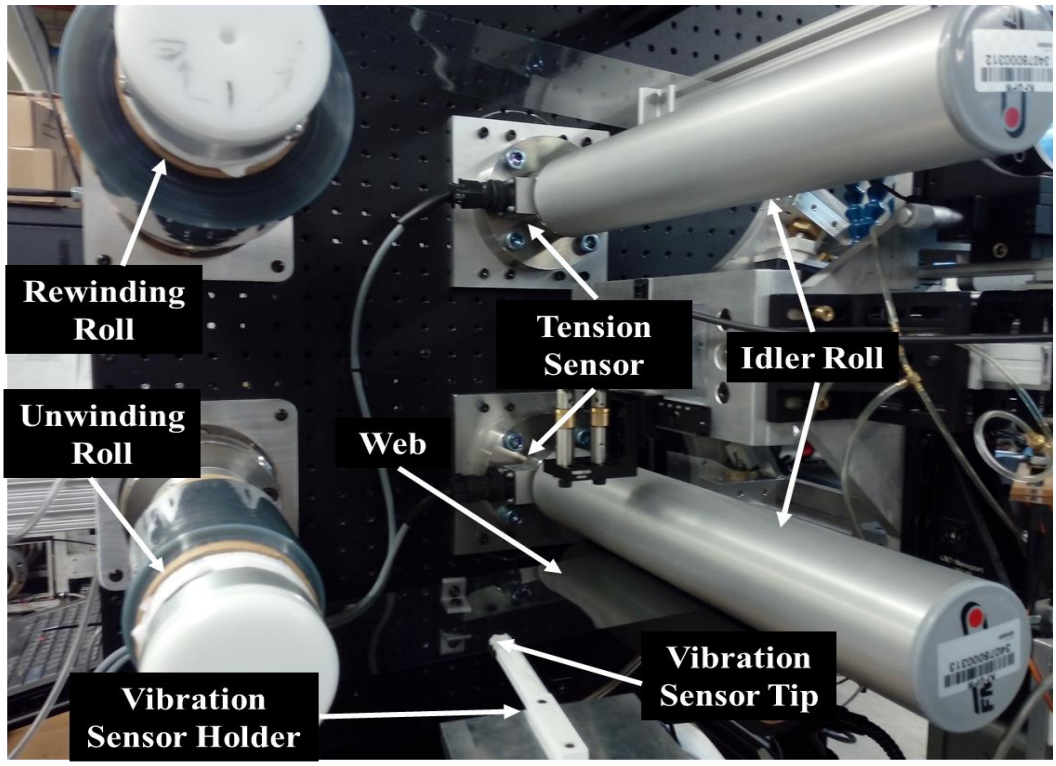

Figure 5.5 Experimental setup

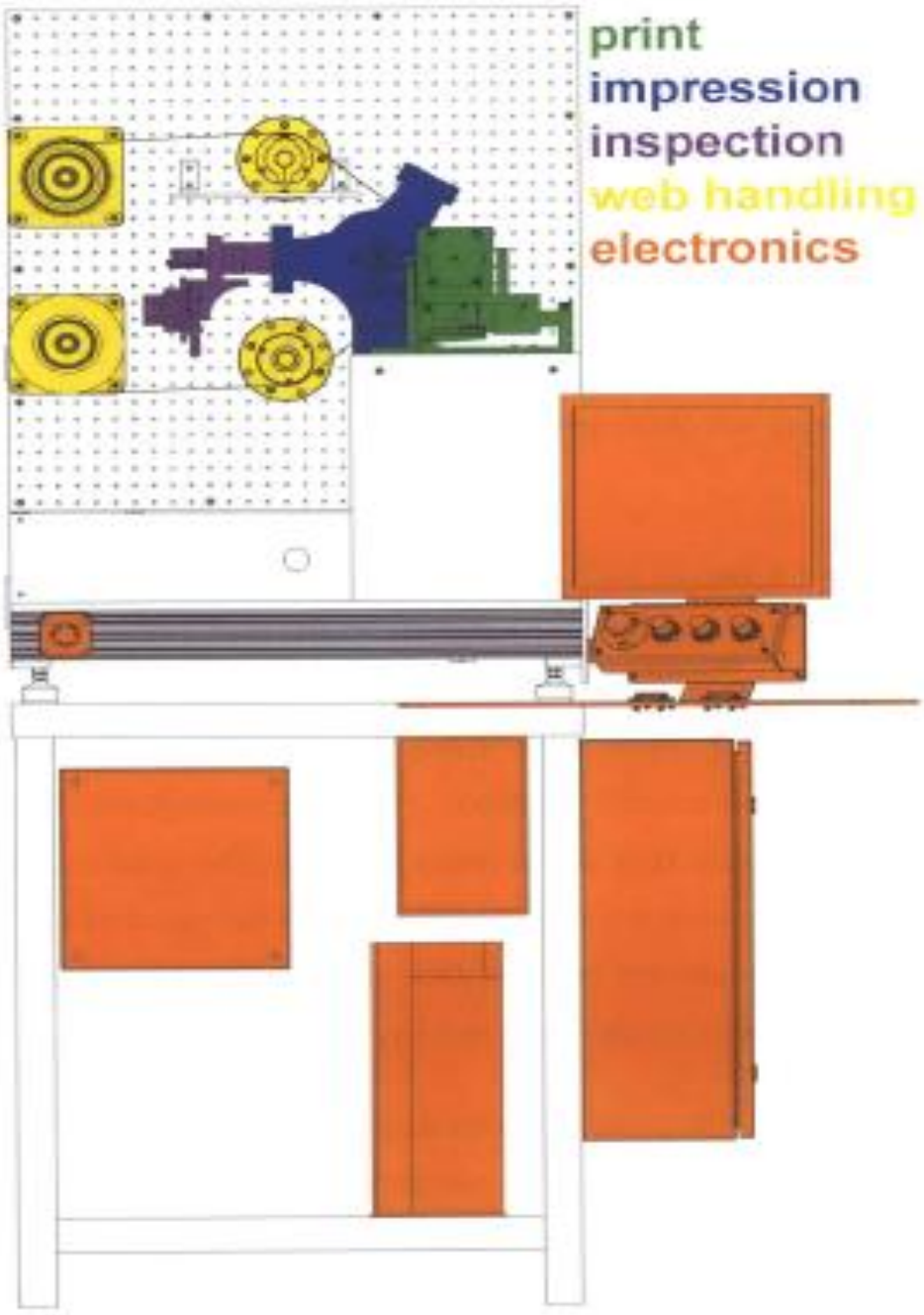

Figure 5.6 System's critical component layout [2]

Micro-contact printing is a promising technology in which a patterned elastomeric stamp is used to transfer patterns of self-assembled monolayers onto a substrate. The simplest web-handling machine might be one with just two rolls: an unwinding and a rewinding roll. The roll-to-roll used is a multi-span machine with two active, two idlers and an impression roll as shown in Fig. 5.6. Web is fed from the unwinding roll, passing through the two idler and an impression roll where microcontact printing is performed on the moving web before it is rewound by the rewinding roll.

The objective of the experiment is to verify the mathematical model by comparing the fundamental frequencies of the system at different web speeds and tensions. A precise tension control system, described in the next section, was installed for this purpose and a micro-measurement displacement sensor was used for vibration measurement.

5.2.1 Tension Measurement/Control System

To measure and control the web tension, the 'FMS CMGZ 309' tension controller was installed in the system alongside the force measuring roll. It is a microprocessor based PID-controller designed for precise closed loop tension control of a running web. The tension controller consists of the following components:

- **Strain Gauge Amplifier**

Strain gauge amplifier delivers a highly accurate supply voltage (5 VDC) for one or two sensors. A highly accurate differential amplifier raises the mV sensor signal up to 10V.

- **Force Sensor**

The operational reliability and accuracy of the measurement determines the productivity and quality of the processing. The type of processing, the material, and factors such as temperature, humidity and the changing winding diameters lead to continuous variations in the tension in the processed material.

The web tension in the material (FB) causes a resulting force in the direction of the bisecting line (FM) on a wrapped roller as shown in Fig. 5.7. The measurement of this force is a direct measure of the web tension. The feedback value can be sent to an FMS closed loop tension controller, which regulates the drive, ensuring constant material tension throughout the process.

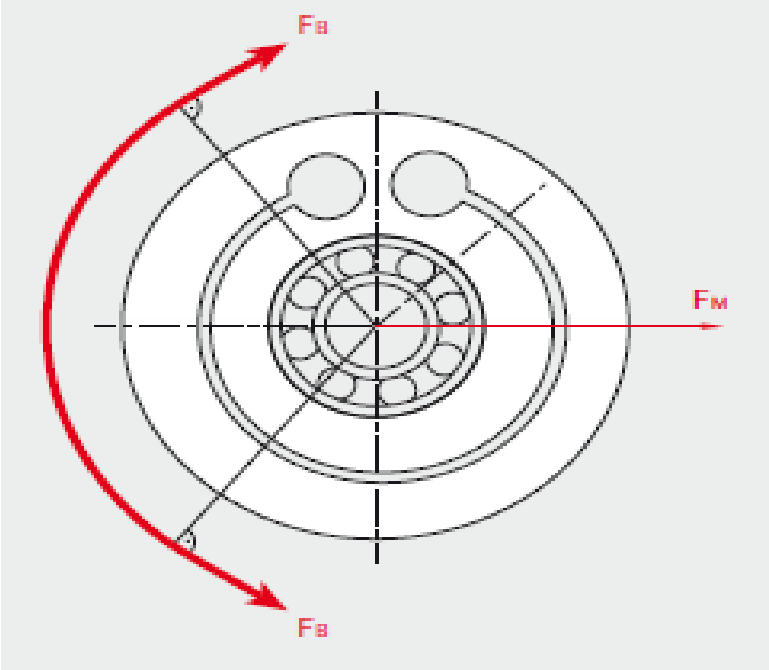

Figure 5.7 FMS web tension measurement

- **PID Controller**

The comparator unit compares the reference value with the measured feedback value and transmit the error to the PID controller. The PID controller calculate the output signal according to the difference. The output signal can be 0-10V or 0-20Ma. The close loop tension control process is summarized in Fig. 5.8.

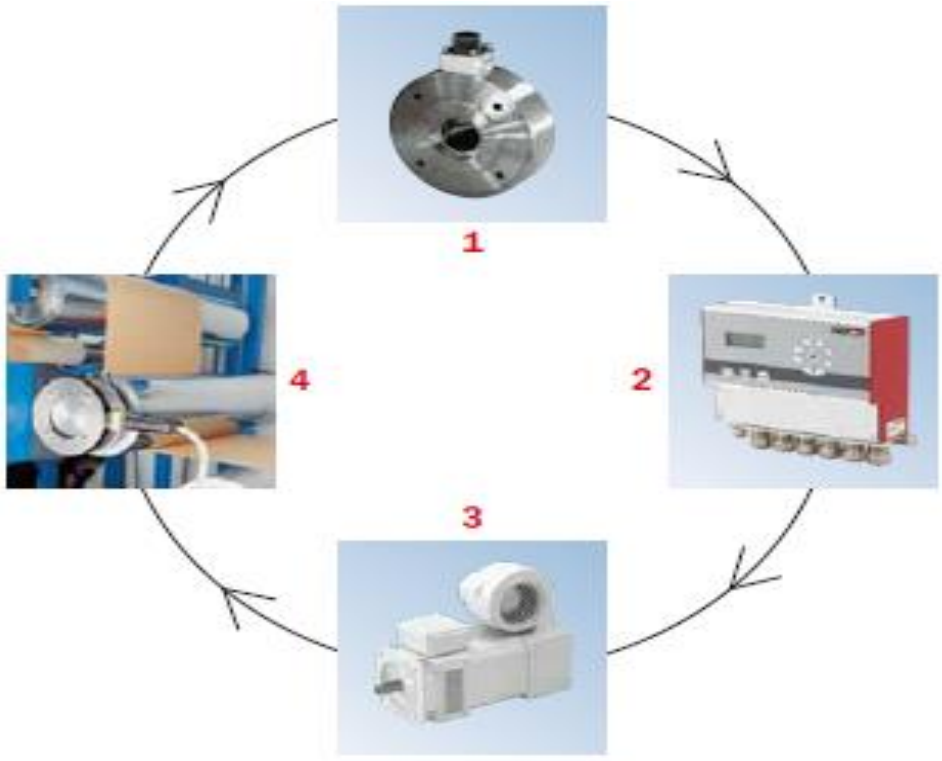

Figure 5.8 Tension control process

1. Force sensors measure the axial tension.

2. The tension controller amplifies the measured signal from the force sensor and calculates an output value from the difference between the reference and feedback values.
3. The drive converts the output value from the tension controller into a corresponding torque or speed.
4. The tension in the web is maintained.

5.2.2 Fiber Optic Micro Displacement Measurement Systems (µDMS)

µDMS is a displacement measurement system with type D-fiber optics which are microprocessor-based systems for providing linearized outputs of distance using the USB 2.0 protocol. There are two types of fiber-optic probes: D and RC models. D-types have a random mixture of transmitting and receiving fibers which are always in round bundles, shown in Fig. 5.9. Whereas RC-models are made of both round and rectangular fiber-optic bundles, shown in Fig. 5.10.

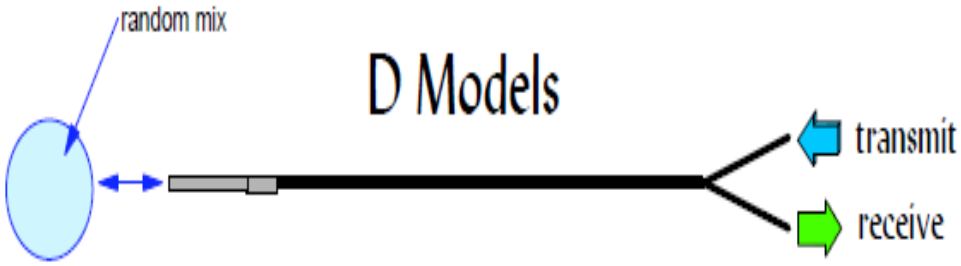

Figure 5.9 Fiber optics probes (D-Model)

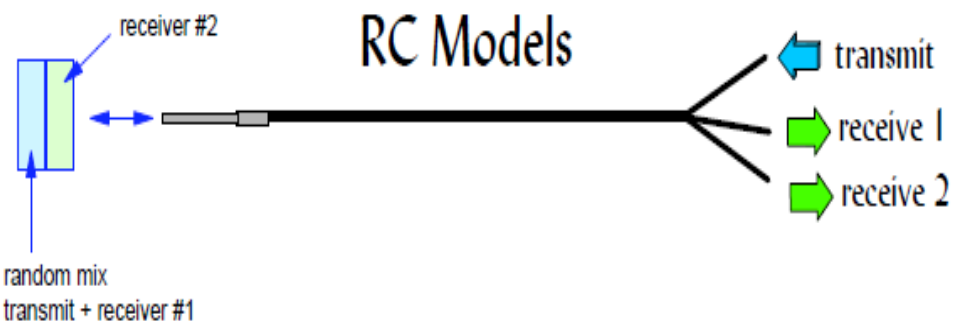

Figure 5.10 Fiber optics probes (RC-Model)

D-type sensors are reflectance compensated and mainly used for one dimensional measurements where the target reflectivity is not changing, shown in Fig. 5.11. RC-types sensors are used for measuring the translation and rotation motion of the target with varying surface reflectivity, shown in Fig. 5.12.

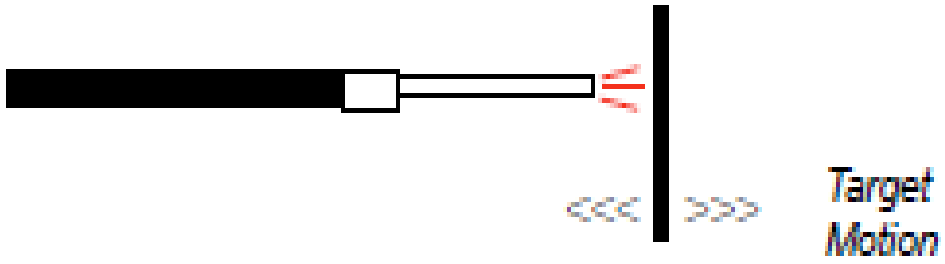

Figure 5.11 D-Model (reflectance dependent)

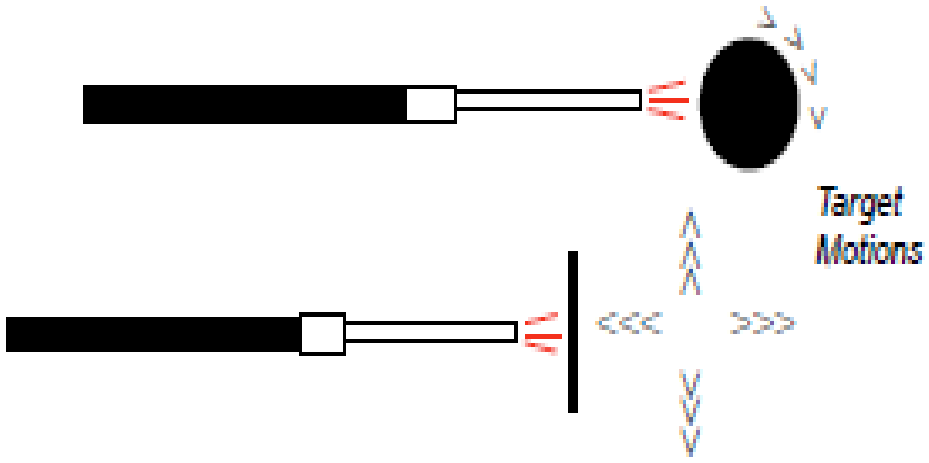

Figure 5.12 RC-Model (reflectance compensated)

5.2.2.1 Operation of Fiber Optic Micro Displacement Measurement Systems (µDMS)

The µDMS control software provided is loaded into PC and Executed. The sensors will first go through an initialization routine. During this process, in addition to many other checks, the software reads and copies all of the calibration tables from the sensor. The sensors will reach to thermal equilibrium in approximately twenty minutes. The Configuration Tab is used to set up the sensor for measurements. The sensor should be fixed and place perpendicular to the target to be measured.

All µDMS sensors have an internal sampling rate of 10 KHz. The average filter controls how many readings the sensor will average together before sending the results to the serial port. Higher averages will slow down the sensor response and increase the resolution. The actual sample rate (readings/second) is displayed below in the live chart. At the slowest speed (4096), the sample rate is approximately 0.4 seconds per data point. At the fastest speed (2), the sample rate is 200 microseconds per point.

5.3 Results & Discussion

To study the moving web case, the transverse vibration of the web is measured for different values of the web tension and the speed of the microcontact printing machine. The thickness of the web used in the experiment was 0.0381 m, its length and width were 0.26 m and 0.127 m, respectively. The transverse displacement of the web was measured, shown in Fig. 5.13, and the FFT algorithm was used to determine the frequency of the transverse vibration, shown in Fig. 5.14.

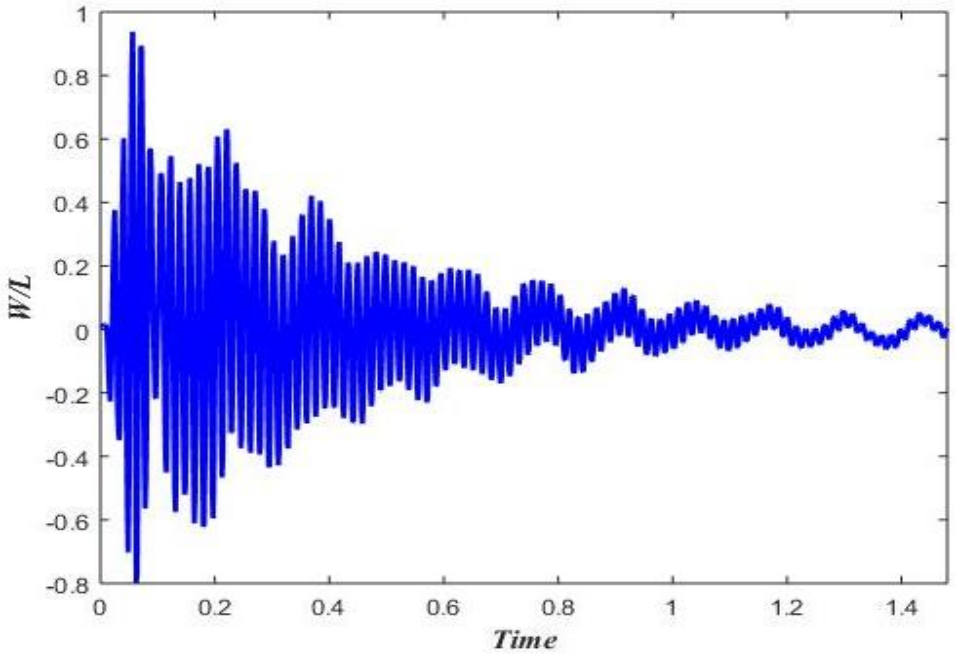

Figure 5.13 Measured transverse displacement

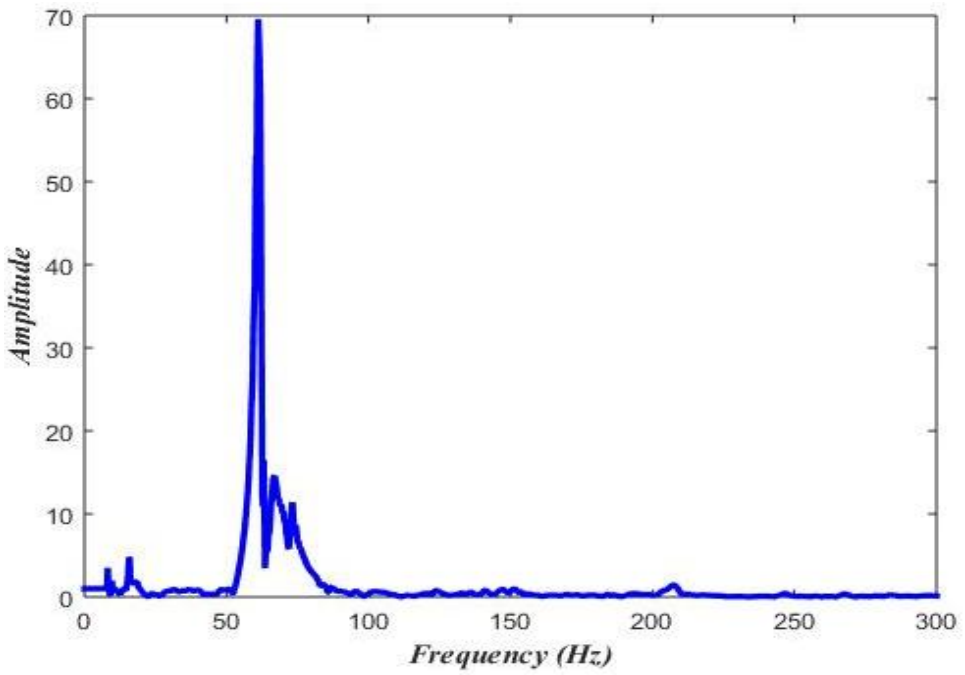

Figure 5.14 Frequency of transverse displacement

The aim of the experiment was to validate the developed mathematical web dynamic model. The frequency response was calculated for the same conditions using the axially moving string model and the axially moving membrane model. Comparisons between the analytical and experimental results are made in the next section.

5.3.1 Frequency Comparison at Different Web Speeds

The frequency of the transverse vibration of an axially moving web is measured at web tensions of 4, 5, 6, 7, 8, 9 and 10 pounds and at web axial speeds of 0, 1, 2, 4, 6, 8 and 10 in/sec, shown in Figs. 5.15.

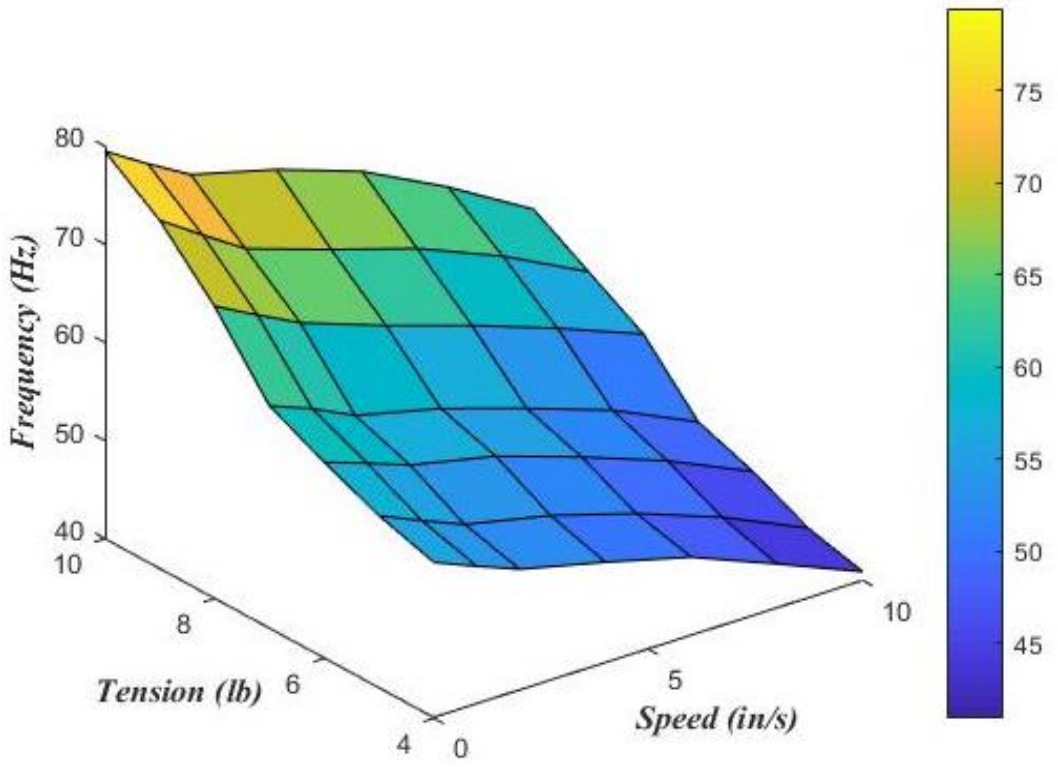

Figure 5.15 Frequency variation against speed & tension (Experimental)

Comparing the frequencies of transverse displacement, increasing the magnitude of the web axial tension results in an increase in the frequencies of the vibration. With the increase in the web axial speed, the values of the vibration frequencies decrease, shown in Fig. 5.15. Vibration frequencies are also obtained from the string and membrane model as shown in Figs. 5.16 and 5.17.

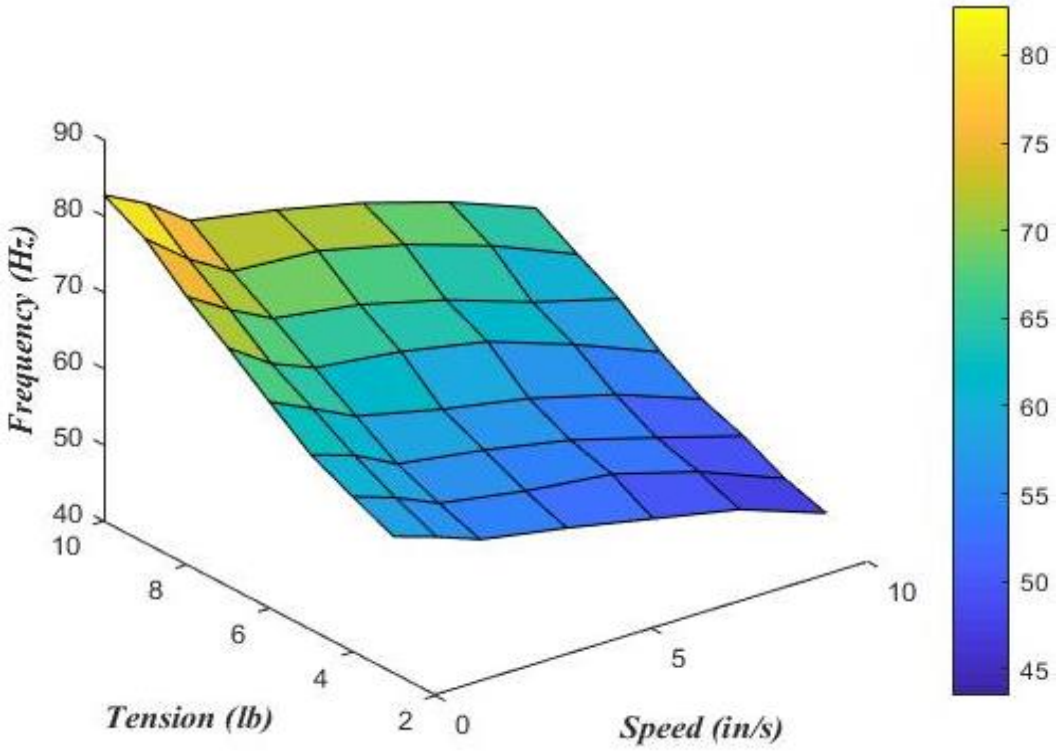

Figure 5.16 Frequency variation against speed & tension (String)

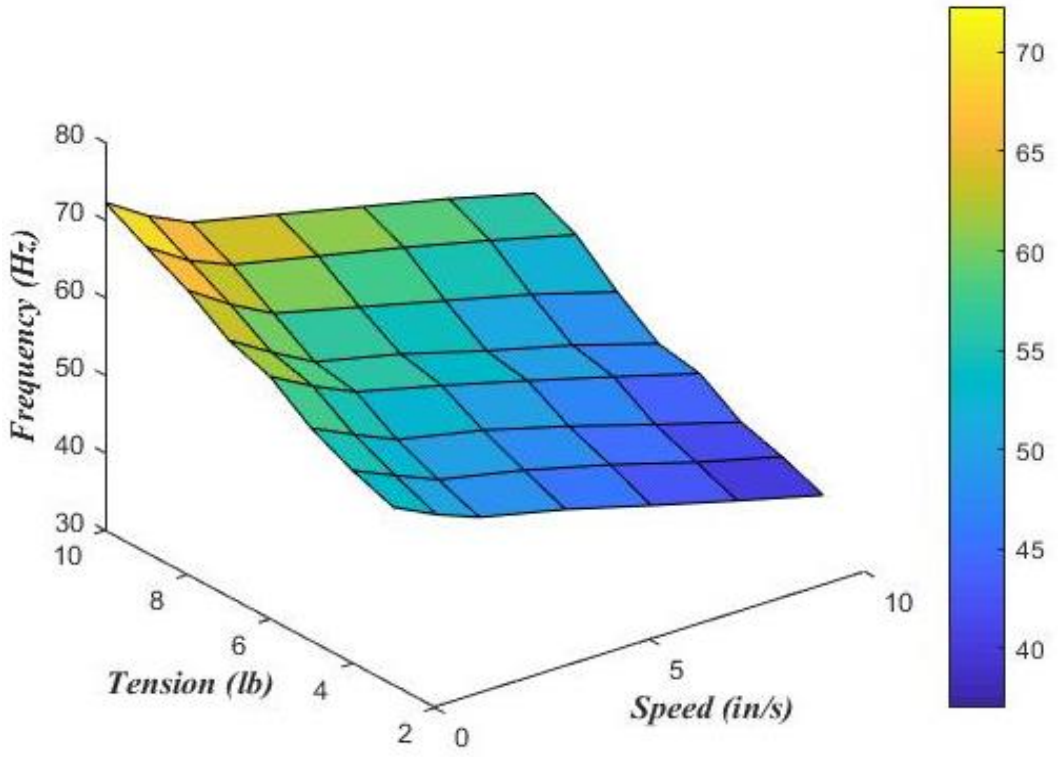

Figure 5.17 Frequency variation against speed & tension (Membrane)

The frequencies of the transverse vibration obtained from both the string and the membrane model follow the same trend observed in the experimental results. Increasing the web axial tension will cause the frequencies to rise, whereas increasing the web axial speed results in lower vibration frequencies as shown in Figs. 5.16 and 5.17. Although both models are in good agreement with the experimental results, the values of frequencies obtained from the string model are in closer agreement with those obtained from the experimental results.

5.3.2 Transverse Displacement Comparison at Variable Web Speed

To validate the coupled model, a comparison of the simulated and experimental transverse displacement is made at variable speed of the web as shown in Fig. 5.18.

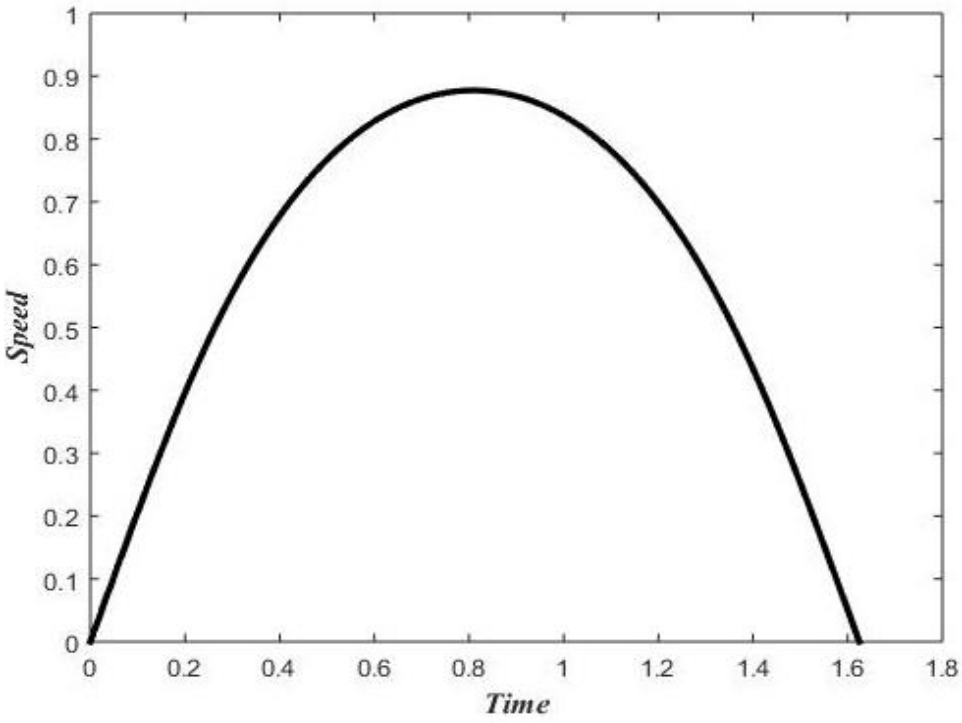

Figure 5.18 Axial web speed

The velocity from the mathematical model is used as an input to the experimental setup, and the transverse vibration data of the web is recorded. The transverse displacement from the experiment is plotted alongside with the simulated results at two representative locations (x_* = 0.50 & 0.75) as shown in Figs. 5.19 and 5.20.

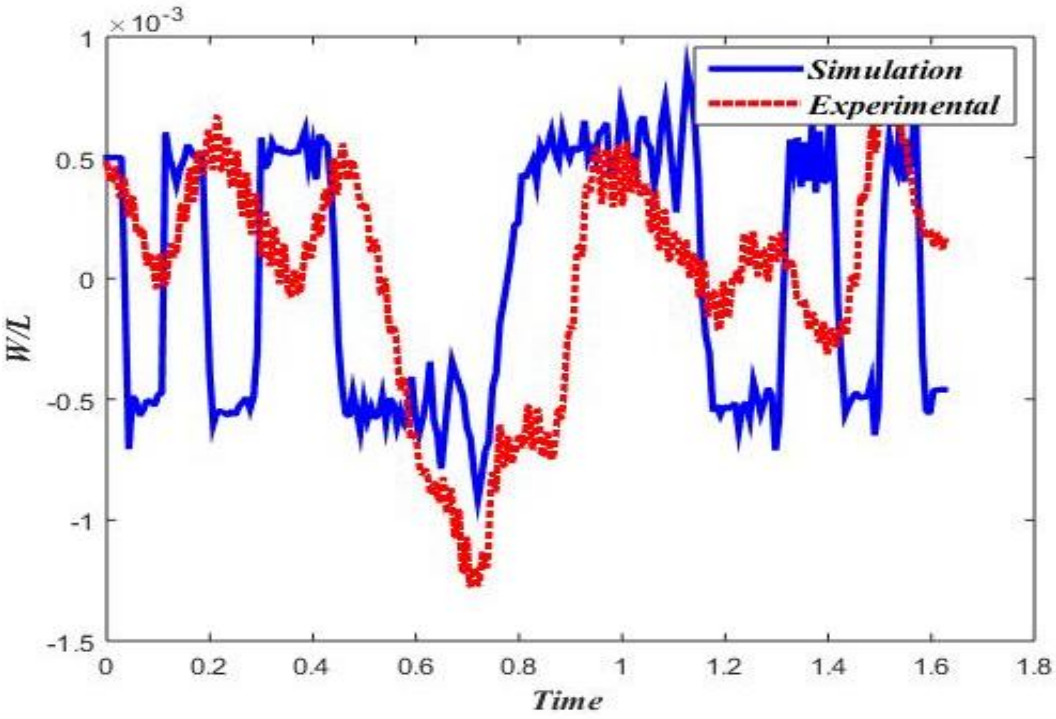

Figure 5.19 Simulated & experimental transverse response comparison at $x_* = 0.50$

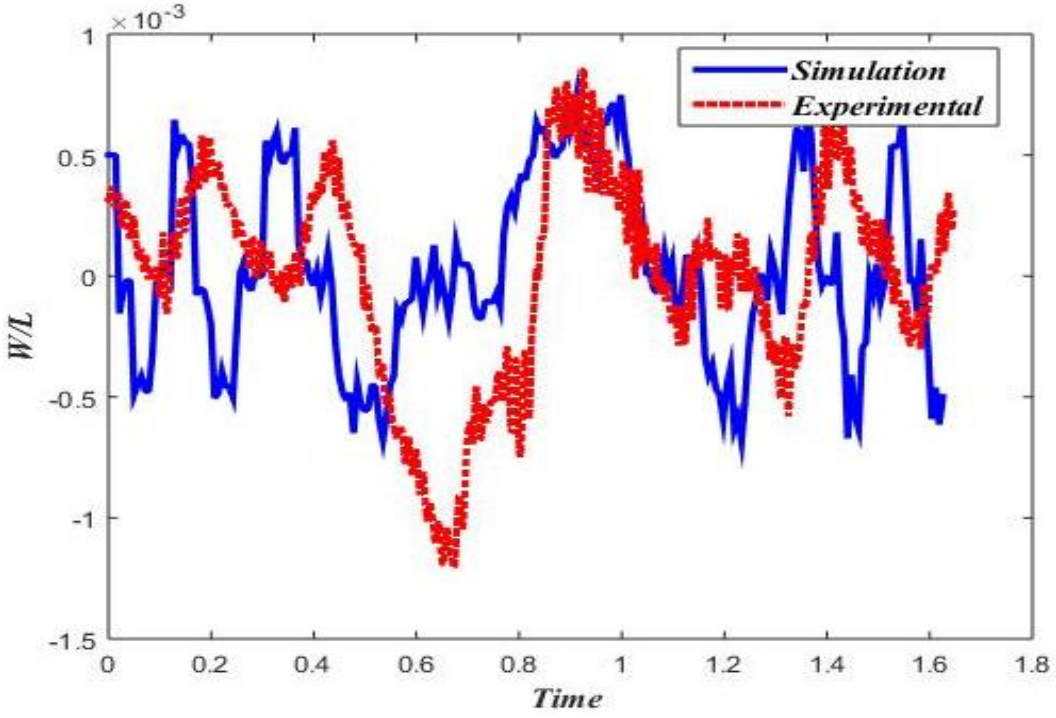

Figure 5.20 Simulated & experimental transverse response comparison at $x_* = 0.75$

A good agreement can be seen between the experimental and simulated response of the axially moving web at variable speed. To observe the effect of varying speed on the response, the web speed is plotted alongside the web response as shown in Figs. 5.21 and 5.22.

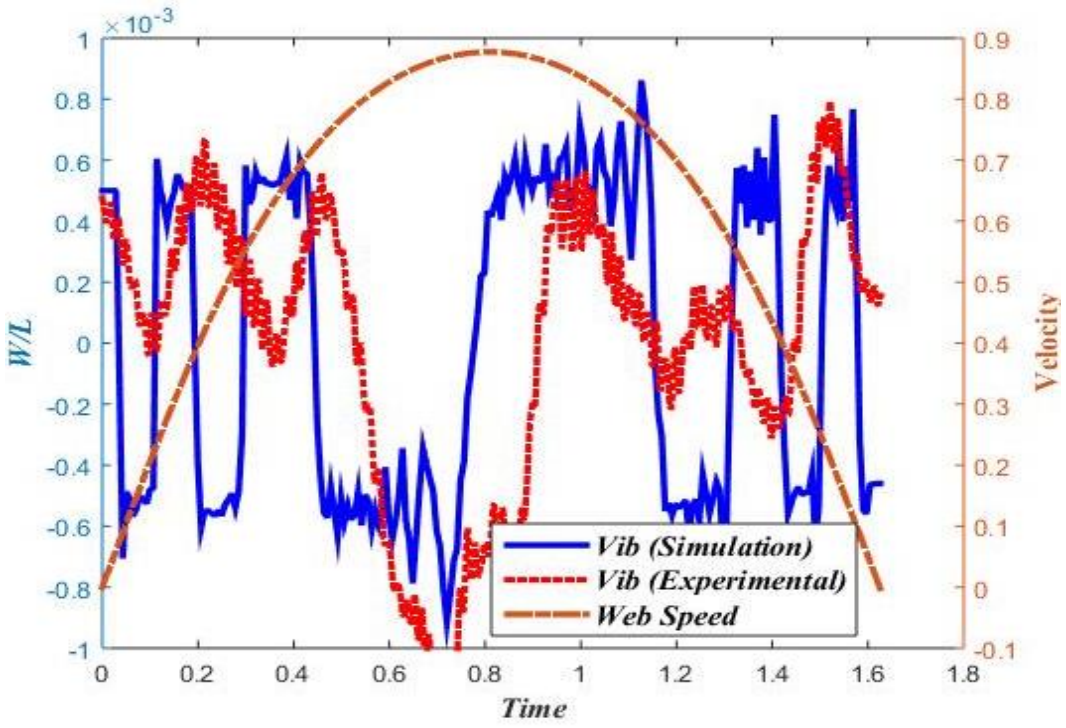

Figure 5.21 Simulated & experimental transverse response comparison with at $x_* = 0.50$

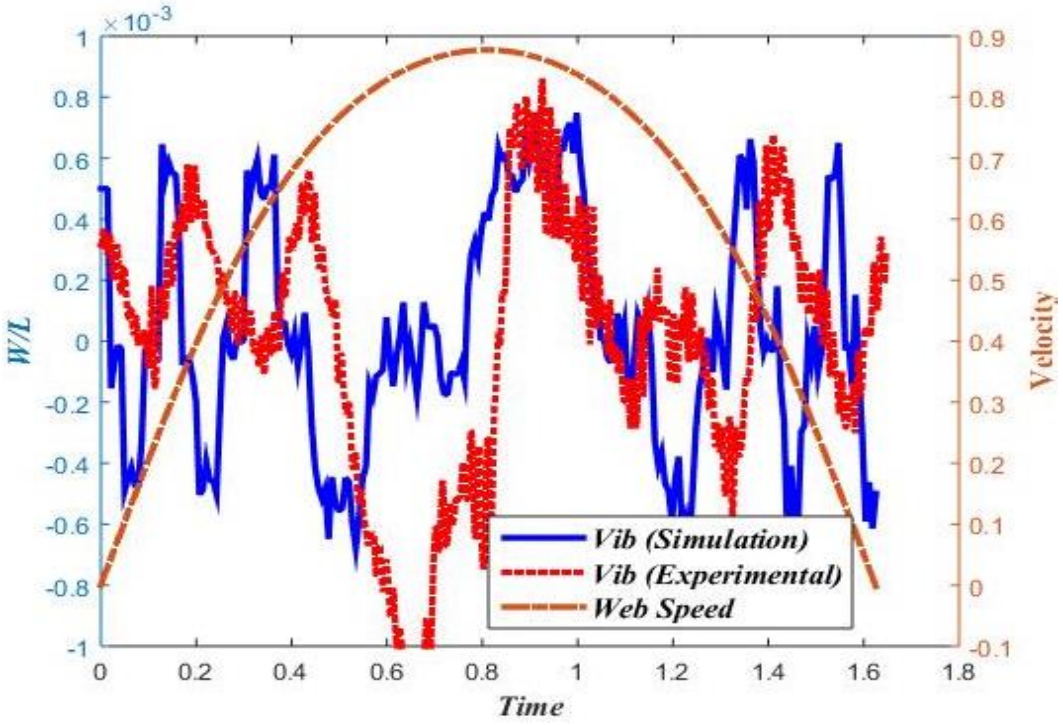

Figure 5.22 Simulated & experimental transverse response comparison with at $x_* = 0.75$

At the early and late phases, the axial web speed changes rapidly with time leading to high frequency fluctuations in the dynamic response. Whereas, low frequency response is noted in the middle of the time span, due to the slow change in the axial web speed with time.

CHAPTER 6

WEB VIBRATION SUPPRESSION

6.1 Mathematical Model

In this section a vibration suppression methodology is proposed. To achieve this suppression, suitable boundary conditions and input driving torques are introduced for an axially moving web to regulate the vibration and axial web speed.

6.1.1 Problem Formulation

Let us consider an axially moving string in a roll-to-roll system with axial tension T, axial speed *v* and transverse deflection *w (x, t).* Mechanical energy of the web is given by

$$E(t) = \tau + U \tag{6.1}$$

Where τ is the kinetic energy and U is the potential energy for the axially moving web are given by

$$\tau = \int_0^l \frac{1}{2}\rho A\left[\left(\frac{\partial w}{\partial t} + v\,\frac{\partial w}{\partial x}\right)^2\right]dx \tag{6.2}$$

$$U = \frac{1}{2}\int_0^l T\left(\frac{\partial w}{\partial x}\right)^2 dx \tag{6.3}$$

where ρ is the density and A is the area of the web. Using equations (6.2) and (6.3), the total mechanical energy $E(t)$ of the system is given by

$$E(t) = \frac{1}{2}\rho \int_0^l \left[\left(\frac{\partial w}{\partial t} + v\,\frac{\partial w}{\partial x}\right)^2\right] dx + \frac{1}{2}\int_0^l T\left(\frac{\partial w}{\partial x}\right)^2 dx \tag{6.4}$$

Normalizing equation (6.4) by utilizing $\sqrt{\frac{\rho A l^2}{T}}$ as a temporal parameter, and $\sqrt{\frac{TA}{\rho}}$ as a reference velocity transforms the equation of total mechanical energy into the following dimensionless one:

$$E(t_*) = \frac{1}{2}\int_0^1 \left[\left(\frac{\partial w_*}{\partial t_*} + v_*\,\frac{\partial w_*}{\partial x_*}\right)^2\right] dx_* + \frac{1}{2}\int_0^1 \left(\frac{\partial w_*}{\partial x_*}\right)^2 dx_* \tag{6.5}$$

Note that variables with stars are dimensionless, and v_* is a dimensionless transport speed that represents the ratio of the physical velocity and the wave velocity in the string material. Applying a material derivative on the mechanical energy and utilizing the equation of motion

$$\dot{E}(t_*) = \int_0^1 \left[\left(\frac{\partial w_*}{\partial t_*} + v_*\,\frac{\partial w_*}{\partial x_*}\right)\left(\frac{\partial^2 w_*}{\partial x_*^2}\right)\right] dx_* + \int_0^1 \left(\frac{\partial w_*}{\partial x_*}\right)\left(\frac{\partial^2 w_*}{\partial t_* \partial x_*} + v_*\,\frac{\partial^2 w_*}{\partial x_*^2}\right) dx_* \tag{6.6}$$

Which can be written as

$$\dot{E}(t_*) = 2 * v_* \int_0^1 \left[\left(\frac{\partial w_*}{\partial x_*}\right)\left(\frac{\partial^2 w_*}{\partial x_*^2}\right)\right] dx_* + \int_0^1 \left(\left(\frac{\partial w_*}{\partial x_*}\right)\left(\frac{\partial^2 w_*}{\partial t_* \partial x_*}\right) + \left(\frac{\partial w_*}{\partial t_*}\right)\left(\frac{\partial^2 w_*}{\partial x_*^2}\right)\right) dx_* \tag{6.7}$$

Simplifying each term in equation (6.7)

1st Term

$$\int_0^1 \left[\left(\frac{\partial w_*}{\partial x_*}\right)\left(\frac{\partial^2 w_*}{\partial x_*^2}\right)\right] dx_* = \left(\frac{\partial w_*}{\partial x_*}\right)\left(\frac{\partial w_*}{\partial x_*}\right)\Big|_0^1 - \int_0^1 \left[\left(\frac{\partial w_*}{\partial x_*}\right)\left(\frac{\partial^2 w_*}{\partial x_*^2}\right)\right] dx_*$$

$$\int_0^1 \left[\left(\frac{\partial w_*}{\partial x_*}\right)\left(\frac{\partial^2 w_*}{\partial x_*^2}\right)\right] dx_* = \left(\frac{\partial w_*}{\partial x_*}\right)^2\Big|_0^1 - \int_0^1 \left[\left(\frac{\partial w_*}{\partial x_*}\right)\left(\frac{\partial^2 w_*}{\partial x_*^2}\right)\right] dx_*$$

$$\int_0^1 \left[\left(\frac{\partial w_*}{\partial x_*}\right)\left(\frac{\partial^2 w_*}{\partial x_*^2}\right)\right] dx_* + \int_0^1 \left[\left(\frac{\partial w_*}{\partial x_*}\right)\left(\frac{\partial^2 w_*}{\partial x_*^2}\right)\right] dx_* = \left(\frac{\partial w_*}{\partial x_*}\right)^2\Big|_0^1$$

$$2 * \int_0^1 \left[\left(\frac{\partial w_*}{\partial x_*}\right)\left(\frac{\partial^2 w_*}{\partial x_*^2}\right)\right] dx_* = \left(\frac{\partial w_*}{\partial x_*}\right)^2\Big|_0^1$$

Therefore,

$$\int_0^1 \left[\left(\frac{\partial w_*}{\partial x_*}\right)\left(\frac{\partial^2 w_*}{\partial x_*^2}\right)\right] dx_* = \frac{1}{2}\left(\left(\frac{\partial w_*}{\partial x_*}\right)^2\Big|_0^1\right) \tag{6.8}$$

2nd Term

$$\int_0^1 \left(\left(\frac{\partial w_*}{\partial x_*}\right)\left(\frac{\partial^2 w_*}{\partial t_* \partial x_*}\right) + \left(\frac{\partial w_*}{\partial t_*}\right)\left(\frac{\partial^2 w_*}{\partial x_*^2}\right)\right) dx_*$$

$$= \int_0^1 \left[\left(\frac{\partial w_*}{\partial t_*}\right)\left(\frac{\partial^2 w_*}{\partial t_* \partial x_*}\right)\right] dx_* + \int_0^1 \left[\left(\frac{\partial w_*}{\partial t_*}\right)\left(\frac{\partial^2 w_*}{\partial x_*^2}\right)\right] dx_*$$

$$\int_0^1 \left(\left(\frac{\partial w_*}{\partial x_*}\right)\left(\frac{\partial^2 w_*}{\partial t_* \partial x_*}\right) + \left(\frac{\partial w_*}{\partial t_*}\right)\left(\frac{\partial^2 w_*}{\partial x_*^2}\right)\right) dx_*$$

$$= \left[\left(\frac{\partial w_*}{\partial x_*}\right)\left(\frac{\partial w_*}{\partial t_*}\right)\Big|_0^1 - \int_0^1 \left[\left(\frac{\partial w_*}{\partial t_*}\right)\left(\frac{\partial^2 w_*}{\partial x_*^2}\right)\right] dx_*\right]$$

$$+ \left[\left(\frac{\partial w_*}{\partial t_*}\right)\left(\frac{\partial w_*}{\partial x_*}\right)\Big|_0^1 - \int_0^1 \left[\left(\frac{\partial^2 w_*}{\partial t_* \partial x_*}\right)\left(\frac{\partial w_*}{\partial x_*}\right)\right] dx_*\right]$$

$$\int_0^1 \left(\left(\frac{\partial w_*}{\partial x_*}\right)\left(\frac{\partial^2 w_*}{\partial t_* \partial x_*}\right) + \left(\frac{\partial w_*}{\partial t_*}\right)\left(\frac{\partial^2 w_*}{\partial x_*^2}\right)\right) dx_*$$

$$= \left[\left(\frac{\partial w_*}{\partial x_*}\right)\left(\frac{\partial w_*}{\partial t_*}\right)\Big|_0^1 - \int_0^1 \left[\left(\frac{\partial w_*}{\partial t_*}\right)\left(\frac{\partial^2 w_*}{\partial x_*^2}\right)\right] dx_*\right]$$

$$+ \left[\left(\frac{\partial w_*}{\partial t_*}\right)\left(\frac{\partial w_*}{\partial x_*}\right)\Big|_0^1 - \left[\left(\frac{\partial w_*}{\partial x_*}\right)\left(\frac{\partial w_*}{\partial t_*}\right)\Big|_0^1 - \int_0^1 \left[\left(\frac{\partial w_*}{\partial t_*}\right)\left(\frac{\partial^2 w_*}{\partial x_*^2}\right)\right] dx_*\right]\right]$$

$$\int_0^1 \left(\left(\frac{\partial w_*}{\partial x_*}\right)\left(\frac{\partial^2 w_*}{\partial t_* \partial x_*}\right) + \left(\frac{\partial w_*}{\partial t_*}\right)\left(\frac{\partial^2 w_*}{\partial x_*^2}\right)\right) dx_*$$

$$= \left[\left(\left(\frac{\partial w_*}{\partial x_*}\right)\left(\frac{\partial w_*}{\partial t_*}\right)\Big|_0^1\right) - \int_0^1 \left[\left(\frac{\partial w_*}{\partial t_*}\right)\left(\frac{\partial^2 w_*}{\partial x_*^2}\right)\right] dx_* + \left(\left(\frac{\partial w_*}{\partial x_*}\right)\left(\frac{\partial w_*}{\partial t_*}\right)\Big|_0^1\right)\right.$$

$$\left. - \left(\left(\frac{\partial w_*}{\partial x_*}\right)\left(\frac{\partial w_*}{\partial t_*}\right)\Big|_0^1\right) + \int_0^1 \left[\left(\frac{\partial w_*}{\partial t_*}\right)\left(\frac{\partial^2 w_*}{\partial x_*^2}\right)\right] dx_*\right]$$

Therefore,

$$\int_0^1 \left(\left(\frac{\partial w_*}{\partial x_*}\right)\left(\frac{\partial^2 w_*}{\partial t_* \partial x_*}\right) + \left(\frac{\partial w_*}{\partial t_*}\right)\left(\frac{\partial^2 w_*}{\partial x_*^2}\right)\right) dx_* = \left(\left(\frac{\partial w_*}{\partial x_*}\right)\left(\frac{\partial w_*}{\partial t_*}\right)\Big|_0^1\right) \tag{6.9}$$

Substituting equations (6.8) and (6.9) into equation (6.7) gives

$$\dot{E}(t_*) = v_* \left(\frac{\partial w_*}{\partial x_*}\right)^2\Big|_0^1 + \left(\left(\frac{\partial w_*}{\partial x_*}\right)\left(\frac{\partial w_*}{\partial t_*}\right)\Big|_0^1\right) \tag{6.10}$$

Applying the limits of integration, time derivative of mechanical energy becomes

$$\dot{E}(t_*) = v_* \left(\left(\frac{\partial w_*(1,t)}{\partial x_*}\right)^2 - \left(\frac{\partial w_*(0,t)}{\partial x_*}\right)^2\right)$$

$$+ \left(\left(\frac{\partial w_*(1,t)}{\partial x_*}\right)\left(\frac{\partial w_*(1,t)}{\partial t_*}\right) - \left(\frac{\partial w_*(0,t)}{\partial x_*}\right)\left(\frac{\partial w_*(0,t)}{\partial t_*}\right)\right) \tag{6.11}$$

or

$$\dot{E}(t_*) = -v_*\left(\frac{\partial w_*(0,t)}{\partial x_*}\right)^2 + \left(\frac{\partial w_*(1,t)}{\partial x_*}\right)\left[\left(\frac{\partial w_*(1,t)}{\partial t_*}\right) + v_*\left(\frac{\partial w_*(1,t)}{\partial x_*}\right)\right] \quad (6.12)$$

In order to make sure that the rate of change of mechanical energy is negative, the following condition is proposed

$$\left(\frac{\partial w_*(1,t)}{\partial t_*}\right) = -v_*\left(\frac{\partial w_*(1,t)}{\partial x_*}\right) \quad (6.13)$$

Regulating the axial speed of the web to a desired setpoint, first we defined the speed setpoint error as

$$e = v - v_d \quad (6.14)$$

where, v is the actual web speed and v_d is the desired web speed. Using the roll-to-roll dynamics, input torques at the unwinding and rewinding rolls are calculated from (see chapter 3)

$$\tau_u(t) = \frac{\mathrm{d}}{\mathrm{d}t}(J_u * \Omega_u) - R_u * T + C_u \quad (6.15)$$

$$\tau_r(t) = \frac{\mathrm{d}}{\mathrm{d}t}(J_r * \Omega_r) + R_r * T + C_r \quad (6.16)$$

Using $v_u = R_u\Omega_u$, $v_r = R_r\Omega_r$, and substituting them in equations (6.15) and (6.16) result in

$$\tau_u(t) = \frac{\mathrm{d}}{\mathrm{d}t}\left(J_u * \frac{v_u}{R_u}\right) - R_u * T + C_u \quad (6.17)$$

$$\tau_r(t) = \frac{\mathrm{d}}{\mathrm{d}t}\left(J_r * \frac{v_r}{R_r}\right) + R_r * T + C_r \quad (6.18)$$

Substituting $v_u = v_r = v$ in equations (6.17) and (6.18) become

$$\tau_u(t) \;=\; \frac{\mathrm{d}}{\mathrm{d}t}\left(J_u * \frac{v}{R_u}\right) - R_u * T + C_u \tag{6.19}$$

$$\tau_r(t) \;=\; \frac{\mathrm{d}}{\mathrm{d}t}\left(J_r * \frac{v}{R_r}\right) + R_r * T + C_r \tag{6.20}$$

Substituting equation (6.14) in equations (6.19) and (6.20), the input control torques at the unwinding and rewinding rolls become

$$\tau_u(t) \;=\; \frac{\mathrm{d}}{\mathrm{d}t}\left(J_u * \frac{v_d}{R_u}\right) + \frac{\mathrm{d}}{\mathrm{d}t}\left(J_u * \frac{e}{R_u}\right) - R_u * T + C_u \tag{6.21}$$

$$\tau_r(t) \;=\; \frac{\mathrm{d}}{\mathrm{d}t}\left(J_r * \frac{v_d}{R_r}\right) + \frac{\mathrm{d}}{\mathrm{d}t}\left(J_r * \frac{e}{R_r}\right) + R_r * T + C_r \tag{6.22}$$

Thus, one can now find the unwinding and rewinding torques by minimizing the error (e).

6.1.2 Finite Difference Solution

A numerical approach based on a finite difference scheme is used for the discretization of spatial coordinates. Applying the backward finite difference scheme to discretize equation (6.13) and applying the central difference scheme to discretize the equation of motion (3.45) result in n second-order ODEs, where n is the total number of spatial points and dx_* is the step size.

$$\left.\begin{aligned}
\frac{\mathrm{d}^2 w_{*1}}{dt_*^2} + \frac{v_*}{\mathrm{d}x_*}\frac{\mathrm{d}w_{*2}}{\mathrm{d}t_*} + \frac{(v_*^2-1)}{{dx_*}^2}(-2*w_{*1}+w_{*2}) + \frac{v_*^{\cdot}}{2*\mathrm{d}x_*}*w_{*2} &= 0 \\
\frac{\mathrm{d}^2 w_{*2}}{dt_*^2} + \frac{v_*}{\mathrm{d}x_*}\left(-\frac{\mathrm{d}w_{*1}}{\mathrm{d}t_*} + \frac{\mathrm{d}w_{*3}}{\mathrm{d}t_*}\right) + \frac{(v_*^2-1)}{{\mathrm{d}x_*}^2}(w_{*1}-2*w_{*2}+w_{*3}) + \frac{v_*^{\cdot}}{2*\mathrm{d}x_*}(-w_{*1}+w_{*3}) &= 0 \\
&\vdots \\
\frac{\mathrm{d}^2 w_{*(n-1)}}{\mathrm{d}t_*^2} + \frac{v_*}{\mathrm{d}x_*}\frac{\mathrm{d}w_{*(n-2)}}{\mathrm{d}t_*} + \frac{(v_*^2-1)}{{\mathrm{d}x_*}^2}\left(w_{*(n-2)}-2*w_{*(n-1)}\right) + \frac{v_*^{\cdot}}{2*\mathrm{d}x_*}*w_{*(n-2)} &= 0 \\
\frac{d^2 w_{*n}}{dt_*^2} = -\frac{v_*}{2*dx_*}\left(\frac{dw_{*(n)}}{dt_*} - \frac{dw_{*(n-1)}}{dt_*}\right)
\end{aligned}\right\} \quad (6.23)$$

To solve the n second-order ODEs, state space representation is used to convert them into $2n$ first-order ODEs, which are given as

$$\left.\begin{aligned}
\frac{\mathrm{d}y_1}{dt_*} &= y_2 \\
\frac{\mathrm{d}y_2}{\mathrm{d}t_*} = \frac{\mathrm{d}^2 w_{*1}}{\mathrm{d}t_*^2} &= -\frac{v_*}{\mathrm{d}x_*}y_4 + \frac{(v_*^2-1)}{{\mathrm{d}x_*}^2}(2*y_1 - y_3) - \frac{v_*^{\cdot}}{2*\mathrm{d}x_*}*y_4 \\
\frac{\mathrm{d}y_2}{\mathrm{d}t_*} = \frac{\mathrm{d}^2 w_{*1}}{\mathrm{d}t_*^2} &= -\frac{v_*}{\mathrm{d}x_*}y_4 + \frac{(v_*^2-1)}{{\mathrm{d}x_*}^2}(2*y_1 - y_3) - \frac{v_*^{\cdot}}{2*\mathrm{d}x_*}*y_4 \\
\frac{\mathrm{d}y_3}{\mathrm{d}t_*} &= y_4 \\
\frac{\mathrm{d}y_4}{\mathrm{d}t_*} = \frac{\mathrm{d}^2 w_{*2}}{\mathrm{d}t_*^2} &= -\frac{v_*}{\mathrm{d}x_*}(y_2 - y_6) + \frac{(v_*^2-1)}{{\mathrm{d}x_*}^2}(-y_1 + 2*y_3 - y_5) - \frac{v_*^{\cdot}}{2*\mathrm{d}x_*}(y_2 - y_6) \\
&\vdots \\
\frac{\mathrm{d}y_{2*(n-1)-1}}{\mathrm{d}t_*} &= y_{2*(n-1)} \\
\frac{\mathrm{d}y_{2*(n-1)}}{\mathrm{d}t_*} &= -\frac{v_*}{\mathrm{d}x_*}y_{2*(n-1)-2} + \frac{(v_*^2-1)}{{\mathrm{d}x_*}^2}\left(-y_{2*(n-1)-3} + 2*y_{2*(n-1)-1}\right) - \frac{v_*^{\cdot}}{2*\mathrm{d}x_*}y_{2*(n-1)-2} \\
\frac{dy_{2*(n)-1}}{dt_*} &= y_{2*(n)} \\
\frac{dy_{2*(n)}}{dt_*} = \frac{d^2 w_{*n}}{dt_*^2} &= -\frac{v_*}{2*dx_*}\left(y_{2*(n)} - y_{2*(n)-2}\right)
\end{aligned}\right\} \quad (6.24)$$

6.1.3 Numerical Results and Discussion

Numerical integrations for the two cases of uncoupled (R2R dynamics independent) & coupled (R2R dynamics dependent) vibrations were carried out to see the effect of the proposed methodology on the vibration suppression in each case. Results are presented in Figs. 6.1-6.3 showing the transverse displacement responses monitored at the three representative locations (x_*= 0.25, 0.50 and 0.75).

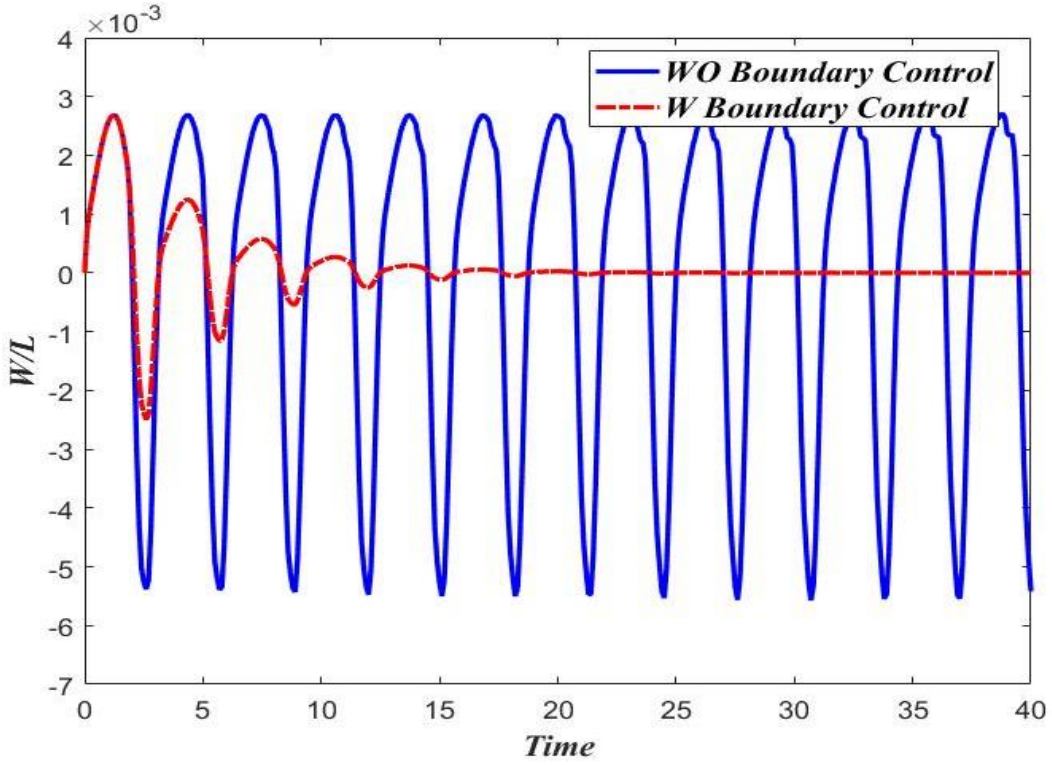

Figure 6.1 With & without control transverse displacement at $x_* = 0.25$ & $v_* = 0.5$

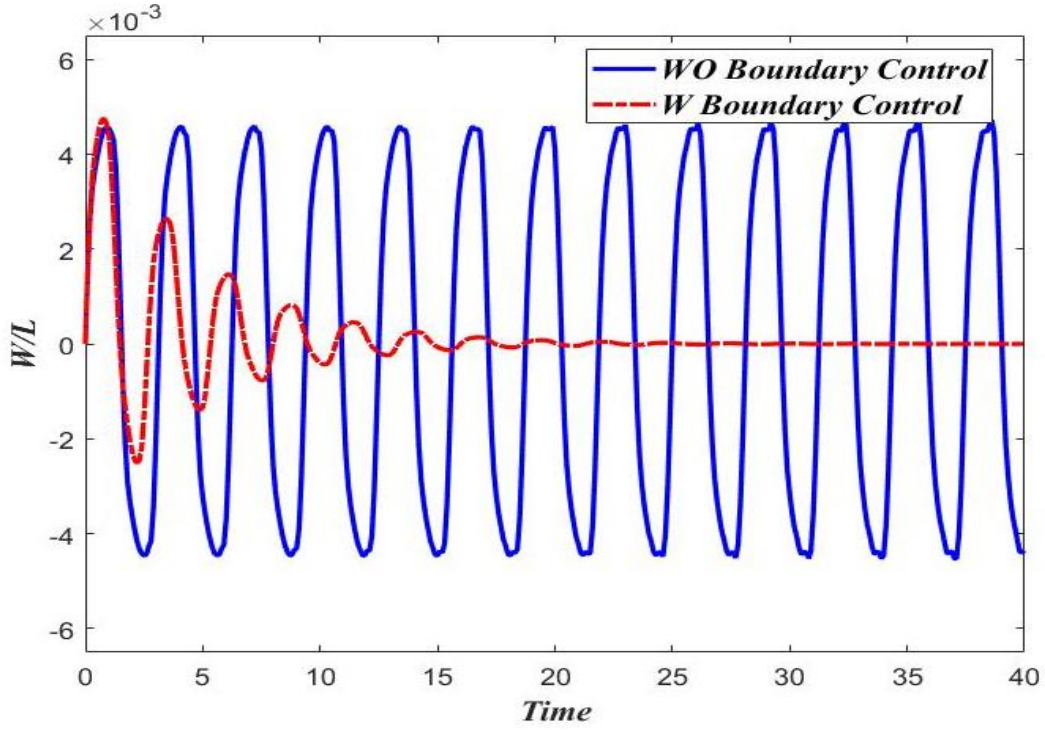

Figure 6.2 With & without control transverse displacement at $x_* = 0.50$ & $v_* = 0.5$

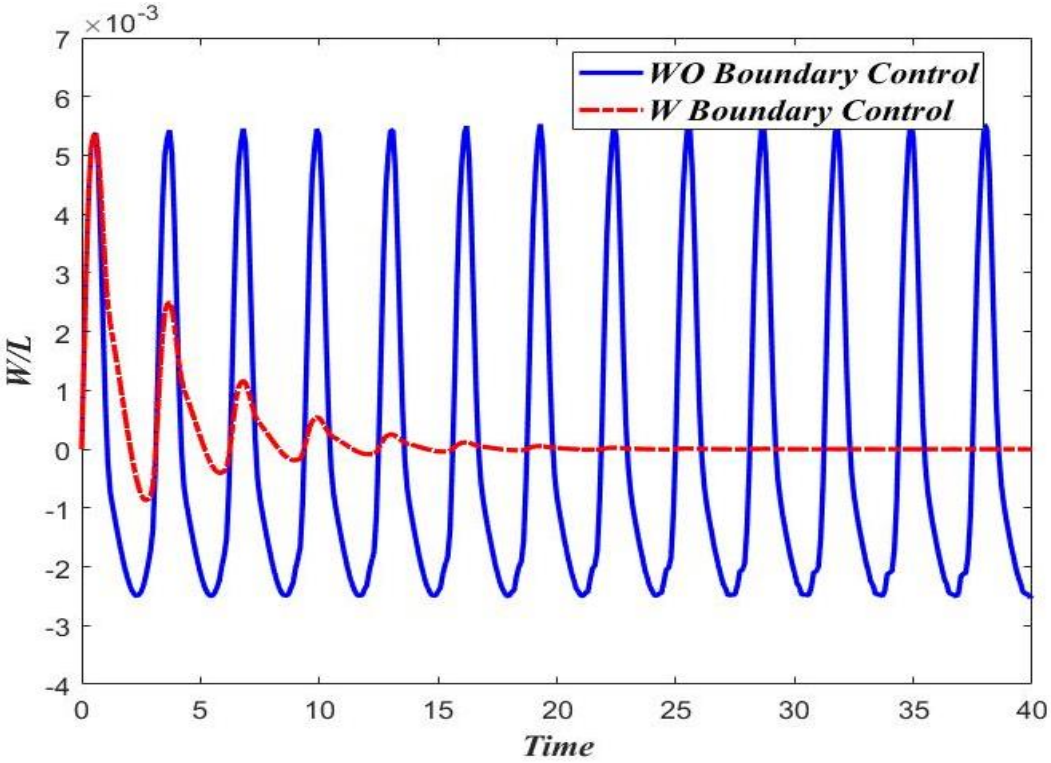

Figure 6.3 With & without control transverse displacement at $x_* = 0.75$ & $v_* = 0.5$

Figures 6.1-6.3 demonstrates the effectiveness of the proposed boundary control condition in reducing the transverse vibration at different locations of the web for the given dimensionless speed. Solid and dashed lines represent the transverse response of the web without boundary control and with boundary control conditions, respectively. With the application of boundary control a significant reduction in the amplitude of web transverse vibration is achieved. Therefore, it can be stated that the proposed condition is effectively reduces the vibrational energy and prevents the web from excessive vibrations.

According to the control condition, energy reduction at the right boundary is directly proportional to axial speed. The higher the speed, the faster energy decay in the string. To see the effect of the axial speed of the web on the vibration reuction, the controlled transverse responses at various dimensionless speeds are plotted at various locations of the web as shown in Figs. 6.4 - 6.6. Comparison is made at three locations (x_*= 0.25, 0.50 and 0.75) and at dimensionless axial speeds of $v_* = 0.1, 0.3, 0.4$ and 0.6.

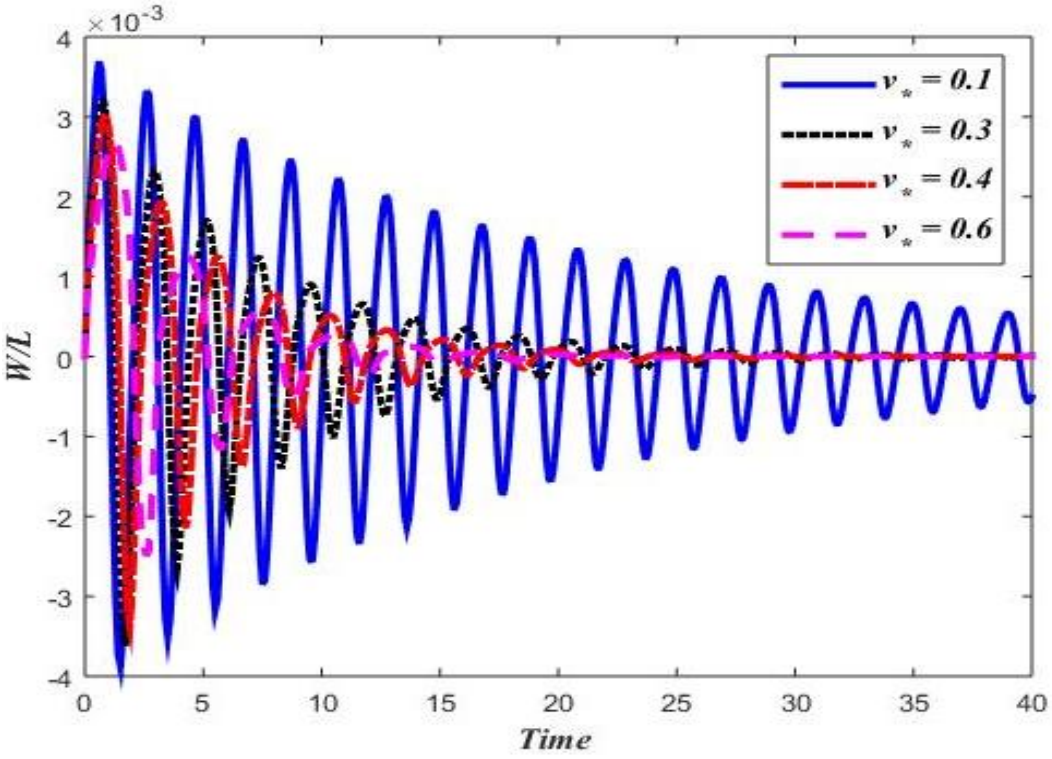

Figure 6.4 Transverse displacement at $x_* = 0.25$ for webs having different speeds

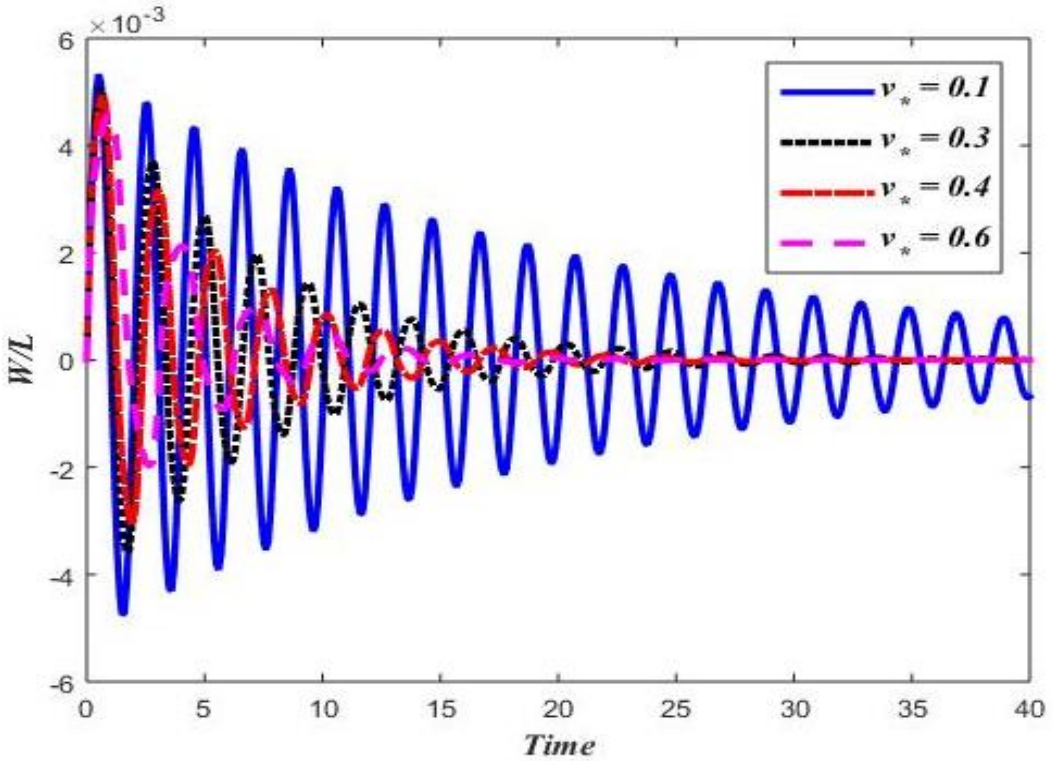

Figure 6.5 Transverse displacement at $x_* = 0.50$ for webs having different speeds

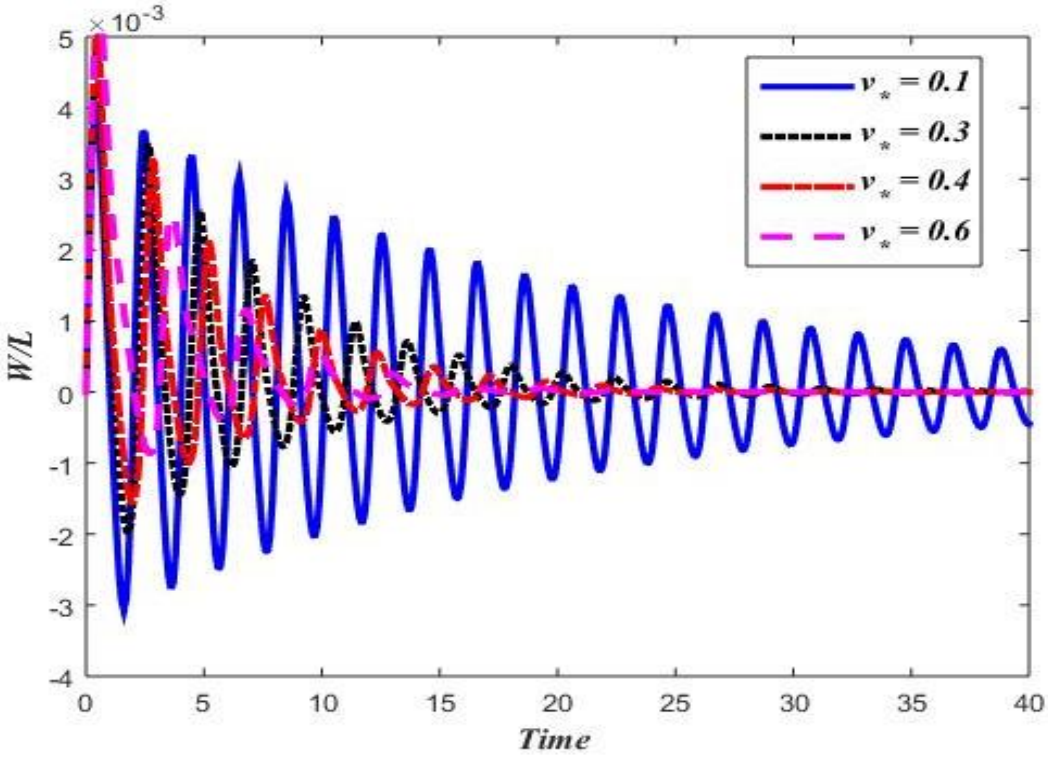

Figure 6.6 Transverse displacement at $x_* = 0.75$ for webs having different speeds

Comparison shows a significant decrease in the amplitude of vibration. Amplitude reduction is more prominent as the dimensionless speed is increased. Consequently, it can be concluded that at higher dimensionless speeds, with the use of controlled boundary condition, a lower amplitude of the transverse response can be achieved at the same location at the string.

Let us now examine the effect of the proposed combined control consisting of (i) applied torques at the rolls and (ii) imposed at the right roll. Equations (6.21), (6.22) and (6.24) are solved together with the system of equations (3.33) - (3.35), as a coupled system that describes the transverse vibration of the controlled axially moving web between the unwinding and the rewinding rolls.

The effect of proposed combined control methodology is web speed is presented in Fig. 6.7. It is noted that the axial web speed remains almost constant for the most of the time of transferring the web material from one roll to another.

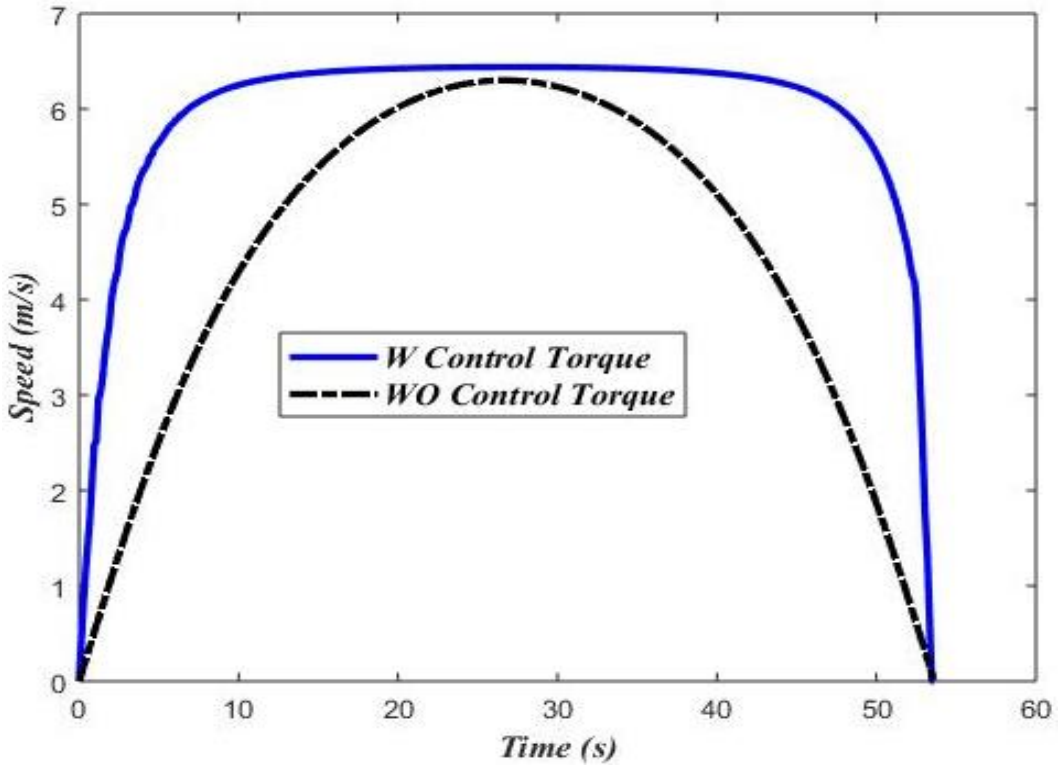

Figure 6.7 Axial speed comparison

A comparison of the R2R dynamic-coupled web vibration is made for three cases (i) R2R system without boundary control while constant torques at the rolls, (ii) R2R system with boundary control and no control torques, and (iii) R2R system with boundary control and control torques. Three web locations (x_*= 0.25, 0.50 and 0.75) have been selected for comparative study as shown in Figs. 6.8-6.10.

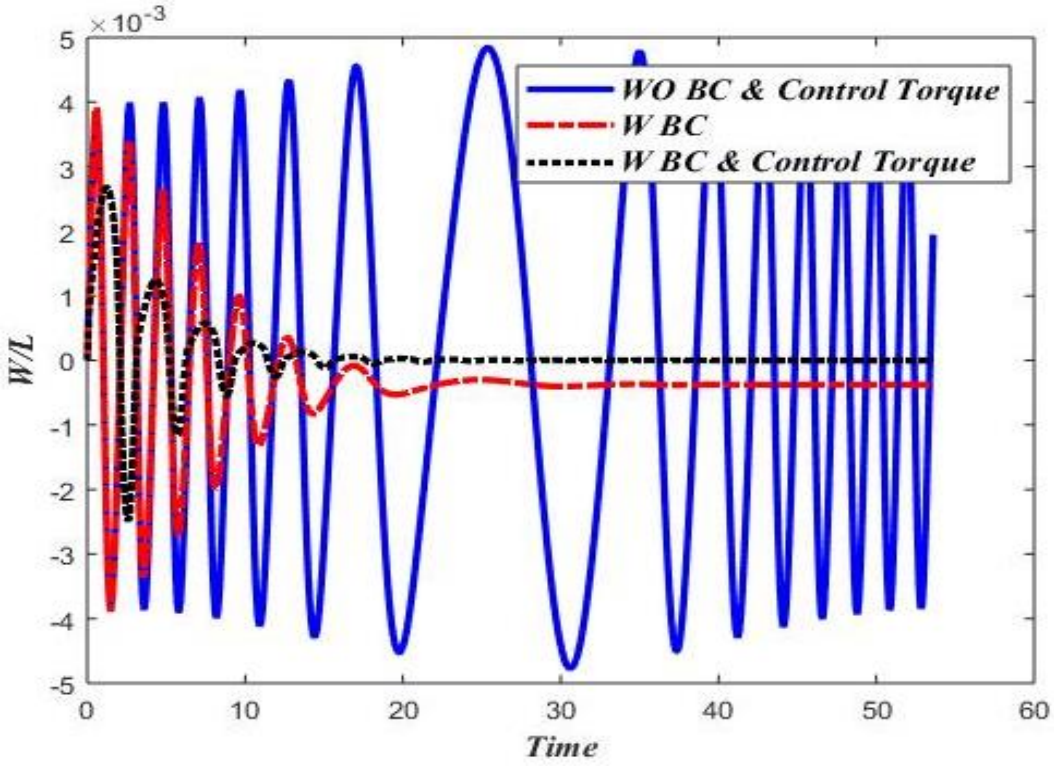

Figure 6.8 Transverse displacement at $x_* = 0.25$ for webs having variable speed

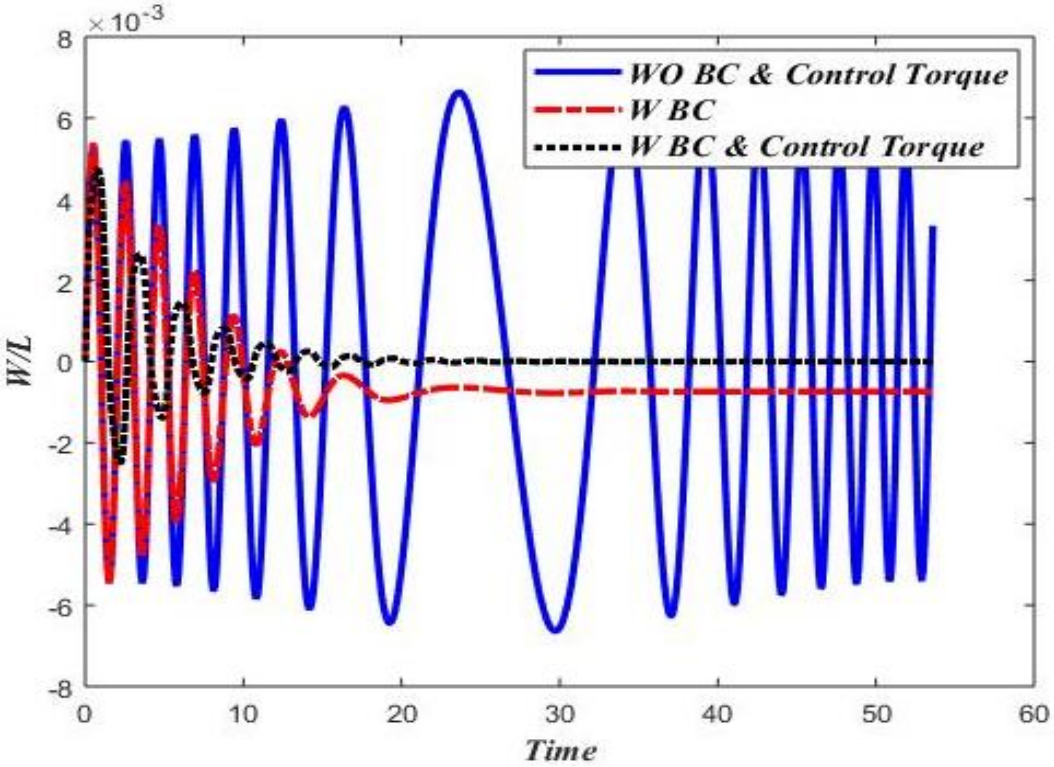

Figure 6.9 Transverse displacement at $x_* = 0.50$ for webs having variable speed

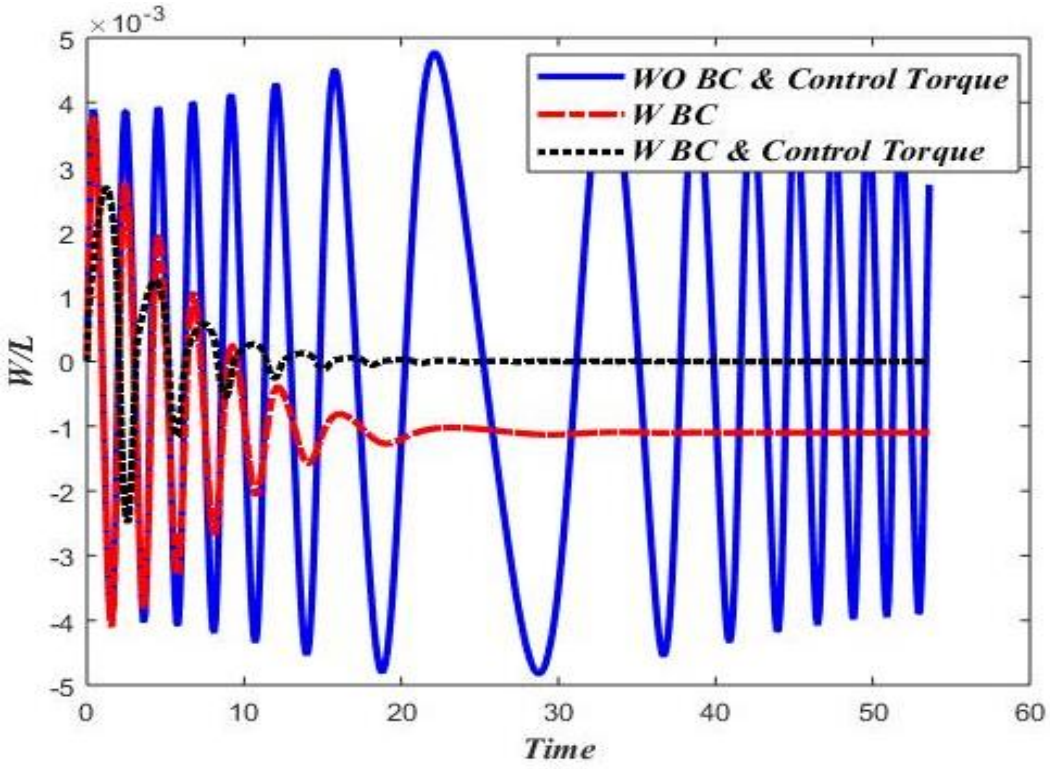

Figure 6.10 Transverse displacement at $x_* = 0.75$ for webs having variable speed

Comparison shows that, in the case of boundary control, a significant decrease in the vibration amplitude is achieved (red dashed). The reduction in the vibration amplitude and settling time is even more prominent in the case of the R2R system with boundary control and applied control torques (black dashed).

6.2 Experimental Verification

To verify the proposed control methodology, experiments were performed in the Laboratory of Manufacturing and Productivity at the Massachusetts Institute of Technology (MIT). A roll-to-roll micro-contact printing machine, shown in Fig. 6.11, is used as test bed.

To implement the boundary control, the original setup is modified as shown in Fig. 6.12 where a foam roll is installed at a slightly offset position at the right boundary.

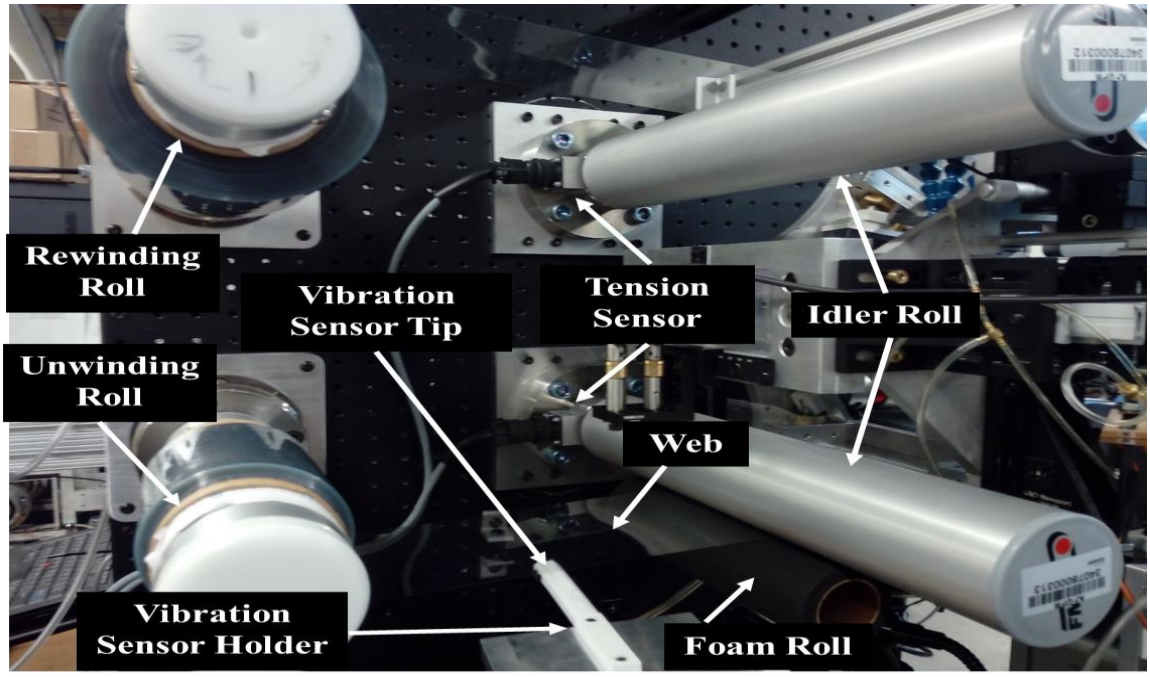

Figure 6.11 Modified Experimental Setup

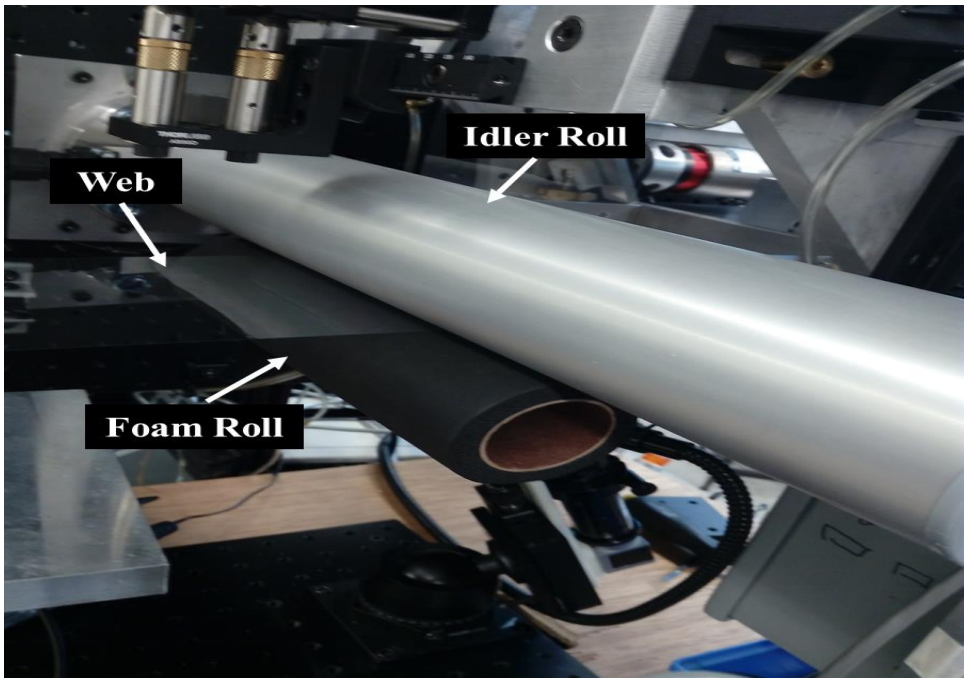

Figure 6.12 Foam roll-idler roll engagement

6.2.1 Results

Experiments are performed to measure the transverse displacement at different locations of the web on both modified and non-modified setups. The transverse displacement of the web was measured by the fiber optic micro displacement measurement system (μDMS) at three locations (x_*= 0.25, 0.50 and 0.75). With and without control condition responses are compared at "v =4 in/sec" and "T=30 N" as shown in Figs. 6.13 – 6.15.

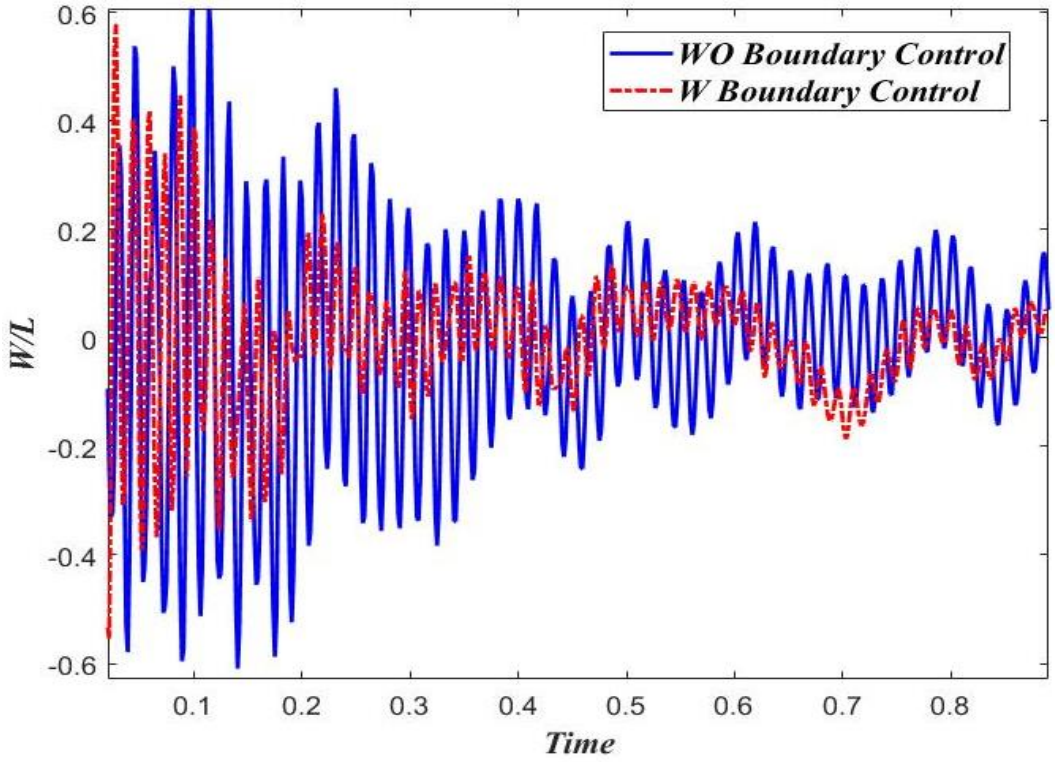

Figure 6.13 Transverse Response Comparison at $x_* = 0.25$

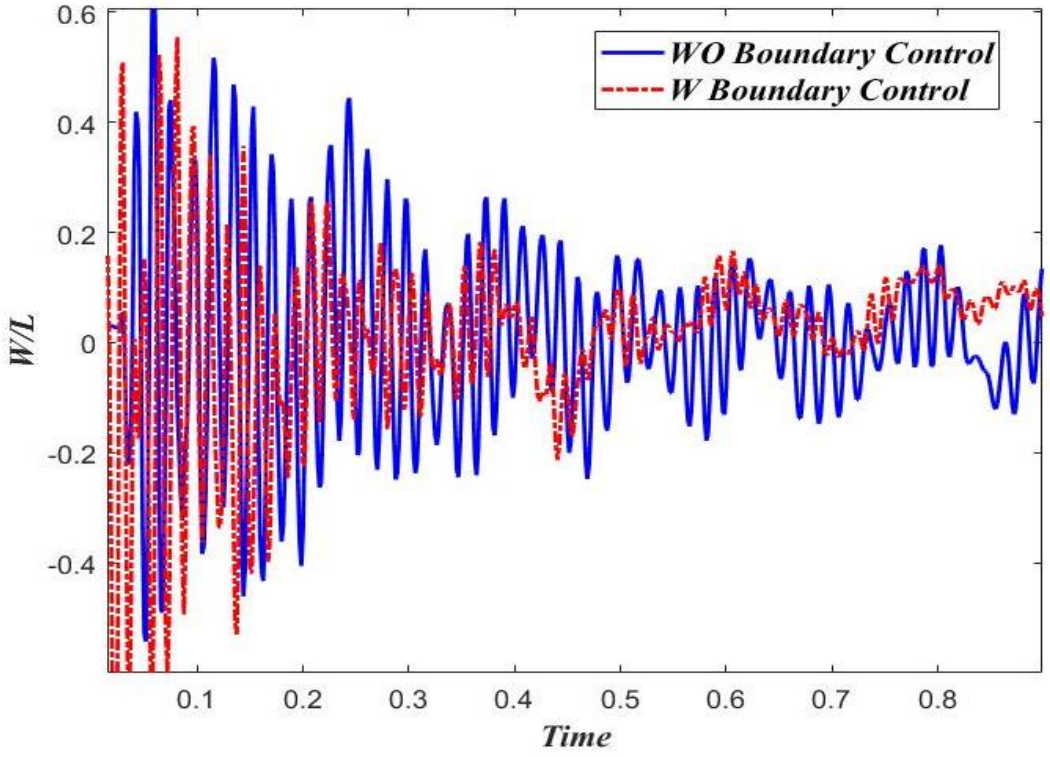

Figure 6.14 Transverse Response Comparison at $x_* = 0.50$

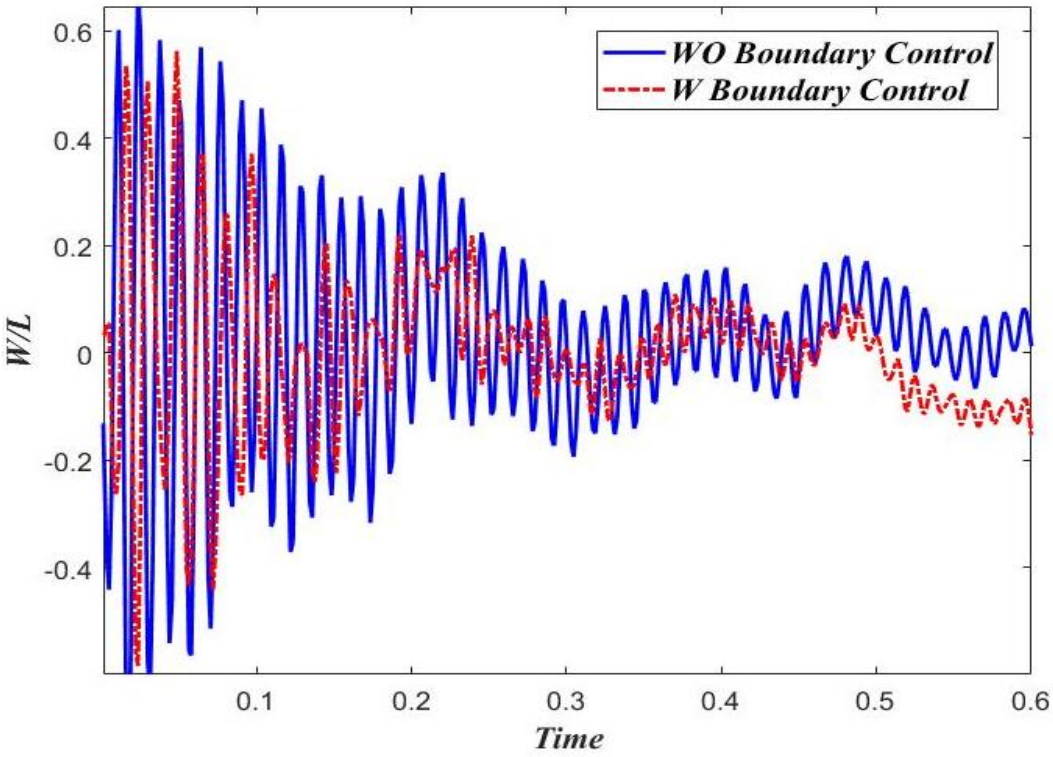

Figure 6.15 Transverse Response Comparison at $x_* = 0.75$

Comparison of the transverse vibration response at different locations clearly shows that applying a boundary control condition at the right boundary results in smaller web vibration. The rate of decay can be increased by properly controlling the slope of the web at the boundary.

CHAPTER 7

CONCLUSIONS AND RECOMMENDATIONS

In this study, the motion of substrates in the form of webs within roll-to-roll systems utilized for printing micro / nano features were considered. The web motion was considered at the following two levels: (i) The level of roll-to-roll system's dynamics describing the axial motion of the web coupled with the angular motion of the rolls. This led to the axial speed-tension relationship. (ii) The level of web transverse vibration that is coupled with the roll-to-roll dynamics. This led to the determination of time and frequency responses, mode shapes, and critical speeds of the axially moving web. Intuitively, the webs under consideration were modeled as strings. As a basic initial study, the case of one web-two rolls was considered. Then, the simplest case of a printing machine of two webs-three rolls was considered. Afterwards, the case of a printing machine having four webs-five rolls (which was actually built at MIT and copied at KFUPM) was investigated.

String mathematical models of coupled differential equations were solved by utilizing a finite difference scheme / state space technique which helped in transforming hyperbolic partial differential equation into first-order ordinary differential equations (ODE's). The utilized numerical approach was found to be efficient with favorable convergence, long-term stability and minimum computational time.

Findings of this study are summarized as follows:

- In order to describe the coupled axial motion / transverse vibration, a certain amount of web material was transferred from the unwinding roll to the rewinding roll.
- While transferring a certain amount of web material from the unwinding roll to the rewinding roll, the angular speed of both rolls varied nonlinearly in time, attaining the same maximum angular speed within the time of the web material transfer.
- All cases of R2R systems' dynamics considered showed that the web-transmitted tension varied varied according to a smooth nonlinear concave path.
- Parametric study on the two web spans-three rolls was conducted to see the effects of web lengths, the moment of inertia of idler impression roll, and the radii of the rewinding / unwinding rolls on the angular speed and web transmitted tension.
- Increasing the idler impression roll moment of inertia led to a reduced amplitude in the roll angular speed.
- Decreasing the length of one of the web spans did not affect tension profile, while it decreases slightly the duration of the transient state.
- Reducing the rewinding roll radius to half of the unwinding radius increased the angular velocity of the rewinding roll at a faster and increased the magnitude of the fluctuations in the transient state.
- Studying the vibration of axially moving web in isolation from the R2R system's dynamics showed that an increase of the axial speed of the web led to a reduction in the transverse vibration frequency.

- An analysis of the non-dimensional frequencies in the range of non-dimensional speed, indicated that divergent instability of the string occurred when the non-dimensional speed reached unity.
- Mode shapes were strongly dependent on the axial speed of the string.
- In order to achieve an optimal design of the systems, the major task is to evaluate all possible resonance frequencies of the system. The effect of the external disturbance frequency on the dynamic response was investigated. It was observed that the instability in transverse response occurred when the first and second frequencies of oscillation converged or when the second frequency of oscillation became a multiple of the first frequency of oscillation.
- The transverse vibration of an axially moving web within a roll-to-roll system was studied, considering the coupling between the vibration governing equation and the roll-to-roll system's dynamic model. The coupled equations were solved numerically using a finite difference approach. Based on the R2R system's dynamics, the transverse vibration of the axially moving web between the rolls was found to be non-periodic, with a faster vibration amplitude variation in time to rapid changes of web axial speed and a slower vibration amplitude variation in time to slow changes of the web axial speed.
- In order to suppress the web transverse vibration, a new vibration suppression method was introduced by using a boundary condition and adjusted driving torques at the unwinding and rewinding rolls.
- This suppression method ensured that the web vibration was mitigated. It was shown through the numerical results that introducing a boundary condition at the

right boundary will cause the vibrational energy to mitigate and prevent the web from excessive vibrations.

- The reduction in the web vibration amplitude and response settling time was prominent in the case of the R2R system with aforementioned boundary control approach and adjusted driving torques at the unwinding and rewinding rolls. Numerical simulations were backed by experiments to show effectiveness.

Recommendation for future investigations:

- Considering the air entrainment between the rolls and web at high speed.
- Conducting the similar studies on small scale (micro / nano).
- Introducing boundary control condition at both boundaries to mitigate the web vibrational energy.

REFERENCES

[1] E. Young and K. Reid, Lateral and longitudinal dynamic behavior and control of moving webs, Journal of Dynamic Systems, Measurement, and Control. 115 (1993) 309–317.

[2] A. Libert, Precision control of cylindrical stamp contact in a continuous roll-to-roll microcontact printing machine, MS. Dissertation, Massachusetts Institute of Technology, USA (2014).

[3] L. Perera, The role of active dancers in tension control of webs, MS. Dissertation, Oklahoma State University, USA (2001).

[4] S. T. Nill, Integrated hardware, software, and sensor design for control of a scalable continuous microcontact printing process, MS. Dissertation, Massachusetts Institute of Technology, USA (2014).

[5] J. Damour, The Mechanics of Tension Control, Converter Accessory Corporation, Wind Gap, PA USA.

[6] Web tension handbook, Advance web process control, www.CMScontrols.com.

[7] K. Chen, K. Ou and Y. Liao, On the influence of roller misalignments on the web behavior during roll-to-roll processing, Journal of the Chinese Institute of Engineers. 1 (2011) 87-97.

[8] K. Jain, M. Klosner, and M. Zemel, Flexible electronics and displays: High-resolution, roll-to-roll, projection lithography and photoablation processing technologies for high-throughput production, Proceedings of IEEE. 93 (2005) 1500–1510.

[9] A. Parsad, P. Toor and S. Sexena, Product Opportunities for Large Scale Micro-Contact Printing and CNT Forest Growth, New Process Development, Massachusetts Institute of Technology, USA (2014).

[10] K. Ou, Material characterization and stress analysis of web material transportation, The 25th Chinese society of mechanical engineering annual meeting, Changhua, Taiwan. (2008).

[11] S. Ahn and L. Guo, High-speed roll-to-roll nanoimprint lithography on flexible plastic substrates, Advanced Materials. 20 (2008) 2044–2049.

[12] D. Roisum, The mechanics of wrinkling, Proceedings of the technical association of the pulp and paper industry. 79 (1996) 217–226.

[13] Q. Nguyen and K. Hong, Transverse vibration control of axially moving membranes by regulation of axial velocity, IEEE Transactions on Control Systems Technology. 20 (2012) 1124–1131.

[14] D. Luo and S. R. Schricker, Handbook of nanomaterials properties. Berlin, Heidelberg: Springer Berlin Heidelberg, 2014.

[15] M. De Volder, S. H. Tawfick, R. H. Baughman, and A. J. Hart, Carbon Nanotubes: Present and Future Commercial Applications, 2014.

[16] Y. Zhang, Study on the synthesis process of carbon nanotubes, Advanced Materials. 22 (2014) 254–257.

[17] J. Hart, Continuous manufacturing of carbon nanotube forests – Presentation, 2013.

[18] S. A. Ruiz and C. S. Chen, Microcontact printing: A tool to pattern, Soft Matter, 3 (2007) 167.

[19] J. L. Wilbur, A. Kumar, and H. A. Biebuyck, Microcontact printing of self-assembled monolayers: applications in microfabrication, Advanced Materials. 6 (1994) 600-604.

[20] Y. Xia and G. M. Whitesides, Soft lithography, Annual Review of Materials Science, 28 (1998) 153-184.

[21] B. Michel, A. Bernard, A. Bietsch, E. Delamarche, M. Geissler, D. Juncker, H. Kind, J. P. Renault, H. Rothuizen, H. Schmid, P. S. Winkel, R. Stutz, and H. Wolf, Printing meets lithography: Soft approaches to high-resolution patterning, IBM Journal, 45 (2001) 697–719.

[22] B. Kruszka, A. P. Terzyk, M. Wiśniewski, P. Gauden, and M. Szybowicz, Synthesis of carbon nanotubes and nanotube forests on copper catalyst, Advanced Materials. 13 (2004) 35-40.

[23] K. Grenfell, Tension control on paper-making and converting machinery, Proceedings of IEEE Annual Conference on Electrical Engineering in the Pulp and Paper Industry, 9 (1963).

[24] D. Whitworth, “Tension variations in pliable material in production machinery”, PhD. dissertation, Loughborough University of Technology. (1979).

[25] D. Whitworth and M. Harrison, “Tension variations in pliable material in production machinery”, Journal of Applied Mathematical Modeling. 7 (1983) 189–196.

[26] H. Koç, D. Knittel, M. Mathelin and G. Abba, “Modeling and robust control of winding systems for elastic webs”, IEEE Transactions on control systems technology. 10 (2) (2002).

[27] H. Koç, D. Knittel, M. Mathelin and G. Abba, Modeling and control of an industrial accumulator in a web transport system, in Proc. Europ. Contr. Conf. ECC. (1999).

[28] H. Koç, D. Knittel, M. Mathelin and G. Abba, “Web tension control in an industrial accumulator”, in Proc. Int. Conf. Web Handling IWEB5. (1999).

[29] S. Yun, C. Han and J. Chung, “A study on the robust control algorithm for an axially moving film”, KSME International Journal. 15 (2001) 1207-1216.

[30] A. Valenzuela, J. Bentley and R. Lorenz, “Sensor less tension control in paper machines”, IEEE Transactions on industry applications. 39 (2) (2003).

[31] C. Chen, K. Chang and C. Chang, “Modeling and control of a web-fed machine”, Applied Mathematical Modelling. 28 (2004) 863–876.

[32] E. Laroche and D. Knittel, “An improved linear fractional model for robustness analysis of a winding system”, Control Engineering Practice. 13 (2005) 659–666.

[33] P. Pagilla, N. Siraskar, and R. Dwivedula, “Decentralized control of web processing lines”, IEEE Transactions on Control Systems Technology.15 (2007) 106–117.

[34] X. Dou and W. Wang, “Robust control of multistage printing systems”, Control Engineering Practice. 18 (2010) 219-229.

[35] T. Tran and K. Choi, “A back stepping-based control algorithm for multi-span roll-to-roll web system”, The International Journal of Advanced Manufacturing Technology. 70 (2014) 45-61.

[36] R. A. Sack, “Transverse oscillations in traveling strings”, British Journal of Applied Physics. 5 (1954) 224-226.

[37] S. Mahalingam, “Transverse vibrations of power transmission chains”, British Journal of Applied Physics. 8 (1957) 145-148.

[38] F. R. Archibald and A. G. Emslie, “The vibrations of a string having a uniform motion along its length”, Journal of Applied Mechanics, ASME. 25 (1958) 347–8.

[39] A. G. Ulsoy, C. D. Mote Jr. and R. Syzmani, “Principal developments in band saw vibration and stability research”, Holzals Roh und Werkstoff. 36 (1978) 273-280.

[40] J. A. Wickert and C. D. Mote Jr, “Current research on the vibration and stability of axially moving materials”, Shock and Vibration Digest. 20 (1988) 3-13.

[41] J. A. Wickert and C. D. Mote, “Classical vibration analysis of axially moving continua”, Journal of Applied Mechanics, ASME. 57 (1990) 738–44.

[42] W. T. Horssen, “On the influence of lateral vibrations of supports for an axially moving string”, Journal of Sound and Vibration. 268 (2003) 323–330.

[43] W. T. Horssen and S. V. Ponomareva, “On the construction of the solution of an equation describing an axially moving string”, Journal of Sound and Vibration. 287 (2005) 359–366.

[44] Y. Wang and X. Liu, “Eigenvalue and stability analysis for transverse vibrations of axially moving strings based on Hamiltonian dynamics”, Acta Mech Sinica. 21 (2005) 485–494.

[45] S. Abrate, “Vibrations of belts and belt drives”, Mach. Theory. 27 (1992) 645-659.

[46] L. Q. Chen and W. J. Zhao, “A computation method for nonlinear vibration of axially accelerating viscoelastic strings”, Applied Mathematics and Computation. 162 (2005) 305–310.

[47] M. H. Ghayesh and N. Mordian, “Nonlinear dynamic response of axially moving stretched viscoelastic strings”, Applied Mechanics. 81 (2011) 781-799.

[48] L. Q. Chen, J. Zhao and W. J. Zu, “Transient response of an axially accelerating viscoelastic string constituted by a fractional differential law”, Journal of Sound and Vibration. 278 (2004) 861–871.

[49] U. Zwiers and M. Braun, “Modeling and stability analysis of strings in axial motion”, 12th IFToMM World Congress, Besancon, France. June 18-21, 2007.

[50] R. F. Fung, J. S. Huang and Y. C Chen, “The transient amplitude of the viscoelastic traveling string: an integral constitutive law”, Journal of Sound and Vibration. 201 (2) (1997) 153–167.

[51] R. F. Fung, J. S. Huang and Y. C. Chen, “Non-linear dynamic analysis of the viscoelastic string with a harmonically varying transport speed”, Computers & Structures. 66(6) (1998) 777-784.

[52] M. Pakdemirli and H. Boyaci, “Effect of non-ideal boundary conditions on the vibrations of continuous systems”, Journal of Sound and Vibration. 249 (2002) 815-823.

[53] G. Suweken and W. T. Horssen, “On the transversal vibrations of a conveyor belt with a low and time-varying velocity. Part I: the string-like case”, Journal of Sound and Vibration. 264 (2003) 117-133.

[54] J. Chung, C. S. Han and K. Yi, “Vibration of an axially moving string with geometric non-linearity and translating acceleration”, Journal of Sound and Vibration. 240(4) (2001) 733–746.

[55] M. Pakdemirli, A. G. Ulsoy and A. Ceranoglu, “Transverse vibration of an axially accelerating string”, Journal of Sound and Vibration. 69(2) (1994) 179–196.

[56] L. Q. Chen and W. J. Zhao, “The energetic and the stability of axially moving Kirchhoff strings”, Acoustical Society of America. (2005) 55–58.

[57] G. Brandenburg, “A mathematical model of a continuous elastic web in a system of driven, looped, rollers”, Control Engineering and Data Processing. 3 (1973) 62–69.

[58] H. Koç, D. Knittel, M. Mathelin and G. Abba, “Modeling and robust control of winding systems for elastic webs”, IEEE Transactions on control systems technology. 10(2) (2002).

[59] W.A. Strauss, “Partial Differential Equations. An Introduction”. New York, John Wiley and Sons (1992).

[60] L. Q. Chen, J. Wu and J. W. Zu, “The chaotic response of the viscoelastic traveling string: an integral constitutive law”, Chaos, Solitons and Fractals. (2004) 349–357.

[61] A. Yurddas, E. Ozkaya and H. Boyaci, “Nonlinear vibrations of axially moving multi-supported strings having non-ideal support conditions”, Nonlinear Dynamics 73 (2013) 1223–1244.

[62] T. K. Senguptai, S. B. Talla and S. C. Pradhan, “Galerkin finite element methods for wave problems”, Sadhana 30 (2005) 611–623.

[63] C. D. Mote, “A study of band saw vibrations”, J. Frankl Inst 279 (1965) 430–444.

[64] C. D. Mote, “Divergence buckling of an edge-loaded axially moving band”, International Journal Mech Science 10 (1968) 281–295.

[65] A. Simpson, “Transverse modes and frequencies of beams translating between fixed end supports”, Journal of Engineering Science 15 (1973) 159–164.

[66] M. Krzystof, and T. Kapitaniak, “Dynamics of axially moving continua”, International Journal Mech Science 8(2014) 26–41.

[67] C. D. Mote, “On the non-linear oscillation of an axially moving string”, Journal of Applied Mechanics, ASME 33(1966) 463–464.

[68] K. Behdinan and B. Tabarrok, “Dynamics of Flexible Sliding Beams: Non-Linear Analysis Part II: Transient Response”, Journal of Sound and Vibration 208 (1997) 541–565.

[69] U. Lee, J. Kim and H. Oh, “Spectral analysis for the transverse vibration of an axially moving Timoshenko beam”, Journal of Sound and Vibration 271 (2004) 685–703.

[70] U. Lee and H. Oh, “Dynamics of an axially moving viscoelastic beam subject to axial tension”, Journal of Sound and Vibration 42 (2005) 2381–2398.

[71] G. Cepon and M. Boltezar, “Computing the dynamic response of an axially moving continuum”, Journal of Sound and Vibration 300 (2007) 316–329.

[72] T. Z. Yang, B. Fang, Y. Chen and Y. X. Zhen, “Approximate solutions of axially moving viscoelastic beams subject to multi-frequency excitations”, International Journal of Non-Linear Mechanics 44 (2009) 230–238.

[73] L. Wang, J. S. Chen and H. Y. Hu, “Radial basis collocation method for dynamic analysis of axially moving beams”, Interaction and Multiscale Mechanics 2 (2009) 333–352.

[74] C. An and J. Su, “Dynamic response of clamped axially moving beams: Integral transform solution”, Applied Mathematics and Computation 218 (2011) 249–259.

[75] Q. Ni, Z. L. Zhang and L. Wang, “Application of the differential transformation method to vibration analysis of pipes conveying fluid”, Applied Mathematics and Computation 217 (2011) 7028–7038.

[76] C. An and J. Su, “Dynamic response of axially moving Timoshenko beams: integral transform solution”, Applied Mathematics and Mechanics 35 (2014) 1421–1436.

[77] H. R. Oz and M. Pakedmirli, “Vibrations of An Axially Moving Beam with Time-Dependent Velocity”, Journal of Sound and Vibration 227 (1999) 239–257.

[78] Y. S. Shih and Z. F. Yeh, “Dynamic stability of a viscoelastic beam with frequency-dependent modulus”, International Journal of Solids and Structures 42 (2005) 2145–2159.

[79] L. Q. Chen, X. D. Yang and C. J. Cheng, “Dynamic stability of an axially accelerating viscoelastic beam”, European Journal of Mechanics and Solids 23 (2004) 659–666.

[80] L. Q. Chen and X. D. Yang, “Stability in parametric resonance of axially moving viscoelastic beams with time-dependent speed”, Journal of Sound and Vibration 284 (2005) 879–891.

[81] L. Q. Chen and X. D. Yang, “Nonlinear free transverse vibration of an axially moving beam: Comparison of two models”, Journal of Sound and Vibration 299 (2007) 348–354.

[82] S. Sui, L. Chen, C. Li and X. Liu, “Transverse Vibration of Axially Moving Functionally Graded Materials Based on Timoshenko Beam Theory”, Mathematical Problems in Engineering (2015) 391–399.

[83] H. Lv, Y. Li, L. Li and Q. Liu, “Transverse vibration of viscoelastic sandwich beam with time-dependent axial tension and axially varying moving velocity”, Applied Mathematical Modelling 38 (2014) 2558–2585.

[84] Q. Ni, M. Li, M. Tang and L. Wang, “Free vibration and stability of a cantilever beam attached to an axially moving base immersed in fluid”, Journal of Sound and Vibration 333 (2014) 2543–2555.

[85] A. M. Zenkour, A. E. Abouelregal and I. A. Abbas, “Generalized Thermo-Elastic Vibration of An Axially Moving Clamped Microbeam Subjected to Ramp-Type Thermal Loading”, Journal of Thermal Stresses 37 (2014) 1302–1323.

[86] M. H. Ghayesh and H. Farokhi, “Thermo-mechanical dynamics of three-dimensional axially moving beams”, Nonlinear Dynamics 80 (2015) 1643–1660.

[87] M. Li, Q. Ni and L. Wang, “Nonlinear dynamics of an underwater slender beam with two axially moving supports”, Ocean Engineering 108 (2015) 402-415.

[88] A. G. Ulsoy and C. D. Mote, “Vibration of wide band saw blades”, ASME, Journal of Engineering for Industry 104 (1982) 71–78.

[89] C. C. Lin and C. D. Mote, “Equilibrium displacement and stress distribution in a two dimensional axially moving web under transverse loading”, ASME, Journal of Applied Mechanics 62 (1995) 772–779.

[90] H. P. Lee, “Dynamic stability of a moving rectangular plate subject to in plane acceleration and force perturbations”, Journal of Applied Acoustics 45 (1995) 47–59.

[91] X. Wang, “Numerical analysis of moving orthotropic thin plates”, Computational Structure 70 (1999) 467–486.

[92] N. S. Bardell, R. S. Langley and J. M. Dunsdon, “On the free in-plane vibration of isotropic rectangular plates”, Journal of Sound and Vibration 191 (1996) 459–467.

[93] S. Hatami, H. R. Ronagh and M. Azhari, “Exact free vibration analysis of axially moving viscoelastic plates”, Computers and Structures 86 (2008) 1738–1746.

[94] X. D. Yang, W. Zhang, L. Q. Chen and M. H. Yao, “Dynamical analysis of axially moving plate by finite difference method”, Nonlinear Dynamics 67 (2012) 997–1006.

[95] H. Koivurova and A. Pramila, “Nonlinear vibration of axially moving membrane by finite element method”, Computational Mechanics 20 (1997) 573 -581.

[96] C. Shin, W. Kim and J. Chung, “Free in-plane vibration of an axially moving membrane”, Journal of Sound and Vibration 272 (2004) 137–154.

[97] C. Shin, J. Chung and W. Kim, “Dynamic characteristics of the out-of-plane vibration for an axially moving membrane”, Journal of Sound and Vibration 286 (2005) 1019–1031.

[98] C. Shin, J. Chung and H. H. Yoo, “Dynamic responses of the in-plane and out-of-plane vibrations for an axially moving membrane”, Journal of Sound and Vibration 297 (2006) 794–809.

[99] T. Saksa, N. Banichuk, J. Jeronen, M. Kurki and T. Tuovinen, “Dynamic analysis for axially moving viscoelastic panels”, International Journal of Solids and Structures 49 (2012) 3355–3366.

[100] J. Wu, W. Lei, Q. Wu, Y. Wang and L. Ma, “Transverse Vibration Characteristics and Stability of a Moving Membrane with Elastic Supports”, Journal of Low Frequency Noise, Vibration and Active Control 33 (2014) 65-78.

[101] J. Wu, J. Lui, W. Yan and Q. Wu, “Study on Membrane Vibration Characteristics Based on Meshless Method”, The 21st International Congress on Sound and Vibration 13-17 July, 2014, Beijing/China.

[102] Y. Wang, X. Liu and L. Huang, “Stability analyses for axially moving strings in nonlinear free and aerodynamically excited vibrations”, Chaos, Solitons and Fractals. 38 (2008) 421–429.

[103] A. Kelleche and N. Tatar, “Control of an axially moving viscoelastic Kirchhoff string”, Applicable Analysis. (2017) 1–18.

[104] R. Viguie, G. Kerschena, J. C. Golinval, D. M. McFarland, L. A. Bergman, A.F. Vakakis and N. V. Wouw, “Using passive nonlinear targeted energy transfer to stabilize drill-string systems”, Mechanical Systems and Signal Processing. 23 (2009) 148–169.

[105] M. A. Foda, “Vibration control and suppression of an axially moving string”, Journal of Vibration and Control. 18 (2011) 58–75.

[106] Y. Zhang, J. Zang, T.Z. Yang, B. Fang, and X. Wen, “Vibration suppression of an axially moving string with transverse wind loadings by a nonlinear energy sink”, Mathematical Problems in Engineering. (2013) 1–7.

[107] A. Berkani, N. Tatar and A. Khemmoudj, “Control of viscoelastic translational Euler–Bernoulli beam”, Mathematical Methods in Applied Sciences. 40 (2017) 237–254.

[108] Z. Zhao, Y. Liu, F. Guo and F. Fu, “Vibration control and boundary tension constraint of an axially moving string system”, Nonlinear Dynamics. 89 (2017) 2431–2440.

[109] A. Kelleche, N. Tatar and A. Khemmoudj, “Uniform Stabilization of an Axially Moving Kirchhoff String by a Boundary Control of Memory Type”, Journal of Dynamics and Control Systems. 23 (2017) 237–247.

[110] B. Yang and C. D. Mote, “Active vibration control of axially moving continua”, Intelligent Structural Systems. (1992) 359-402.

[111] J. Lin and J. Hu, “Vibration attenuation of an axially moving string via active in-domain control methods”, Asian Journal of Control. 4 (1999) 270-282.

[112] C. A. Tan and S. Ying, “Active wave control of the axially moving string: Theory and Experiment”, Journal of Sound and Vibration. 236 (2000) 861–880.

[113] Y. Li, D. Aron and C. D. Rahn, “Adaptive vibration isolation for axially moving strings: Theory and Experiment”, Automatica. 38 (2002) 379–390.

[114] S. P. Nagarkatti, F. Zhang, B. T. Costic and D. M. Dawson, “Speed tracking and transverse vibration control of an axially accelerating Web”, Mechanical Systems and Signal Processing. 16 (2002) 337–356.

[115] K. J. Yang, K. S. Hong and F. Matsuno, “Robust adaptive boundary control of an axially moving string under a spatiotemporally varying tension”, Journal of Sound and Vibration. 273 (2004) 1007–1029.

[116] C. W. Kim, K. S. Hong and H. Park, “Boundary control of an axially moving string" Actuator Dynamics Included”, Journal of Mechanical Science and Technology. 19 (2005) 40–50.

[117] L. Q. Chen and W. Zhang, “Adaptive vibration reduction of an axially moving string via a tensioner”, Journal of Sound and Vibration. 48 (2006) 1409–1415.

[118] Y. Liu, Z. Zhao and Y. He, “Stabilization of an axially moving accelerated/decelerated system via an adaptive boundary control”, ISA Transactions. 64 (2016) 394–404.

[119] Y. Liu, Z. Zhao and W. He, “Boundary control of an axially moving system with high acceleration/deceleration and disturbance observer”, Journal of the Franklin Institute. 354 (2017) 2905–2923.

[120] K. W. Wang and C. D. Mote, “Band/wheel system vibration under impulsive excitation”, Journal of Sound and Vibration 115 (1987) 203–216.

APPENDIX

$$A * S^{\cdot}(t) + B * S(t) = 0 \tag{A1}$$

$$S(t) = \begin{Bmatrix} \frac{dw_*}{dt_*} \\ w_* \end{Bmatrix} \tag{A2}$$

$$(B + \lambda_n * A)S_0 \; = \; 0 \tag{A3}$$

For string

$$A = \begin{bmatrix} M & 2 * v_* * G \\ 0 & \{(v_*^2 - 1)K_1 + v_* * G + \alpha K_2\} \end{bmatrix} \tag{A4}$$

$$B = \begin{bmatrix} 0 & \{(v_*^2 - 1)K_1 + v_* * G + \alpha K_2\} \\ \{(v_*^2 - 1)K_1 + v_* * G + \alpha K_2\} & 0 \end{bmatrix} \tag{A5}$$

For beam

$$A = \begin{bmatrix} M & 2 * v_* * G \\ 0 & \{(v_*^2 - 1) * K + v_* * G\} \end{bmatrix} \tag{A6}$$

$$B = \begin{bmatrix} 0 & \{(v_*^2 - 1) * K + v_* * G\} \\ \{(v_*^2 - 1) * K + v_* * G\} & 0 \end{bmatrix} \tag{A7}$$

For membrane

Adopting the methodology of [95], the kinetic energy (τ) and the potential energy (U) of an axially moving membrane is given as

$$\tau = \int_0^A \frac{1}{2}(\rho A)v^2 dA = 0 \tag{A8}$$

$$U = \int_0^A (q_x \epsilon_x + q_y \epsilon_y + 2q_{xy} \epsilon_{xy} +) dA \qquad (A9)$$

where

$$v = \left(V + \left(\frac{\partial u}{\partial t}\right) + V\left(\frac{\partial u}{\partial x}\right)\right) i + \left(\left(\frac{\partial v}{\partial t}\right) + V\left(\frac{\partial v}{\partial x}\right)\right) j + \left(\left(\frac{\partial w}{\partial t}\right) + V\left(\frac{\partial w}{\partial x}\right)\right) k \qquad (A10)$$

$$q_x = \frac{Eh}{(1-r^2)}\left(\frac{\partial u}{\partial x} + r\frac{\partial v}{\partial y}\right),\ q_y = \frac{Eh}{(1-r^2)}\left(\frac{\partial y}{\partial y} + r\frac{\partial u}{\partial x}\right),\ q_{xy}$$

$$= \frac{Eh}{2(1+r)}\left(\frac{\partial u}{\partial y} + \frac{\partial v}{\partial x}\right) \qquad (A11)$$

$$\epsilon_x = \frac{\partial u}{\partial x} + \frac{1}{2}\left(\frac{\partial w}{\partial x}\right)^2, \epsilon_y = \frac{\partial v}{\partial y} + \frac{1}{2}\left(\frac{\partial w}{\partial y}\right)^2, \epsilon_{xy} = \frac{1}{2}\left(\frac{\partial u}{\partial y} + \frac{\partial v}{\partial x} + \frac{\partial w}{\partial x}\frac{\partial w}{\partial y}\right) \qquad (A12)$$

where r is Poisson's ratio and E is Young's modulus. Substituting equations (A8) - (A11) into equation (3.36) results in equations of motion as

$$\rho h\left(\frac{\partial^2 u}{\partial t^2} + 2\,V\frac{\partial^2 u}{\partial t \partial x} + V^2\frac{\partial^2 u}{\partial x^2} + V\cdot\frac{\partial u}{\partial x}\right) - \frac{\partial q_x}{\partial x} - \frac{\partial q_{xy}}{\partial x} = 0 \qquad (A13)$$

$$\rho h\left(\frac{\partial^2 v}{\partial t^2} + 2\,V\frac{\partial^2 v}{\partial t \partial x} + V^2\frac{\partial^2 v}{\partial x^2} + V\cdot\frac{\partial v}{\partial x}\right) - \frac{\partial q_y}{\partial x} - \frac{\partial q_{xy}}{\partial x} = 0 \qquad (A14)$$

$$\rho h\left(\frac{\partial^2 w}{\partial t^2} + 2\,V\frac{\partial^2 w}{\partial t \partial x} + V^2\frac{\partial^2 w}{\partial x^2} + V\cdot\frac{\partial w}{\partial x}\right) - \frac{\partial}{\partial x}\left(q_x\frac{\partial w}{\partial x} + q_{xy}\frac{\partial w}{\partial y}\right)$$

$$-\frac{\partial}{\partial y}\left(q_y\frac{\partial w}{\partial y} + q_{xy}\frac{\partial w}{\partial x}\right) = 0 \qquad (A15)$$

Converting equations (A13) - (A15) into a weak form by multiplying them with the weighing functions $\overline{u}$, $\overline{v}$ and $\overline{w}$ and integrating the resultant equation.

$$\int_0^b \int_0^l \left[\rho h\overline{u}\left(\frac{\partial^2 u}{\partial t^2} + 2\,V\frac{\partial^2 u}{\partial t\partial x} + V^2\frac{\partial^2 u}{\partial x^2} + + V\cdot\frac{\partial u}{\partial x}\right) + \frac{\partial \overline{u}}{\partial x}q_x + \frac{\partial \overline{u}}{\partial x}q_{xy}\right] dxdy$$

$$+ \int_0^b \int_0^l \left[\rho h\overline{v}\left(\frac{\partial^2 v}{\partial t^2} + 2\,V\frac{\partial^2 v}{\partial t\partial x} + V^2\frac{\partial^2 v}{\partial x^2} + V\cdot\frac{\partial v}{\partial x}\right) + \frac{\partial \overline{v}}{\partial x}q_y\right.$$

$$\left. + \frac{\partial \overline{v}}{\partial x}q_{xy}\right] dxdy = \int_0^b T\,(\overline{u}|_{x=l} - \overline{u}|_{x=0})dy \qquad (A16)$$

$$\int_0^b \int_0^l \left[\rho h\overline{w}\left(\frac{\partial^2 w}{\partial t^2} + 2\,V\frac{\partial^2 w}{\partial t\partial x} + V^2\frac{\partial^2 w}{\partial x^2} + V\cdot\frac{\partial w}{\partial x}\right) + \frac{\partial \overline{w}}{\partial x}q_x + \frac{\partial \overline{w}}{\partial x}q_{xy} + \frac{\partial \overline{w}}{\partial y}q_y\right.$$

$$\left. + \frac{\partial \overline{w}}{\partial y}q_{xy}\right] dxdy = 0 \qquad (A17)$$

Assuming the approximated solution to be

$$u = \sum_{i=0}^{N}\sum_{j=0}^{N} T_{ij}^{u}(t)Z_{ij}^{u}(x,y) \qquad (A18a)$$

$$v = \sum_{i=0}^{N}\sum_{j=0}^{N} T_{ij}^{v}(t)Z_{ij}^{v}(x,y) \qquad (A18b)$$

$$w = \sum_{i=0}^{N}\sum_{j=0}^{N} T_{ij}^{w}(t)Z_{ij}^{w}(x,y) \qquad (A18c)$$

where

$$Z_{ij}^{u}(x,y) = Z_{ij}^{u}(x,y) = Z_{ij}^{w}(x,y) = X_i(x)Y_j(y)$$

The weighing functions are

$$\overline{u} = \sum_{m=0}^{N}\sum_{n=0}^{N} T_{mn}^{\overline{u}}(t)Z_{mn}^{u}(x,y) \qquad (A19a)$$

$$\overline{v} = \sum_{m=0}^{N}\sum_{n=0}^{N} T_{mn}^{\overline{v}}(t) Z_{mn}^{v}(x,y) \qquad (A19b)$$

$$\overline{w} = \sum_{m=0}^{N}\sum_{n=0}^{N} T_{mn}^{\overline{w}}(t) Z_{mn}^{w}(x,y) \qquad (A19c)$$

Assuming

$$D = \frac{Eh}{1-v^2}$$

$$D_0 = \frac{Eh}{2(1+v)}$$

and

$$\bar{Z}(x,y) = Derivative\ w.r.t\ to \quad x$$

$$Z'(x,y) = Derivative\ w.r.t\ to \quad y$$

Therefore equation (A16) becomes

$$\int_0^b \int_0^l \rho h \left[\sum_{m=0}^{N} \sum_{n=0}^{N} T_{mn}^{\overline{u}}(t) Z_{mn}^{u}(x,y) \left\{ \sum_{i=0}^{N} \sum_{j=0}^{N} \left(\ddot{T}_{ij}^{u} Z_{ij}^{u}(x,y) + 2V \dot{T}_{ij}^{u} \bar{Z}_{ij}^{u}(x,y) \right. \right. \right.$$

$$\left. \left. \left. + V^2 T_{ij}^{u} \bar{\bar{Z}}_{ij}^{u}(x,y) \right) \right\} dxdy \right]$$

$$+ \int_0^b \int_0^l \left[\sum_{m=0}^{N} \sum_{n=0}^{N} \bar{T}_{mn}^{\overline{u}}(t) \bar{Z}_{mn}^{u}(x,y)\, D \left\{ \sum_{i=0}^{N} \sum_{j=0}^{N} T_{ij}^{u}(t) \bar{Z}_{ij}^{u}(x,y) \right. \right.$$

$$\left. \left. + v \sum_{i=0}^{N} \sum_{j=0}^{N} T_{ij}^{v}(t) Z_{ij}^{\prime v}(x,y) \right\} dxdy \right]$$

$$+ \int_0^b \int_0^l \left[\sum_{m=0}^{N} \sum_{n=0}^{N} \bar{T}_{mn}^{\overline{u}}(t) Z_{mn}^{\prime u}(x,y)\, D_0 \left\{ \sum_{i=0}^{N} \sum_{j=0}^{N} T_{ij}^{u}(t) Z_{ij}^{\prime u}(x,y) \right. \right.$$

$$\left. \left. + \sum_{i=0}^{N} \sum_{j=0}^{N} T_{ij}^{v}(t) \bar{Z}_{ij}^{v}(x,y) \right\} dxdy \right] = \int_0^b T \left(\overline{u}|_{x=l} - \overline{u}|_{x=0} \right) dy$$

$$\sum_{m=0}^{N}\sum_{n=0}^{N}\sum_{i=0}^{N}\sum_{j=0}^{N}\left[\left\{\rho h\int_0^b\int_0^l \ddot{T}_{ij}^u Z_{ij}^u(x,y)Z_{mn}^u(x,y)+2V\rho h\int_0^b\int_0^l \dot{T}_{ij}^u \bar{Z}_{ij}^u(x,y)Z_{mn}^u(x,y)\right\}\right.$$

$$+\left\{\rho hV^2\int_0^b\int_0^l Z_{mn}^u(x,y)\bar{\bar{Z}}_{ij}^u(x,y)+D\int_0^b\int_0^l \bar{Z}_{mn}^u(x,y)\bar{Z}_{ij}^u(x,y)\right.$$

$$\left.+D_0\int_0^b\int_0^l Z_{mn}'^u(x,y)Z_{ij}'^u(x,y)\right\}T_{ij}^u dxdy$$

$$\left.+\left\{vD\int_0^b\int_0^l \bar{Z}_{mn}^u(x,y)Z_{ij}'^v(x,y)+D_0\int_0^b\int_0^l Z_{mn}'^u(x,y)\bar{Z}_{ij}^v(x,y)\right\}T_{ij}^v dxdy\right]$$

$$=\ f_{mn}$$

where

$$f_{mn}=\ [1-(-1)^m]\,T\ \int_0^b Y_n dy$$

The discretized in-plan equations of motion are

$$\sum_{i=0}^{N}\sum_{j=0}^{N}\left(M_{mnij}^u\ddot{T}_{ij}^u+2\,VG_{mnij}^u\dot{T}_{ij}^u+K_{mnij}^{uu}T_{ij}^u+V^{\cdot}G_{mnij}^u T_{ij}^u+K_{mnij}^{uv}T_{ij}^v\right)$$

$$=\ f_{mn} \qquad (A20)$$

$$\sum_{i=0}^{N}\sum_{j=0}^{N}\left(M_{mnij}^v\ddot{T}_{ij}^v+2\,VG_{mnij}^v\dot{T}_{ij}^v+K_{mnij}^{vv}T_{ij}^v+V^{\cdot}G_{mnij}^v T_{ij}^v+K_{mnij}^{vu}T_{ij}^u\right)$$

$$=\ 0 \qquad (A21)$$

where the coefficients are

$$M_{mnij}^u=M_{mnij}^v=\ \rho h\left[\int_0^l X_m(x)X_i(x)dx\int_0^b Y_n(y)Y_j(y)dy\right]$$

$$G_{mnij}^u=G_{mnij}^v=\ \rho h\left[\int_0^l X_m(x)\frac{dX_i(x)}{dx}dx\int_0^b Y_n(y)Y_j(y)dy\right]$$

$$K_{mnij}^{uu} = \rho h V^2 \left[\int_0^l X_m(x)\frac{d^2X_i(x)}{dx^2}dx \int_0^b Y_n(y)Y_j(y)dy\right] + D\left[\int_0^l \frac{dX_m(x)}{dx}\frac{dX_i(x)}{dx}dx \int_0^b Y_n(y)Y_j(y)dy\right] + D_0\left[\int_0^l X_m(x)X_i(x)dx \int_0^b \frac{dY_n(y)}{dy}\frac{dY_j(y)}{dy}dy\right]$$

$$K_{mnij}^{vv} = \rho h V^2 \left[\int_0^l X_m(x)\frac{d^2X_i(x)}{dx^2}dx \int_0^b Y_n(y)Y_j(y)dy\right] + D_0\left[\int_0^l \frac{dX_m(x)}{dx}\frac{dX_i(x)}{dx}dx \int_0^b Y_n(y)Y_j(y)dy\right] + D\left[\int_0^l X_m(x)X_i(x)dx \int_0^b \frac{dY_n(y)}{dy}\frac{dY_j(y)}{dy}dy\right]$$

$$K_{mnij}^{uv} = vD\left[\int_0^l \frac{dX_m(x)}{dx}X_i(x)dx \int_0^b Y_n(y)\frac{dY_j(y)}{dy}dy\right] + D_0\left[\int_0^l X_m(x)\frac{dX_i(x)}{dx}dx \int_0^b \frac{dY_n(y)}{dy}Y_j(y)dy\right]$$

$$K_{mnij}^{vu} = vD\left[\int_0^l X_m(x)\frac{dX_i(x)}{dx}dx \int_0^b \frac{dY_n(y)}{dy}Y_j(y)dy\right] + D_0\left[\int_0^l \frac{dX_m(x)}{dx}X_i(x)dx \int_0^b Y_n(y)\frac{dY_j(y)}{dy}dy\right]$$

Equations (A20) and (A21) in matrix form

$$M\ddot{S} + 2VG\dot{S} + (K + V\cdot G)S = F \qquad (A22)$$

Similarly, equation (A17) becomes

$$\int_0^b \int_0^l \rho h \left[\sum_{m=0}^{Mx} \sum_{n=0}^{My} T_{mn}^{\overline{w}}(t) Z_{mn}^{w}(x,y) \left\{ \sum_{i=0}^{Mx} \sum_{j=0}^{My} \left(\ddot{T}_{ij}^{w} Z_{ij}^{w}(x,y) + 2V\dot{T}_{ij}^{w} \bar{Z}_{ij}^{w}(x,y) \right. \right. \right.$$

$$\left. \left. \left. + V^2 T_{ij}^{w} \bar{\bar{Z}}_{ij}^{w}(x,y) \right) \right\} dxdy \right]$$

$$+ \sum_{m=0}^{Mx} \sum_{n=0}^{My} \bar{T}_{mn}^{\overline{w}}(t) \bar{Z}_{mn}^{w}(x,y) \int_0^b \int_0^l \left[D \sum_{i=0}^{Mx} \sum_{j=0}^{My} T_{ij}^{w}(t) Z_{ij}^{w}(x,y) \left\{ \sum_{i=0}^{Nx} \sum_{j=0}^{Ny} T_{ij}^{u}(t) \bar{Z}_{ij}^{u}(x,y) \right. \right.$$

$$\left. \left. + v \sum_{i=0}^{Nx} \sum_{j=0}^{Ny} T_{ij}^{v}(t) Z_{ij}^{\prime v}(x,y) \right\} dxdy \right.$$

$$\left. + D_0 \sum_{i=0}^{Mx} \sum_{j=0}^{My} T_{ij}^{w}(t) Z_{ij}^{\prime w}(x,y) \left\{ \sum_{i=0}^{Nx} \sum_{j=0}^{Ny} T_{ij}^{u}(t) Z_{ij}^{\prime u}(x,y) + \sum_{i=0}^{Nx} \sum_{j=0}^{Ny} T_{ij}^{v}(t) \bar{Z}_{ij}^{v}(x,y) \right\} dxdy \right]$$

$$+ \sum_{m=0}^{Mx} \sum_{n=0}^{My} \bar{T}_{mn}^{w}(t) \bar{Z}_{mn}^{w}(x,y) \int_0^b \int_0^l \left[\sum_{i=0}^{Mx} \sum_{j=0}^{My} T_{ij}^{w}(t) Z_{ij}^{\prime w}(x,y) \, D \left\{ \sum_{i=0}^{Nx} \sum_{j=0}^{Ny} T_{ij}^{v}(t) Z_{ij}^{\prime v}(x,y) \right. \right.$$

$$\left. \left. + v \sum_{i=0}^{Nx} \sum_{j=0}^{Ny} T_{ij}^{u}(t) \bar{Z}_{ij}^{u}(x,y) \right\} dxdy \right.$$

$$\left. + D_0 \sum_{i=0}^{Nx} \sum_{j=0}^{Ny} T_{ij}^{u}(t) \bar{Z}_{ij}^{u}(x,y) \left\{ \sum_{i=0}^{Nx} \sum_{j=0}^{Ny} T_{ij}^{u}(t) Z_{ij}^{\prime u}(x,y) + \sum_{i=0}^{Nx} \sum_{j=0}^{Ny} T_{ij}^{v}(t) \bar{Z}_{ij}^{v}(x,y) \right\} dxdy \right]$$

$$= 0$$

$$\bar{T}_{ij}^{w}\sum_{m=0}^{Mx}\sum_{n=0}^{My}\sum_{i=0}^{Mx}\sum_{j=0}^{My}\left[\left\{\rho h\int_{0}^{b}\int_{0}^{l}\ddot{T}_{ij}^{w}Z_{ij}^{w}(x,y)Z_{mn}^{w}(x,y)\right.\right.$$

$$+2V\rho h\int_{0}^{b}\int_{0}^{l}\dot{T}_{ij}^{w}\bar{Z}_{ij}^{w}(x,y)Z_{mn}^{w}(x,y)$$

$$\left.+\rho hV^{2}\int_{0}^{b}\int_{0}^{l}T_{ij}^{w}(t)Z_{mn}^{w}(x,y)\bar{\bar{Z}}_{ij}^{w}(x,y)\right\}$$

$$+\sum_{i=0}^{Nx}\sum_{j=0}^{Ny}\left\{D\int_{0}^{b}\int_{0}^{l}\bar{Z}_{mn}^{w}(x,y)\bar{Z}_{ij}^{u}(x,y)\bar{Z}_{ij}^{w}(x,y)T_{ij}^{u}(t)\right.$$

$$+vD\int_{0}^{b}\int_{0}^{l}\bar{Z}_{mn}^{w}(x,y)Z_{ij}^{\prime v}(x,y)\bar{Z}_{ij}^{w}(x,y)T_{ij}^{v}(t)$$

$$+D_{0}\int_{0}^{b}\int_{0}^{l}\bar{Z}_{mn}^{w}(x,y)Z_{ij}^{\prime u}(x,y)Z_{ij}^{\prime w}(x,y)T_{ij}^{u}(t)$$

$$+D_{0}\int_{0}^{b}\int_{0}^{l}\bar{Z}_{mn}^{w}(x,y)\bar{Z}_{ij}^{v}(x,y)Z_{ij}^{\prime w}(x,y)T_{ij}^{v}(t)$$

$$+D\int_{0}^{b}\int_{0}^{l}Z_{mn}^{\prime w}(x,y)Z_{ij}^{\prime v}(x,y)Z_{ij}^{\prime w}(x,y)T_{ij}^{v}(t)$$

$$+vD\int_{0}^{b}\int_{0}^{l}Z_{mn}^{\prime w}(x,y)Z_{ij}^{\prime w}(x,y)\bar{Z}_{ij}^{u}(x,y)T_{ij}^{u}(t)$$

$$+D_{0}\int_{0}^{b}\int_{0}^{l}Z_{mn}^{\prime w}(x,y)Z_{ij}^{\prime u}(x,y)Z_{ij}^{\prime w}(x,y)T_{ij}^{u}(t)$$

$$\left.\left.+D_{0}\int_{0}^{b}\int_{0}^{l}Z_{mn}^{\prime w}(x,y)\bar{Z}_{ij}^{w}(x,y)\bar{Z}_{ij}^{v}(x,y)T_{ij}^{v}(t)+\right\}T_{ij}^{w}\,dxdy\right]=0$$

The discretized out-of-plan equation of motion is

$$M^w\ddot{T}^w + 2VG^w\dot{T}^w + [V^2H^w + V\cdot G + (K^{wu}T^u + K^{wv}T^v)]T^w = 0 \qquad (A23)$$

where the coefficients are

$$M^w = \sum_{m=0}^{Mx}\sum_{n=0}^{My}\sum_{i=0}^{Mx}\sum_{j=0}^{My}\left[\rho h\int_0^l X_m^w X_i^w dx\int_0^l Y_n^w Y_j^w dy\right]$$

$$G^w = \sum_{m=0}^{Mx}\sum_{n=0}^{My}\sum_{i=0}^{Mx}\sum_{j=0}^{My}\left[\rho h\int_0^l X_m^w \frac{dX_i^w}{dx} dx\int_0^l Y_n^w Y_j^w dy\right]$$

$$H^w = \sum_{m=0}^{Mx}\sum_{n=0}^{My}\sum_{i=0}^{Mx}\sum_{j=0}^{My}\left[\rho h\int_0^l X_m^w \frac{d^2X_i^w}{dx^2} dx\int_0^l Y_n^w Y_j^w dy\right]$$

$$\begin{aligned}K^{wu} = \sum_{m=0}^{Mx}\sum_{n=0}^{My}\sum_{i=0}^{Mx}\sum_{j=0}^{My}\Bigg[\sum_{i=0}^{Nx}\sum_{j=0}^{Ny}\Bigg\{ & D\left(\int_0^l \frac{dX_m^w}{dx}\frac{dX_i^w}{dx}\frac{dX_i^u}{dx}dx\int_0^l Y_n^w Y_j^w Y_j^u dy\right)\\ & + D_0\left(\int_0^l \frac{dX_m^w}{dx}X_i^w X_i^u dx\int_0^l Y_n^w \frac{dY_j^w}{dy}Y_j^u dy\right)\\ & + vD\left(\int_0^l X_m^w X_i^w \frac{dX_i^u}{dx}dx\int_0^l \frac{dY_n^w}{dy}\frac{dY_j^w}{dy}Y_j^u dy\right)\\ & + D_0\left(\int_0^l X_m^w \frac{dX_i^w}{dx}X_i^u dx\int_0^l \frac{dY_n^w}{dy}Y_j^w\frac{dY_j^u}{dy}dy\right)\Bigg\}\Bigg]T_{ij}^u\end{aligned}$$

$$K^{wv} = \sum_{m=0}^{Mx}\sum_{n=0}^{My}\sum_{i=0}^{Mx}\sum_{j=0}^{My}\left[\sum_{i=0}^{Nx}\sum_{j=0}^{Ny}\left\{ vD\left(\int_0^l \frac{dX_m^w}{dx}\frac{dX_i^w}{dx}X_i^v dx \int_0^l Y_n^w Y_j^w \frac{dY_j^v}{dy} dy\right)\right.\right.$$

$$+ D_0\left(\int_0^l \frac{dX_m^w}{dx} X_i^w \frac{dX_i^v}{dx} dx \int_0^l Y_n^w \frac{dY_j^w}{dy} Y_j^v dy\right)$$

$$+ D\left(\int_0^l X_m^w X_i^w X_i^v dx \int_0^l \frac{dY_n^w}{dy}\frac{dY_j^w}{dy}\frac{dY_j^v}{dy} dy\right)$$

$$\left.\left. + D_0\left(\int_0^l X_m^w \frac{dX_i^w}{dx}\frac{dX_i^v}{dx} dx \int_0^l \frac{dY_n^w}{dy} Y_j^w Y_j^v dy\right)\right\}\right] T_{ij}^v$$

$$A = \begin{bmatrix} M & 2 * V * G \\ 0 & K \end{bmatrix} \qquad (A24)$$

$$B = \begin{bmatrix} 0 & K \\ K & 0 \end{bmatrix} \qquad (A25)$$

VITAE

Name:	SAJID ALI
Place of Birth:	Haripur, Pakistan
Nationality:	Pakistani
Permanent Address:	District and Tehsile Haripur, Village and Post Office Kotnajibullah 22660, Mohallah Saeedabad, KPK, Pakistan
Telephone:	+92-3459634469, +966-591719669
Email Address:	sajidali@kfupm.edu.sa; maliksajidalikhan@gmail.com
Education Qualification:	MSc (Mechanical Engineering) October, 2013 Department of Mechanical Engineering University of Engineering and Technology, Peshawar, Pakistan BSc (Mechanical Engineering) August, 2009 Department of Mechanical Engineering University of Engineering and Technology, Peshawar, Pakistan